WWCB

characterizing, modelling and optimizing the sound absorption of wood wool cement boards

Botterman, B.

Award date:
2016

WWCB

CHARACTERIZING, MODELLING AND OPTIMIZING THE SOUND ABSORPTION OF WOOD WOOL CEMENT BOARDS

BY
B. (BRAM) BOTTERMAN

Author: Bram Botterman
Student number: s070551
E-mail: b.botterman@gmail.com

Date: 08-07-2016

Supervisors:

Building Acoustics
dr. ir. M.C.J. (Maarten) Hornikx

Building Materials
ir. G.C.H. (Guillaume) Doudart de la Grée
dr. Q. (Qingliang) Yu
Prof. dr. ir. H.J.H. (Jos) Brouwers

University: Eindhoven University of Technology
Den Dolech 2
Postbus 513
5600 MB Eindhoven
The Netherlands

SAMENVATTING

In dit afstudeeronderzoek wordt er onderzoek gedaan naar het karakteriseren, modelleren en het uiteindelijk optimaliseren van de geluidsabsorptie van houtvezelcementplaten (Engelse afkorting: WWCB). Deze platen worden door de goede thermische, brandwerende en akoestische eigenschappen al sinds 1920 geproduceerd en toegepast, voornamelijk als plafondplaten (zowel binnen als buiten) en als geluidsschermen. Door eerst fundamentale kennis over de geluidsabsorberende eigenschappen van de platen te vergaren en deze platen te karakteriseren, zullen daarna de akoestische eigenschappen, door middel van impedantiemodellen, worden gemodelleerd en daarna worden verbeterd en geoptimaliseerd.

Verschillende modellen, die in staat zijn de akoestische impedantie van poreuze materialen te modelleren, zijn geanalyseerd en de toepasbaarheid voor de houtvezelcementplaat is geëvalueerd. Uiteindelijk bleek het Johnson-Champoux-Allard (JCA) model het beste in staat de gemeten geluidsabsorptie in de impedantiebuis van de WWCB-samples te kunnen voorspellen. Dit model maakt gebruikt van vijf parameters; de open porositeit, stromingsweerstand, tortuositeit en de visceuze en thermische karakteristieke lengtes. Van deze vijf parameters is de stromingsweerstand gemeten en zijn de andere vier parameters bepaald met de omgekeerde rekenmethode op basis van de resultaten verkregen uit de impedantiebuis-metingen.

Een relatie is gevonden tussen bulkdichtheid en de vijf verschillende parameters. Gebruikmakend van deze relaties, kan worden geconcludeerd dat het mogelijk is om de normaal invallende geluidsabsorptie te voorspellen, alleen gebruikmakend van de bulkdichtheid en de dikte van de geanalyseerde platen.

De platen die zijn getest in deze studie bestaan uit verschillende vezeldiameters (1.0, 1.5 en 2.0 mm) en verschillende diktes (15, 25, 35 en 50 mm). Door de inhomogeniteit van het product verschillen de samples (diameter 40 tot 100 mm), genomen uit deze platen, niet alleen in dikte en vezel diameter, maar ook in dichtheid en hout-bindmiddel ratio.

Gebruikmakend van het gevalideerde model, is de invloed van de dichtheid, dikte en vezeldiameter op de akoestische eigenschappen geëvalueerd. Daarnaast zal de invloed van een spouwconstructie, systemen met verschillende lagen en het toepassen van minerale wool worden geanalyseerd.

Uiteindelijk kan er geconcludeerd worden dat het mogelijk is om de akoestische eigenschappen van houtvezelcementplaten te modelleren en te optimaliseren.

ABSTRACT

The present study aims to characterize, model and optimize the sound absorption of wood wool cement boards (WWCB). These boards are, due to their thermal, fire resisting and acoustical properties, produced and applied since 1920 in parking lots and underneath balconies as in- and outdoor ceiling material and used as sound barriers. The main challenges in this study are the suitability of the existing impedance models for the WWCB and the inhomogeneity of the WWCB; the samples taken from different commercial boards do not only greatly differ in density, but also in wood-to-binder ratio.

By first gathering fundamental knowledge about the sound absorbing properties of the WWCB and to acoustic characterize these boards, will it be evaluated if it is possible to model the sound absorption by making use of impedance models. Different models, able to predict the acoustic impedance of rigid-frame porous materials, have been analyzed and their suitability for the WWCB has been evaluated. It is concluded that the Johnson-Champoux-Allard (JCA) model is the most appropriate to fit the normal incidence sound absorption values as measured in an impedance tube.

From the five input parameters for this impedance model, the flow resistivity has been measured. The open porosity, tortuosity and viscous and thermal characteristic lengths, have been determined by making use of an inverse calculation method, a curve fitting approach, based on the measured acoustic absorption coefficients in the impedance tube.

The tested WWCBs are made of three different strand widths (1.0, 1.5 and 2.0 mm) and of different thicknesses (15, 25, 35 and 50 mm), and samples taken from these boards differ in density and wood to binder ratio. By making use of the found relations between the bulk density and the input parameters for the impedance model, it is concluded to be possible to predict the normal incidence sound absorption of the WWCB by only making use of the bulk density and thickness as input parameters.

Using the JCA-model, the influence of the thickness, density, wood-cement ratio, strand diameters and air-cavity on the sound absorption is evaluated and the results show that it is possible to model and optimize the sound absorption of the existing inhomogeneous WWCB.

PREFACE

After completing my pre-university degree at the Huygens lyceum in Voorburg, I started the bachelor Architecture, Building and Planning at the Eindhoven University of Technology. During my minor Integral Design, where I combined the disciplines Architecture and Building Acoustics, it were Renz van Luxemburg and Constant Hak who made me enthusiastic about architectural acoustics. After this project I decided to start the mastertrack Building Physics and Services. Due to the theoretical, as well as the practical, point of view of the project, I decided to start my final project about the 'characterizing, modelling and optimization the sound absorption of wood wool cement boards'.

I would like to thank my supervisors, dr. ir. M.C.J. Hornikx, ir. ing. G.C.H. Doudart de la Grée, dr. Q. Yu and prof. dr. ir. H.J.H. Brouwers for sharing their knowledge and helping me to reach my goal. I believe that the combination between Building Acoustics and Building Materials was of great value for this thesis.

Besides my supervisors I would also like to the STW-foundation which realized the transfer of knowledge between technical sciences and its users, in my project different companies. These companies provided materials for the project and their knowledge. Presenting my work for these companies, was a great experience for me.

B. (Bram) Botterman

TABLE OF CONTENTS

LIST OF FIGURES

LIST OF TABLES

LIST OF SYMBOLS

Roman		
c	Speed of sound in air	m/s
d	Thickness	m
f	Frequency	Hz
i	Imaginary number $\sqrt{(-1)}$	-
k_c	Propagation wave number	$1/m$
K_e	Effective bulk modulus	kg/ms^2
N_p	Prandtl number (≈0.71)	-
P_0	Atmospheric pressure (≈101,320)	N/m^2
R	Reflection coefficient	-
s_b	Shape factor	-
T	Bessels function	
Z_c	Characteristic impedance	$Pa{\cdot}s/m$
Z_s	Surface impedance	$Pa{\cdot}s/m$
Z_0	Characteristic impedance of air	$Pa{\cdot}s/m$
Z_n	Normalized impedance	$Pa{\cdot}s/m$

Greek

α_p	Practical sound absorption coefficient	-
α_w	Weighted sound absorption coefficient	-
α_∞	Tortuosity	-
γ	Ratio of the specific heat capacity (≈1.4)	-
η	Viscosity of air ($\approx 1.84 \cdot 10^{-5}$)	*Pa·s*
θ	Temperature	*°C*
Λ	Viscous characteristic length	*m*
Λ'	Thermal characteristic length	*m*
μ	Coefficient of dynamic viscosity of air	-
λ	Wave length	*m*
ρ	Bulk density	kg/m^3
ρ_e	Effective density	kg/m^3
ρ_0	Specific density of air (≈1.204)	kg/m^3
σ	Flow resistivity	Ns/m^4
ϕ	Porosity	-
ω	Angular frequency	*1/s*

Subscript

b	Signifies bulk material property
c	Bulk material characteristic
e	Signifies effective property
n	Normal incidence
o	Relating to air
p	Relating to pore (arbitrary shape)
s	Relating to surface

Abbreviations

NRC	Noise Reduction Coefficient	-
WWCB	Wood Wool Cement Board	
SAA	Sound Absorption Average	-

1. INTRODUCTION

1.1 WOOD WOOL CEMENT BOARDS (WWCB)

A wood wool cement board (WWCB) is a building product produced since 1920, consisting of wood-wool mineralized by Portland Cement (PC). The boards are mainly applied in parking lots and underneath balconies as in- and outdoor ceiling material and used as sound barriers. The boards possess high thermal insulation, high fire resistance, good sound absorption properties, have a high durability and low maintenance necessity, hence are still popular in designs nowadays (Doudart de la Grée et al., 2014).

Figure 1.1: *Application of WWCBs at the Flux building on the campus of Eindhoven University of Technology.*

Due to the high porosity (± 80%) and a high pore wall contact area, a WWCB can acoustically be considered as a porous absorber. Its sound absorption has been measured previously (Doudart de la Grée et al., 2014) and it can be concluded that the sound absorption is relatively high in the frequencies between 1000 and 4000 Hz, which is illustrated in Figure 1.2.

The sound absorbing properties of building materials are compared to each other based on the middle octave band and single number sound absorption values, mainly in the range of 125-4000 Hz. Since the sound absorption of the WWCB is significantly lower for the lower frequencies compared to that of the higher frequencies, it is of main interest of this study to investigate the possibilities to increase the sound absorption by changing the WWCB characteristics.

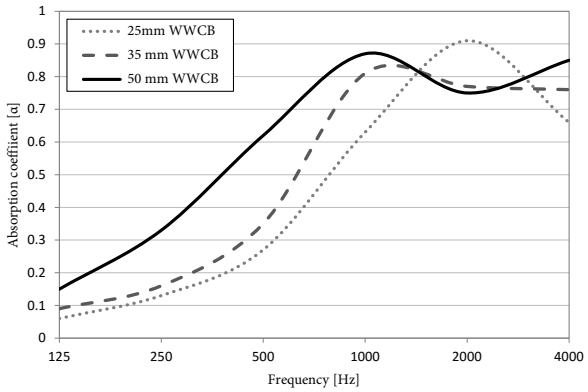

Figure 1.2: *Absorption coefficients for the WWCB with 25, 35 and 50 mm thickness with a 1.5 mm strand width (according to ISO 354:2003) (Doudart de la Grée et al., 2014).*

1.2 PROBLEM STATEMENT

Currently, no systematic study exists explaining the sound absorbing behaviour of the WWCB, which would enable to increase and finally optimize its acoustical properties. It is not known what the influential parameters are for the sound absorption for the WWCB and, therefore, the first goal of this study is to fundamentally understand the sound absorption performance of WWCBs. The second goal is to investigate if it is possible to model the sound absorbing properties of the inhomogeneous WWCB. If a suitable model can be found, this model will be used to evaluate the influence of the different parameters and properties and finally the WWCB will be optimized with respect to the sound absorption.

The main research question in this study is:

Is it possible, by making use of impedance models, to characterize, increase and optimize the sound absorption of wood wool cement boards?

1.3 METHODOLOGY

Firstly, a literature study is performed. The focus in this literature study is on the production process, the existing knowledge of the composition and properties of the WWCB and the existing impedance models which are able to predict the sound absorption of porous materials.

Secondly, based on this literature study, an impedance model is chosen which is suitable for the WWCB. This model will be validated by measurements performed using an impedance tube. For the simulation model several input parameters will be required and these parameters are directly measured or will be obtained by an inverse calculation method (curve fitting approach) on the results of the acoustic impedance measurements. Finally, based on analysing the results of the validated simulation model, an optimisation study will be performed.

For this study, WWCBs with different strand diameters (1.0, 1.5 and 2.0 mm) and different thicknesses (15, 25, 35 and 50 mm) are tested. Samples taken from these boards do not only differ in strand diameter or thickness, but also in density and wood-to-binder ratio, which makes them

inhomogeneous. The influence of these variables will be evaluated. Moreover, the influence of combining different WWCB and adding an air-cavity behind the WWCB on the sound absorption will be analysed.

While this study mainly focusses on physical modelling, it also contains a practical part which is interesting for the companies involved in this project. This study will give an increased acoustical knowledge of their products and will for example give an insight on how to adjust the WWCB product to increase the sound absorption of the WWCB.

1.4 CONTENT OF THIS REPORT

First the wood wool cement board in general, its production process and its properties are addressed in Chapter 2. Secondly, the sound absorption of the WWCB is described in Chapter 3 and in Chapter 4 a more detailed description will be provided regarding acoustic impedance models (describing all relevant parameters and existing theoretical models). In this chapter also the most suitable model for the WWCB will be chosen based on a validation study. In Chapter 5 the practical measurements are explained and results are shown. In Chapter 6, a demonstration of the model will be given and the influence of the board characteristics on the sound absorption will be shown. In Chapter 7 the optimisation study will be performed and the influence on other WWCB properties will be described. In Chapter 8 the results will be discussed, conclusions will be drawn and recommendations for further research will be provided.

1.5 STUDIES RELATED TO WWCB AT THE EINDHOVEN UNIVERSITY OF TECHNOLOGY

This study is part of a project funded by STW, which is a foundation that realizes a transfer of knowledge between technical science and its users. They are doing this by funding research projects and bringing together researchers and companies to form a user committee. A WWCB research has been set up, which is a PhD-study performed by Guillaume Doudart de la Grée in combination with different companies, like Knauf Insulation, Eltomation, van Gansewinkel Minerals and Enci. His research is about the characteristics and the potentials of the WWCB and the main focus point is to make the WWCBs more sustainable by, for example, making use of a more sustainable binder. Part of this study was the graduation project of Veronica Caprai (Caprai, 2015). Next to this and also part of this STW-project, is the graduation project performed by Marco de Groot (de Groot, 2016) about the thermal insulation of the WWCB.

2. WOOD WOOL CEMENT BOARDS (WWCB)

2.1 INTRODUCTION INTO WWCB

A wood wool cement board generally consists of spruce wood wool mixed with Portland Cement (PC) and limestone powder. The boards have a high porosity (+/- 80%) and a relatively low density (measured range 350 to 550 kg/m^3).

2.2 PRODUCTION PROCESS

In order to understand the composition and properties of the WWCB, first the production process is investigated. For the WWCB, forest trees such as spine, poplar and eucalyptus (mostly soft wood species) with a stem diameter between 16-25 cm are harvested at 30-50 cm above ground level and the first 2 m of the trees are used for the production of WWCB (van Elten, 2006). The branches and bark of the trees are removed on site. After cutting, the wood logs are transported to the WWCB factory and stored on site for 3-6 months depending on the season (summer or winter). The tree sap, mainly consisting of sugars, is leached out.

WWCB is produced following the flow chart as presented in Figure 2.1. First the outside stored wood logs are cut into blocks of 50 cm in length (+/- 2%) so that they can be screened for metal parts and then cut into 25 cm pieces and shredded into wood wool. The final dimensions of the wood wool are therefore max. 25 cm in length, 1-4 mm in width and 0.1-0.5 mm in thickness. Depending on the aesthetic requirements super fine (≤ 1 mm in width), fine (+/- 1-3 mm in width), relatively thick (≥ 3 mm in width) wood wool is produced. In this study the influence on the sound absorption for the 1.0, 1.5 and 2.0 mm will be investigated.

The wood wool is then dipped in a solution to accelerate the compatibility between the wood wool and cement paste and is afterwards pressed to decrease the water content. The wet wood wool with 50-65% moisture content, together with cement power, is fed into a continuous mixer. The irregular flow of wet wood wool is continuously controlled by an electronic device for a continuous flow of cement. This process is called the mineralization of the wood wool.

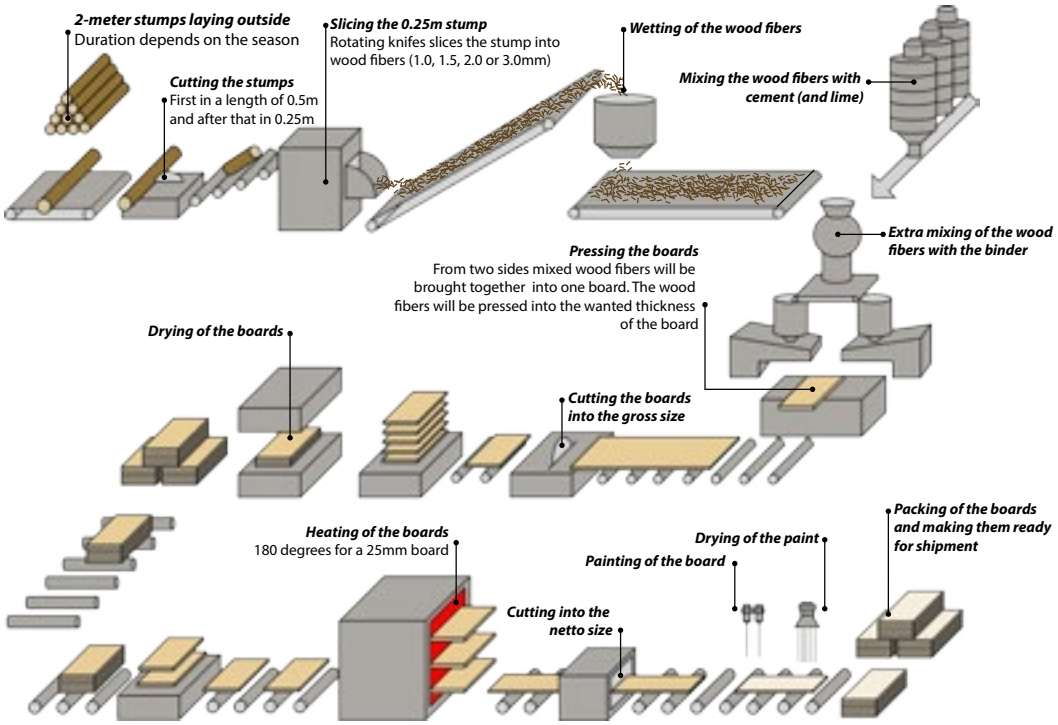

Figure 2.1: *Schematically overview of the production process of the WWCB.*

The mixture is then transported to the so-called double distribution machine. This machine spreads two different layers of a continuous mat of wood wool cement into the molds. After having passed a hydraulic pre-press roll (with a small force, enough to press the plate together), the molds are separated by a circular saw and moved to the hydraulic stacking press. This machine stacks the molds with fresh material under pressure (the mold height is used as a reference pressure). As soon as the stack is full, the stack is moved out and stored under pressure (e.g. by a concrete block of 1500 kg for 24 h). After the setting of cement, the boards are taken from the molds for further curing, while the molds can be cleaned and oiled for re-use.

2.3 WWCB PROPERTIES

The production process and recipe results in WWCBs with specific properties. The thermal conductivity, fire resistance, resistance to bio-degradation, strength and the final colour will be discussed in this paragraph. The sound absorption properties will be described in Chapter 3.

2.3.1 Thermal conductivity

The total open porosity of the board is around 80%. The high porosity in combination with the use of low density wood wool and low dosage of cement results in a low thermal conductivity of +/- 0.08 W/mK for boards with a thickness ranging from 15-30 mm (Doudart de la Grée et al., 2014).

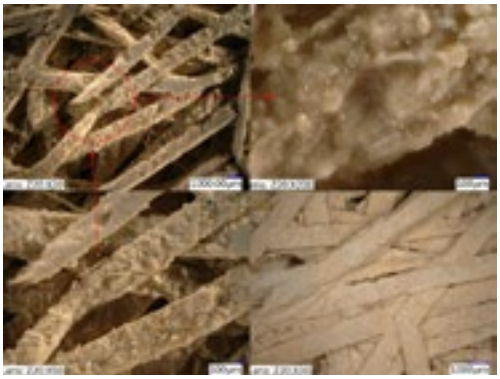

Figure 2.2: *Visualization of the mineralization of the wood-wool by cement using a Keyence VHX 5000 microscope (Caprai, 2015).*

2.3.2 Fire and bio-degradation resistance

Due to the mineralisation of the wood wool by the applied binder, visualised in Figure 2.2, the board possess high resistance to bio-degradation (Pereira et al., 2006) and fire (Aro, 2008). Normally wood ignites before reaching 300 °C, but by applying the cement and limestone binder covering the wood wool, ignition can be delayed and therefore, the product can meet the stated requirements in EN 13501-1 for a low combustible material (category B2).

2.3.3 Strength

The measured bending strengths for the WWCB are in the range of 1.4-4.25 MPa (De Groot, 2016), with average values of 3.25 MPa (1.0 mm strand width), 2.1 MPa (1.5 mm strand width) and 2.0 MPa (2.0 mm strand width).

2.3.4 Colour

At the final step in the production process the boards can be painted in any desired colour. Since grey cement can never be completely invisible, white cement is often used (Doudart de la Grée et al., 2014). The WWCBs used in this study are not painted and therefore have a natural appearance.

2.4 APPLICATION OF THE WWCB

Due to the before mentioned board properties, high durability and low maintenance necessity, the WWCB can be used in- and outdoors. It is mainly used as a ceiling covering material, but can be also be used as wall elements. Currently, the WWCB is mainly applied in utility buildings, e.g. parking lots, sport halls, offices, schools, and shopping malls, or as a ceiling material for balconies in residential buildings.

The boards, widely applied since 1920, can still be labelled as old-fashioned and are therefore not very popular by designers or interior architects. Due to its practical usage, a company in Sweden, called Baux, decided to re-design the WWCB and to make them more interesting as a style-element. Examples are given in Figure 2.3.

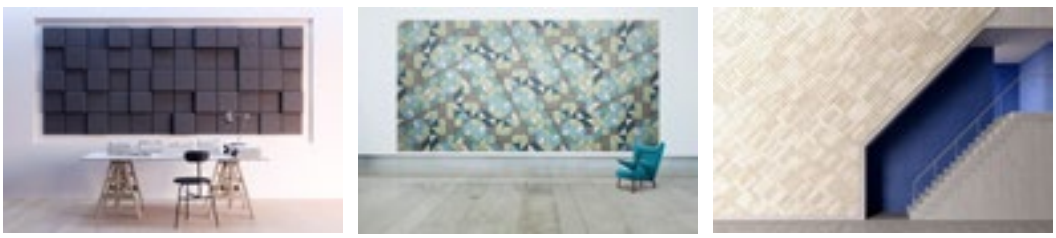

Figure 2.3: *Projects by Baux (Baux, 2016).*

3. SOUND ABSORPTION OF THE WWCB

3.1 INTRODUCTION

In this chapter a brief introduction is given on the sound absorption of the WWCB. Due to the high porosity and the complex internal pore structure of the WWCB, sound waves can relatively easy be absorbed. When an incident sound wave reaches the board, part of the energy is directly reflected and part is transmitted into the WWCB. The energy transmitted by the boundary layer is then either absorbed due to viscous and thermal effects or is reflected against the solid wall and will leave the WWCB again, as illustrated in Figure 3.1.

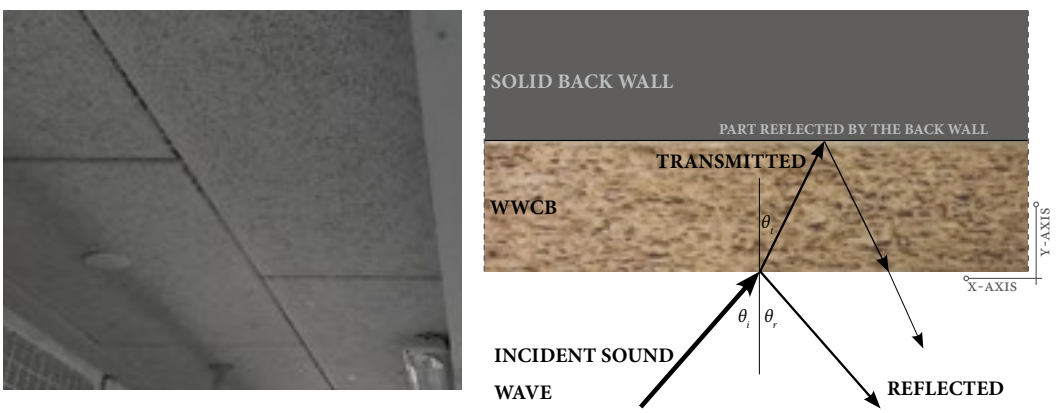

Figure 3.1: *Simplified representation of the sound absorption of the WWCB.*

The WWCB can be described as a porous sound absorbing material, which means that the WWCB is able to reduce the acoustic energy of the incoming sound waves (Seddeq, 2009). Compared to the case of free air, the velocity of the wave first changes because of reduced volume of air inside the WWCB. And after that it changes because of the irregularity in the shape and volumes of the pores. When the sound waves travel through the network of interconnected pores, energy is dissipated due to viscous and thermal effects (Cox & D'Antonio, 2009).

The sound absorption of a material can be expressed by the sound absorption coefficient (α) which is a dimensionless value between 0 and 1 and is dependent both on frequency and angle of incidence. This random incidence sound absorption coefficient is expressed by the average absorption of the incident sound waves from different directions with indication of the frequency.

The practical sound absorption coefficient (α_p) is the average value over the 125-4000 Hz octave bands following:

$$\alpha_p = \frac{\alpha_{125\,Hz} + \alpha_{250\,Hz} + \alpha_{500\,Hz} + \alpha_{1000\,Hz} + \alpha_{2000\,Hz} + \alpha_{4000\,Hz}}{6} \quad [3.1]$$

Where α_p is the practical sound absorption coefficient [-] and $\alpha_{frequency}$ is the sound absorption for that specific octave band [-].

Weighted sound absorption (α_w)

The weighted sound absorption (α_w) is the single number frequency independent value which equals the value of the reference curve at 500 Hz after shifting it as specified in ISO 11654 and is divided into the classes given in Figure 3.2.

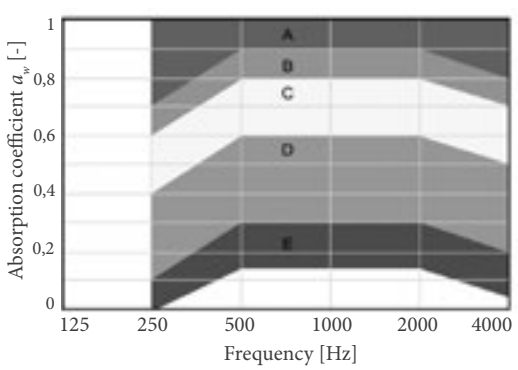

Figure 3.2: *Different classes for the α_w (according to ISO 11654).*

Noise Reduction Coefficient (NRC)

Instead of the α_w, the Noise Reduction Coefficient (NRC) is also often mentioned in product sheets and can be used to compare the sound absorption of materials. This is the average sound absorption over the octave bands 250 - 2000 Hz and following ASTM-C423 this value is rounded up to 0.05.

$$NRC = \frac{\alpha_{250\,Hz} + \alpha_{500\,Hz} + \alpha_{1000\,Hz} + \alpha_{2000\,Hz}}{4} \quad [3.2]$$

Where *NRC* is the Noise Reduction Coefficient [-].

The NRC calculation is based on the results of the reverberation chamber method, the classification standard is listed in Table 3.1.

Table 3.1 *NRC-range for the different sound absorption levels.*

Sound absorption level			
1 - Excellent	2 - Good	3 - Medium	4 - Poor
NRC ≥ 0.80	0.80 > NRC ≥ 0.60	0.60 > NRC ≥ 0.40	0.40 > NRC ≥ 0.20

Sound Absorption Average (SAA)

Also mentioned in ASTM-C423 is the Sound Absorption Average (SAA), which is the average value over the 1/3 octave bands in the frequency range 200 to 2500 Hz.

$$SAA = \frac{\begin{array}{r}\alpha_{200\,Hz} + \alpha_{250\,Hz} + \alpha_{315\,Hz} + \alpha_{400\,Hz} + \\ \alpha_{500\,Hz} + \alpha_{630\,Hz} + \alpha_{800\,Hz} + \alpha_{1000\,Hz} + \\ \alpha_{1250\,Hz} + \alpha_{1600\,Hz} + \alpha_{2000\,Hz} + \alpha_{2500\,Hz}\end{array}}{12} \quad [3.3]$$

Where *SAA* is the Sound Absorption Average [-] and $\alpha_{frequency}$ is the sound absorption for that specific 1/3 octave band [-].

In contrast to the NRC, the SAA is rounded up to 0.01, which is of more interest for the optimization study. It needs to be noted that the used frequency range for the NRC and SAA is limited compared to the α_w. Especially the third octave bands around the 4000 Hz are not used in these values, which is also of importance for understanding of speech, according to (Kuzniarz, 1973).

3.2 SOUND ABSORPTION MEASUREMENTS

The techniques in this study to measure the sound absorption use a reverberation chamber and in an impedance tube. The first one measures the sound absorption coefficient of random incidence sound waves (diffuse field) on a big surface (10-12 m^2). The impedance tube measures the sound absorption of a standing wave on a small sample (in this study samples with a diameter of 40 mm). In the reverberation chamber, the sound absorption values are determined according to Sabine's equation and it is assumed the sound field in the chamber is completely diffuse and the total absorption is a simple sum of the absorption areas of the individual surfaces (Jeong, 2013). A consequence of this is that absorption coefficient sometimes exceed 1.

The random incidences of sound waves are close to the indoor practical conditions and therefore,

this method is superior to other methods in case just the sound absorption in practice needs to be known. However, the working space is much larger than the impedance tube facility, requiring a high amount of material and important acoustic properties of the material, like the acoustical impedance are missing. Therefore for studying the sound absorption of a specific material and product optimization and laboratory measurements, the impedance tube is more suitable. Besides the smaller sample size, the measurements are better controlled in the impedance tube. Hence, the impedance tube will be used in this study. Some measurements will be done in the reverberation chamber to validate the diffuse incidence values computed based on the impedance model.

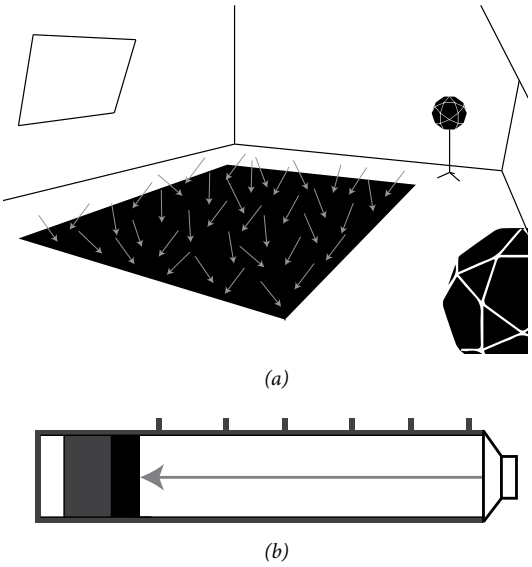

Figure 3.3: *Different incidences of sound waves (a) diffuse (reverberation room) (b) standing waves (impedance tube).*

3.3 SOUND ABSORPTION OF POROUS MATERIALS

As described in the Introduction section, the sound absorption of the WWCB in the higher frequencies (1000-4000 Hz) is relatively good and for the low- and middle frequencies (125-1000 Hz) relatively poor. In general, porous absorbers, such as the WWCB, are less efficient as low frequency sound absorbers due to the long wave length of low frequencies compared to the relatively small thickness of the board. The wavelength for the higher frequencies is relatively short in comparison with the wavelength for the low frequencies as provided in Table 3.2 according to equation 3.6 and 3.7.

$$\lambda = \frac{c}{f} \qquad [3.4]$$

where λ is the wavelength in [m] and f is the frequency in [Hz] and c is the speed of sound in air in [m/s].

$$c = 331 + 0.6T \qquad [3.5]$$

where T is the temperature in [°C]

Table 3.2: *Wavelengths for different octave center frequency bands (for T = 20 °C).*

Frequency [Hz]	*125*	*250*	*500*	*1000*	*2000*	*4000*
Wavelength [m]	2.744	1.372	0.686	0.343	0.172	0.086

In order to be absorbed, the sound wave needs to be 'seen' by the porous material. As a rule of thumb the thickness of the porous material needs to be at least 15% of a wavelength to allow a significant sound absorption and must be 25% of a wavelength to be able to absorb all incident sound. The

thickness of the investigated WWCBs (ranging from 15 to 50 mm) is able to absorb the high frequency sound waves better than the low frequency ones because it meets these requirements. Hence, the thickness of the WWCB plays an important role in the sound absorption of the lower frequency octave bands and makes them inefficient and not particularly useful at low frequencies (Cox & D'Antonio, 2009).

Besides the thickness of the board, the efficiency of sound absorption is depending on the placement against a wall or a ceiling. The particle velocity close to these boundaries is usually small and the sound absorption is lower when placing material there in comparison to a place where the particle velocity is higher. The parts of the WWCB furthest from the backing surface are often most effective. Therefore, either thick WWCBs should be applied or they should be placed on a considerable distance of the wall to reach a point where the particle velocity is significant (Cox & D'Antonio, 2009). Therefore, in this study the influence and optimum thickness of the air-cavity for a WWCB will also be tested and evaluated.

When sound propagates in small spaces, such as interconnected pores in the WWCB, energy is lost. This is primarily due to the viscous effects of the boundary layer. Air is a viscous fluid, and consequently sound energy is dissipated via friction within the porous walls. Besides viscous effects, there will be losses due to the thermal conduction. To be an effective porous absorber, there must be interconnected air paths through the surface, thus an open pore structure is preferable (Cox & D'Antonio, 2009). Not only the presence of open pore structure is important, also the shape of the internal pores is important. A simple internal pore structure, consisting of straight cylindrical pores, will lead to a lower sound absorption compared to the same material that has a more complex pore structure, due to an increase of the viscous and thermal effects. In this way the porous material can be made 'acoustically thicker' (Cox & D'Antonio, 2009).This aspect is described by the pore shape factors and the tortuosity, which will be described in the next chapter in more detail.

Another way to make a porous absorber absorb low frequency sound more effectively is to make use of resonant structures or active absorbers. Since in this study the focus will be on the WWCB itself and optimizing the sound absorption of this material, this aspect is out of scope.

3.4 SOUND ABSORPTION OF THE EXISTING WWCB

Currently, the WWCB has a good sound absorption coefficient for a frequency of 1000 Hz and higher, as presented earlier in Figure 1.2 and listed in Table 3.3. Other relevant absorption coefficients are taken from product sheets, based on reverberation room measurements. These values show for example indeed an increase of the sound absorption for the lower frequencies if the thickness is increased, as presented in Table 3.3. Currently, no knowledge is available about the influence of the strand width, the thickness of the air-cavity and density or the porosity regarding the sound absorption of the WWCB. It is also not known what the effects on the sound absorption is of a multi-layer systems.

Table 3.3: *Absorption coefficients for the WWCB with 25, 35 and 50 mm thickness according to ISO 354:2003 (Doudart de la Grée et al. 2014).*

	Frequency [Hz]							
Thickness of the WWCB [mm]	**125**	**250**	**500**	**1000**	**2000**	**4000**	**NRC**	α_w
25	0.06	0.13	0.27	0.63	0.91	0.66	0.50	0.35
35	0.09	0.16	0.35	0.81	0.77	0.76	0.50	0.40
50	0.15	0.33	0.62	0.87	0.75	0.85	0.65	0.60

4. MODELLING THE SOUND ABSORPTION OF WWCB

4.1 INTRODUCTION

In this study it will be evaluated if an impedance model exists that can be used to predict the sound absorption of the WWCB. By making use of a simulation model, measuring time can be saved and a quick insight will be provided in what happens with the sound absorbing properties in case bulk properties of the WWCB will be changed. In this chapter the focus will be on describing the different impedance models, their input parameters and equations and finally the used models will be compared based on a validation study to determine their suitability.

Based on different input parameters, impedance models are able to predict the sound absorption of a porous material. Which model, specified by a range of input parameters, will be suited for a specific material depends on the material morphology. The models can be divided in: (1) rigid frame models and (2) elastic frame models. The elastic frame models are used for materials that are able to support elastic wave propagation or, for example, a WWCB is mounted as a free element at a ceiling and where it has elastic frames that can support wave propagation. The rigid frame models are used when the material is placed directly to a solid wall or placed within a rigid frame without supporting wave propagation (Cox & D'Antonio, 2009). To verify from what frequency the WWCB can described as motionless, the phase decoupling frequency should be calculated (Zwikker et al., 1949). This is the frequency for which the inertial effects in the frame equals in magnitude the viscous effects in the fluid phase. For frequencies larger than this decoupling frequency the solid and the fluid media of the WWCB can be considered as decoupled and the material skeleton can be considered as motionless.

$$f_d = \frac{\sigma \phi^2}{2\pi \rho_1} \qquad [4.1]$$

where f_d is the phase decoupling frequency [Hz], σ is the flow resistivity [Ns/m^4], ϕ is the porosity [-] and ρ_1 is the mass density of the WWCB [kg/m^3].

Based on the measurements and the results presented in Chapter 5 and 6 the maximum decoupling frequency is 1-2 Hz for the WWCB and therefore the boards can be assumed to behave as a rigid-frame.

4.2 IMPEDANCE MODELS

An overview of the different impedance models is given in Figure 4.2. The different material morphologies are provided in combination with the propagation models that belong to it. Also the different input parameters are given. A material with a simple internal structure, like straight cylindrical pores, requires a more simplified model (less input parameters) in comparison to a material with non uniform cross sections.

The first studies regarding propagation of sound in circular tubes with an arbitrary diameter were conducted by Kirchoff (Kirchhoff, 1868) and Rayleigh (Lord Rayleigh, 1945). These theories account both for the viscous and thermal conductivity. Where this theory is unnecessarily complicated for many applications and is very difficult to solve in case of non-circular cross-section (Champoux et al., 1991), which is the case for the WWCB, a simplified model has been worked out by Zwikker and Kosten (Zwikker et al., 1949).

4.2.1 Zwikker and Kosten model

Zwikker and Kosten constructed a model for sound propagation in materials containing cylindrical pores. They restricted Kirchhoff's theory to a more narrow frequency range and a more narrow radius range (Leclaire, 2012). The effects of viscosity and thermal conductivity are treated separately and summarized in terms of complex density and complex bulk modulus as mentioned in Table 4.2. These parameters are complex because of the dissipative viscous effects introduced by the presence of the pores and due to the heat exchange between the rigid frame and air in the pores. From the work of Zwikker and Kosten the wave equation for the acoustic pressure wave inside a tube is:

$$\Delta p + \omega^2 \frac{\rho_{eq}}{K_{eq}} p = 0 \qquad [4.2]$$

where p is the acoustic pressure [Pa], ω the angular frequency [1/s], ρ_{eq} is the effective density [kg/m^3] and K_{eq} is the effective bulk modulus [kg/m·s^2].

This equation is analogous to the Helmholtz equation that is used to describe the sound propagation in free air (without any dissipation). However, for porous media, the effective density and effective bulk modulus are complex functions of the frequency and material morphology.

In 1956, Biot published a refined model of the acoustic wave propagation in fluid saturated porous media (Biot, 1956). In this model, the medium is poro-elastic and viscous frictions between the solid and the fluid are included. Only since 1970 this theory became popular and it formed the base for propagation models used nowadays. The following described propagation models are developed and based on this theory of which some of them are simple and empirical.

4.2.2 Delany-Bazley-Miki model

In 1970, Delany and Bazley proposed an empirical model describing the sound wave propagation in fibrous materials (Delany et al., 1970). From a large number of measurements on fibrous materials with porosities close to 1.00, Delany and Bazley have proposed empirical expressions for the values of the complex wave number and characteristic impedance. This model is simple and has been very popular in engineering acoustics. Miki extended the work of Delany and Bazley and proposed several empirical expressions for the wave number and the characteristic impedance for several materials and for several frequency ranges (Miki, 1990). This was done because in case of multiple layers, he noticed that the real part of the surface impedance sometimes becomes negative at low frequencies using the Delany and Bazley equations, which is physically impossible.

The Miki model only requires one parameter, the flow resistivity (σ), to calculate the sound absorption coefficients. The restrictions for this model are:

- Porosity (ϕ) needs to be close to 1;
- $0.01 < f/\sigma < 1.00$;
- $2{,}000 < \sigma < 80{,}000$ Ns/m^4 .

4.2.3 Attenborough model

This model is developed to predict the acoustical characteristics of rigid fibrous absorbents and granular materials. By comparing theoretical predictions with measurements, it shows that the theory can give reasonable predictions for resin-bonded fibrous materials, e.g. lead shot, soils, and sands (Attenborough, 1983). These materials are not showing similarities with the WWCB, although the Attenborough model was used in a study (Hucheng & Martin, 2014) on the material wood-concrete, named Durisol (Martin et al., 2008). It is therefore evaluated as well in this study. In this model it is assumed that all the pores are identical in shape, but are oriented differently. The Attenborough model requires four parameters; the porosity, flow resistivity, tortuosity and a pore shape factor. In the pore shape factor, the dynamic and static shape factor are translated to one dimensionless parameter, related to the thickness of the viscous boundary layer at the pore wall. With this model Attenborough has shown the importance of the tortuosity and of the parameters related to the complexity of the pore geometry at high frequencies.

4.2.4 Johnson-Champoux-Allard (JCA) model

The Johnson-Champoux-Allard model is based on the work by Johnson, Koplik and Dashen (*Johnson et al. 1987*) to describe viscous effects inside the porous material with a motionless skeleton having arbitrary pore shapes. They introduced the concepts of dynamic tortuosity and dynamic permeability and studied the low and high frequency behaviours of these functions proposing a function linking these two behaviours. In this process, they defined a physical macroscopical parameter (Λ), named viscous characteristic length. This parameter is related to the pore micro-geometry. Following the work by Johnson et al., Champoux and Allard (Champoux et al., 1991) studied the thermal exchanges between the different fluid layers in the boundary layers in the vicinity of the pore walls for air saturated materials. They introduced the thermal characteristic

length (Λ'). The model incorporating both the viscous and thermal characteristic lengths is one of the most popular in engineering acoustics nowadays. It is referred to the Johnson-Champoux-Allard (JCA) model and involves 5 physical parameters: the porosity, flow resistivity, tortuosity, viscous characteristic length and thermal characteristic length.

4.2.5 Johnson-Champoux-Allard-Lafarge (JCAL) model

Due to problems in the low frequency range (Matelys, 2016), Lafarge (Lafarge et al., 1997) brought a further refinement to the JCA-model by defining a new parameter, the thermal permeability (k'_0). This parameter is used to model the thermal exchanges between the solid and the fluid at the low frequencies. Therefore, this model involves six parameters in total.

4.2.6 Summary

The WWCB will be considered as an equivalent fluid in the rigid frame approximation. As will be described in the next chapter, the porosity of the WWCB is not close to 1 and the flow resistivity is relatively low. Moreover due to the fact the WWCB does not contain cylindrical pores it is not expected that the Miki model will work. The WWCB has a more complex internal pore structure and where the different models derived from Biot's theory (Attenborough, Johson et al., Johnson-Champoux-Allard and Lafarge et al.) are taking into account the tortuosity and pore shapes on a more detailed level, it is expected that the predicted sound absorption for the WWCB is more in line with the measured values in the impedance tube.

Table 4.1: *Overview of the different parameters.*

	Parameter	Symbol	Unit	Description
Input parameters	Flow resistivity	σ	Ns/m^4	Is the resistance that an airflow meets through the structure.
	Porosity	ϕ	-	Ratio of the total open pore volume to the total volume of the porous material.
	Tortuosity	α_∞	-	Ratio of the way a wave has to travel through a material compared to the thickness of the material.
	Viscous characteristic length	Λ	m	Describes the viscous effects inside the board.
	Thermal characteristic length	Λ'	m	Describes the thermal effects.
	Pore shape factor	s_b	-	Describes the influence of the shape of the pore shape on the viscous and thermal effects
	Static thermal permeability	k'_0	m^2	Describes the thermal exchanges between WWCB and saturating fluid at low frequencies
Acoustical properties	Effective density	$\rho_e(\omega)$	kg/m^3	The term effective is used to signify that this is the density experienced by the acoustic waves rather than the more normal definition of mass divided by volume.
	Bulk modulus	$K_e(\omega)$	$kg/m{\cdot}s^2$	Ratio of the pressure applied to a material to the resultant fractional change in the volume it undergoes.
	Propagation wave number	k_c	m^{-1}	Number of radians the wave changes in one meter / the amount of phase change of the waveform per meter.
	Characteristic impedance	Z_c	$Pa{\cdot}s/m$	Ratio of the resistance of a material to propagate a sound wave. Ratio of pressure to velocity.
	Absorption coefficient	α	-	Ratio of the sound energy absorbed by the material divided by the incident sound energy.
	Reflection factor	R	-	The fraction of the sound wave that is reflected from the porous material
	Normal surface impedance	Z_s	$Pa{\cdot}s/m$	Resistance of a surface to propagate a sound wave

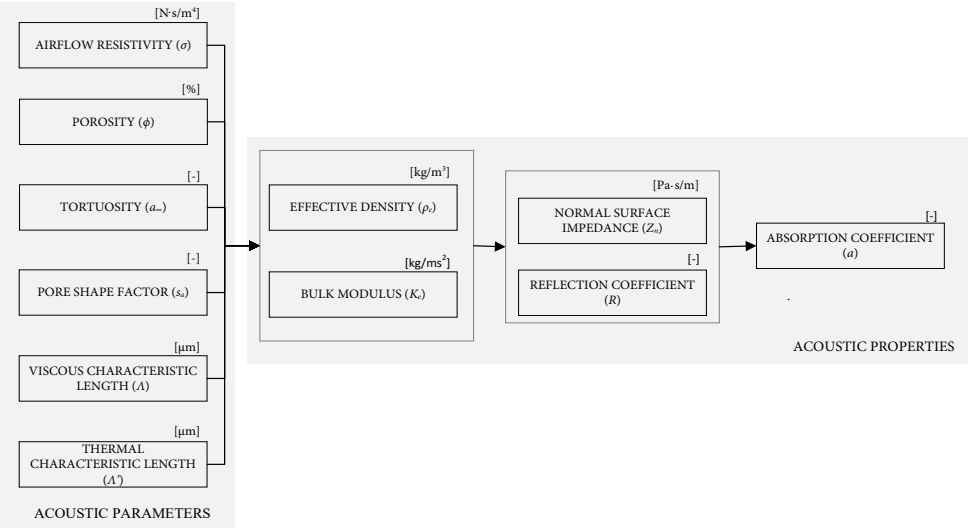

Figure 4.1: *Simplified overview of determining the sound absorption by propagation models.*

4.3 FROM INPUT PARAMETERS TO THE NORMAL INCIDENCE SOUND ABSORPTION

Which input parameters need to be taken into account, depends on the chosen propagation model. The acoustical properties, the effective density and bulk modulus describe the overall properties related to the input parameters. They describe the interaction between a sound wave and the acoustic absorber but are independent of the thickness of the material and the total surface area. The propagation models and the equations used in this study are given in Table 4.2.

$$Z_c = \sqrt{K_e(\omega) \cdot \rho_e(\omega)} \qquad k_c = \omega \sqrt{\frac{\rho_e(\omega)}{K_e(\omega)}} \qquad [4.3] \text{ \& } [4.4]$$

$$Z_s = -iZ_c \cot(k_c \cdot d) \qquad [4.5]$$

$$Z_n = \frac{Z_s}{Z_0} \qquad [4.6]$$

Where Z_n is the normalized surface impedance [Pa·s/m], i the imaginary number [$\sqrt{-1}$] and d the thickness of the sample [m] and Z_0 the characteristic impedance of air [Pa·s/m].

Finally, the acoustical parameters are used to describe the acoustical properties of the WWCB. This are the characteristic impedance, surface impedance, reflection coefficient and the absorption coefficient of the porous media.

$$R = \frac{Z_n - 1}{Z_n + 1} \qquad [4.7]$$

And the absorption coefficient α can be determined following equation 4.8.

$$\alpha = 1 - |R|^2 \qquad [4.8]$$

where α is the sound absorption coefficient [-]

Figure 4.2: *Schematic overview of the propagation models and its input parameters for different material morphologies.*

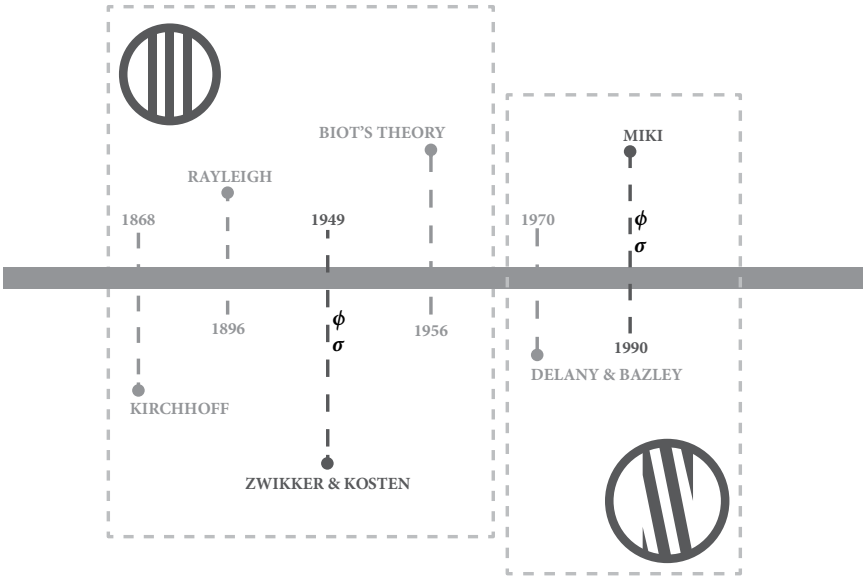

Table 4.2: *Equations for the different propagation models*

Models	Characteristic impedance	Characteristic wave number
Delany-Bazley-Miki	$Z_c = \rho_0 c_0 \left(1 + 5.50\left(10^3 \frac{f}{\sigma}\right)^{-0.632} - i8.43\left(10^3 \frac{f}{\sigma}\right)^{-0.632}\right)$	$k_c = \frac{\omega}{c_0}\left(1 + 7.81\left(10^3 \frac{f}{\sigma}\right)^{-0.618} - i11.41\left(10^3 \frac{f}{\sigma}\right)^{-0.618}\right)$
Miki (1990)		
	Effective density	**Effective bulk modulus**
Zwikker and Kosten	$\rho_e(\omega) = \frac{\rho_0}{\phi}\left(1 + \frac{2}{\lambda\sqrt{-i}} \cdot \frac{J_1(\lambda\sqrt{-i})}{J_0(\lambda\sqrt{-i})}\right)^{-1}$ $\lambda = \sqrt{\frac{8\omega k_s \rho_0}{\phi\sigma}}$	$K_e(\omega) = \frac{\gamma P_0}{\phi}\left(1 + \frac{2(\gamma-1)}{\sqrt{N_{pr}}\lambda\sqrt{-i}} \cdot \frac{J_1(\sqrt{N_{pr}}\lambda\sqrt{-i})}{J_0(\sqrt{N_{pr}}\lambda\sqrt{-i})}\right)^{-1}$ $\lambda = \sqrt{\frac{8\omega k_s \rho_0}{\phi\sigma}}$
Zwikker and Kosten (1949) & J.F. Allard (1993)		
Attenborough	$\rho_e(\omega) = \frac{\alpha_\infty \rho_0}{\phi}\left(1 - \frac{2}{\lambda\sqrt{-i}} \cdot \frac{J_1(\lambda\sqrt{-i})}{J_0(\lambda\sqrt{-i})}\right)^{-1}$ $\lambda = \frac{1}{2s_a}\sqrt{\frac{8\omega\rho_0\alpha_\infty}{\phi\sigma}}$	$K_e(\omega) = \frac{\gamma P_0}{\phi}\left(\gamma - \frac{2(\gamma-1)}{\sqrt{N_{pr}}\lambda\sqrt{-i}} \cdot \frac{J_1(\lambda\sqrt{-i})}{J_0(\lambda\sqrt{-i})}\right)^{-1}$ $\lambda = \frac{1}{2s_a}\sqrt{\frac{8\omega\rho_0\alpha_\infty}{\phi\sigma}}$
Champoux Stinson (1991)		
Johnson-Champoux-Allard (JCA)	$\rho_e(\omega) = \frac{\alpha_\infty \rho_0}{\phi}\left(1 + \frac{\sigma\phi}{i\omega\rho_0\alpha_\infty}\sqrt{1 + \frac{4i\alpha_\infty^2\eta\rho_0\omega}{\sigma^2\Lambda'^2\phi^2}}\right)$	$K_e(\omega) = \frac{\frac{\gamma P_0}{\phi}}{\gamma - (\gamma-1)/\left(1 + \frac{8\eta}{i\Lambda'^2 N_{pr}\omega\rho_0}\sqrt{1 + \frac{i\rho_0\omega N_{pr}\Lambda'^2}{16\eta}}\right)}$
Johnson et al. (1987)		*Champoux et al. (1991)*

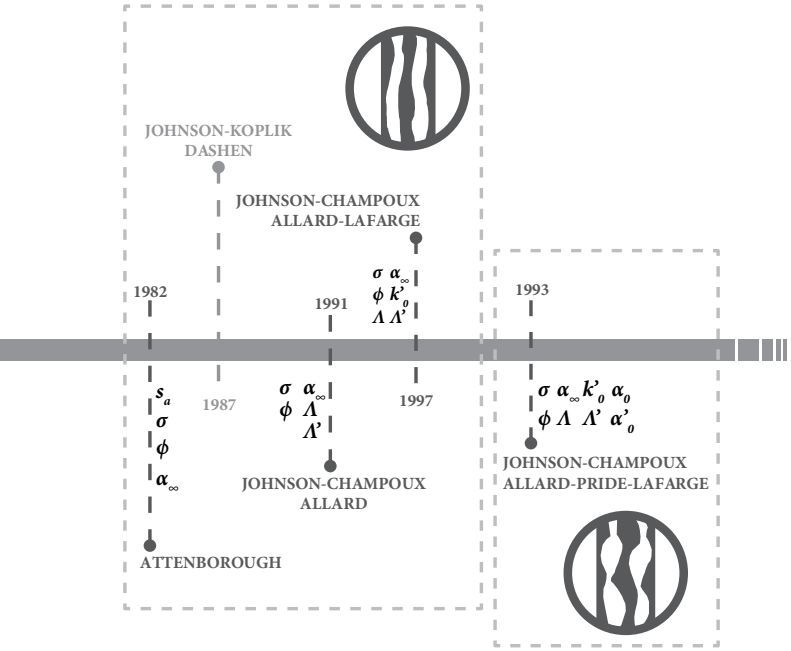

	Effective density	Effective bulk modulus
Johnson-Champoux-Allard-Lafarge (JCAL)	$\rho_e(\omega) = \frac{\alpha_\infty \rho_0}{\phi}\left(1 + \frac{\sigma\phi}{i\omega\rho_0\alpha_\infty}\sqrt{1 + \frac{4i\alpha_\infty^2\eta\rho_0\omega}{\sigma^2\Lambda^2\phi^2}}\right)$	$K_e(\omega) = \frac{\frac{\gamma P_0}{\phi}}{\gamma - (\gamma-1)/\left(1 - i\frac{\phi\eta}{k_0' N_{pr}\omega\rho_0}\sqrt{1 + i\frac{4k_0'^2\rho_0\omega N_{pr}}{\eta\Lambda'^2\phi^2}}\right)}$
	Johnson et al. (1987)	*Lafarge et al. (1997)*

Parameters	Symbol		Unit
	f	*Frequency*	*[Hz]*
	ϕ	*Porosity*	*[-]*
	Z_c	*Characteristic impedance*	*[Pa·s/m]*
	k_c	*Characteristic wavenumber*	*[1/m]*
	$\rho_e(\omega)$	*Effective density*	*[Kg/m³]*
	$K_e(\omega)$	*Effective bulk modulus*	*[Kg/m·s²]*
	ρ_0	*Value in air where ambiguity might otherwise arise*	*[Kg/m³]*
	c_0	*Speed of sound in air*	*[m/s]*
	ω	*Angular frequency*	*[1/s]*
	σ	*Flow resistivity*	*[Ns/m⁴]*
	λ	*Dimensionless parameter*	*[-]*
	k_s	*Structure factor*	
	s_a	*Pore shape factor*	*[-]*
	T	*Ratio between Bessel functions of the first and zero order*	*[-]*
	α_∞	*Tortuosity*	*[-]*
	i	*Imaginary number*	*[-]*
	N_{pr}	*Prandtl number (≈ 0.71)*	*[-]*
	γ	*Ratio of the specific heat capacity (≈1.4)*	*[-]*
	P_0	*Atmospheric pressure (≈101,320)*	*[N/m²]*
	η	*Viscosity of air (≈1.84·10⁻⁵)*	*[Pa·s]*
	Λ	*Viscous characteristic length*	*[m]*
	Λ'	*Thermal characteristic length*	*[m]*
	k_0'	*Static thermal permeability*	*[m²]*

4.4 IMPEDANCE TUBE MEASUREMENTS

Before the previous discussed impedance models will be compared in Section 4.6, an explanation will be given on how the surface impedance was measured. To determine the normal incidence sound absorption coefficient out of the surface impedance under well-defined and controlled conditions, the impedance tube at Echo, the Acoustical Lab at the Eindhoven University of Technology is used.

Inside the impedance tube the standing wave shows modes. To avoid deviations because of these modes and in this way increase the accuracy of the measurement, the impulse responses are measured at six different measurement positions (Beekman, 2012 & Tijsma, 2014).

(a) *(b)*

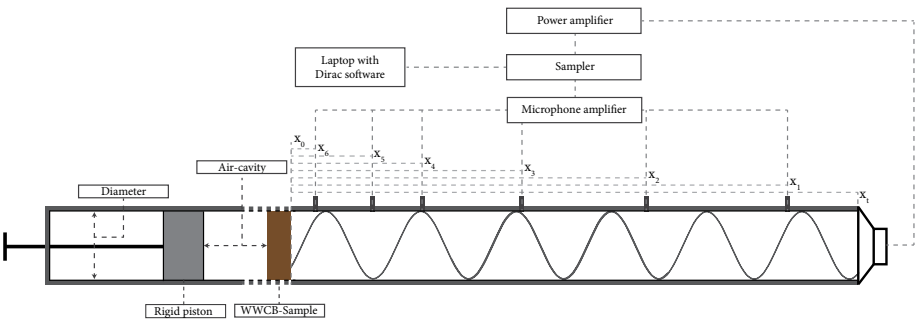

(c)

Figure 4.3: *(a) and (b) are pictures of the used impedance tube and (c) is a schematic overview of the tube.*

The laptop generates a digital signal using the Dirac software. This signal is converted to an analogue signal by the sampler, then amplified and converted by the power amplifier and a plane wave is generated by the speaker. In this way a standing wave is set up within the tube, which is measured at six different locations. The measured sound wave will be amplified by the microphone amplifier and is converted into a digital signal by the sampler. By making use of Dirac, the digital signal is recorded and the impulse responses are extracted and saved.

Table 4.3: *Measurement equipment for the impedance tube*

		Type	Serial number
Impedance tube			
Dirac	Acoustical Engineering	6.0	
Sampler	EMU	0204	YDFM 8740 2350 0194 8B
Power amplifier	Brüel & Kjær	2706	397946
Speaker	Dynaudio	D54 AF	82450
Microphone 1	Endevco	8510B-2	13898
Microphone amplifier 1	Endevco	136	BE79

Finally, the impedance of the sample (diameter 40 mm) alters the reflected wave, and by measuring the resulting standing wave, it is possible to calculate the surface impedance of the sample.

4.4.1 Measurement script

The complete MATLAB-script used for the impedance tube measurements can be found in Appendix B. In this paragraph a short overview will be given of the different steps taken to finally obtain the normal incidence sound absorption of the sample. This work has been done in collaboration with Niels Hoekstra (2016).

Step 1: The microphone positions

The acoustic centres of the microphones need to be filled in into the script, which make it impossible to determine the distances geometrically (Peerlings, 2015). These positions are very sensitive and were, in the old script, determined by measuring the temperature outside the tube and assuming the speed of sound inside the tube. This method seemed not accurate enough, since it was found the temperature fluctuates between in- and outside the tube and also in time, which is important because the microphone needs to be repositioned every time. Therefore, to determine the exact microphone distances, a very small temperature sensor was used in combination with a data logger (Squirrel SQ2020 2F8). The found distances are presented in Table 4.4.

The influence of the different microphone positions on the reflection factors are given in Figure 4.4. In this figure the reflection factor is given for an empty tube, without a sound absorbing material in it, which actually means the value should be one. The fluctuations visible are due to the measurement accuracy of the used impedance tube, which is influenced by the microphone position, mechanical vibrations, temperature and the impedance of the microphones (Peerlings, 2015). It is visible in the figure that the graph, making use of the microphone positions determined by the small temperature sensors are giving the most accurate results.

Table 4.4: *Microphone positions in meter for the different measurement techniques*

Microphone position	**(Tijsma, 2014)**	**Tape-measure**	**Temperature sensor**
1	1.1763	1.188	1.1939
2	0.8405	0.8480	0.8523
3	0.5446	0.5500	0.5521
4	0.3080	0.3100	0.3106
5	0.1892	0.1890	0.1904
6	0.06	0.0596	0.0588

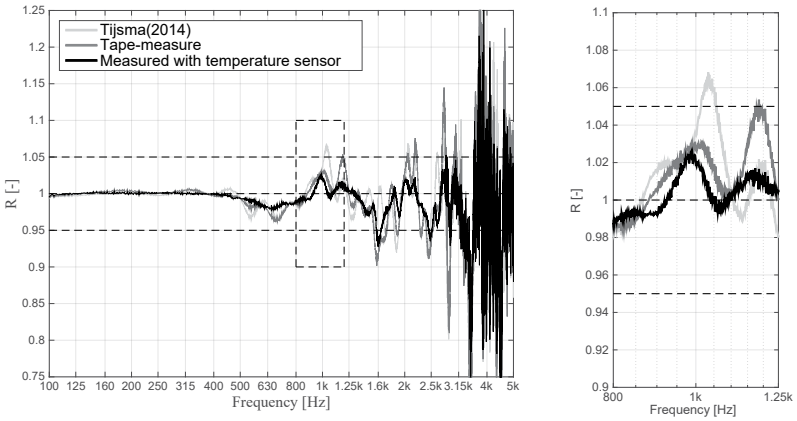

Figure 4.4: *Comparing the different reflection factor curves for the different microphone position techniques.*

Step 2: Determination of the speed of sound

The speed of sound is calculated by analysing the microphone located at the first microphone position, which is 1.1939 m removed from back wall of the tube. An e-sweep of 2.73 seconds in 192000 samples per second is produced by the loudspeaker. In Figure 4.5 the impulse response is shown for the first microphone position in an empty tube. Based on this figure the speed of sound can be determined by making use of equation 4.9.

$$c = \frac{\frac{1}{192000}}{\Delta peak} \cdot 2 \cdot l_{mic.pos1 \rightarrow sample} \qquad [4.9]$$

where: c is the speed of sound in air [m/s], Δpeak is the difference in peaks [Pa], $l_{mic.pos1-sample}$ is the length between microphone position 1 and the sample [m].

Step 3: Calculation of the attenuation constant k' for correcting plane wave attenuation by the impedance tube according to ISO 10534-2.

$$k' = -0.02 \cdot \left(\frac{\sqrt{f}}{c \cdot 0.04} \right) \qquad [4.10]$$

where: k' is the attenuation constant [-], f the frequency [Hz] and c the speed of sound [m/s].

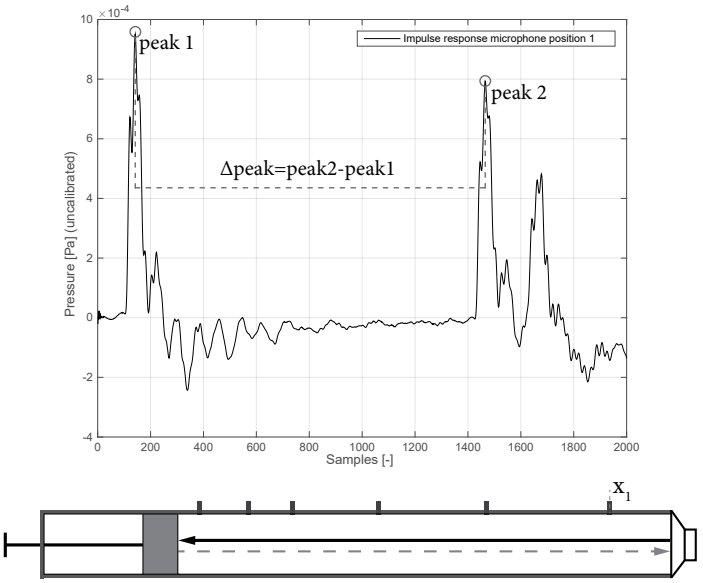

Figure 4.5: *Impulse response for microphone position 1 (sample 0 till 2000) Peak 1 is measured for the incident solid black line and peak 2 is measured for the reflected dashed grey line.*

Step 4: Only the number of samples before the direct sound reaches the back wall is taking into account for the cross correlation of the signals.

Step 5: Impulse responses are measured separately, which may cause a phase difference. To account for this, the difference in sample numbers of the first peak in the impulse response is compared to the expected difference in sample numbers caused by the increased distance from the loudspeaker. The phases are corrected for microphone positions 2 till 6.

Step 6: A Fourier transformation is performed to transform the time-domain of the impulse responses into frequency-domain.

Step 7: The propagation of the wave over the length of the tube is modelled and compared to the wave reflected by the specimen and back wall. Based on this comparison the reflection factor can be determined and finally surface impedance and the normal incidence sound absorption can be determined making use of equations 4.11 and 4.12.

$$Z_n = -\frac{R+1}{R-1} \qquad [4.11]$$

4.4.2 Accuracy of the impedance tube

Theoretically the impedance tube should reflect the complete sound wave if no sample is placed the tube. In Figure 4.6 the reflection coefficient is shown. As it is visible the reflection coefficient is not 1 for the whole frequency range. Till the 2800 Hz the impedance tube is relatively reliable (error maximum 5%). Due to resonances inside the tube peaks and dips are visible. These peaks and dips will also be visible later on in the sound absorption curves for the WWCB. These errors, caused by the tube, will be taken into account by analysing the results.

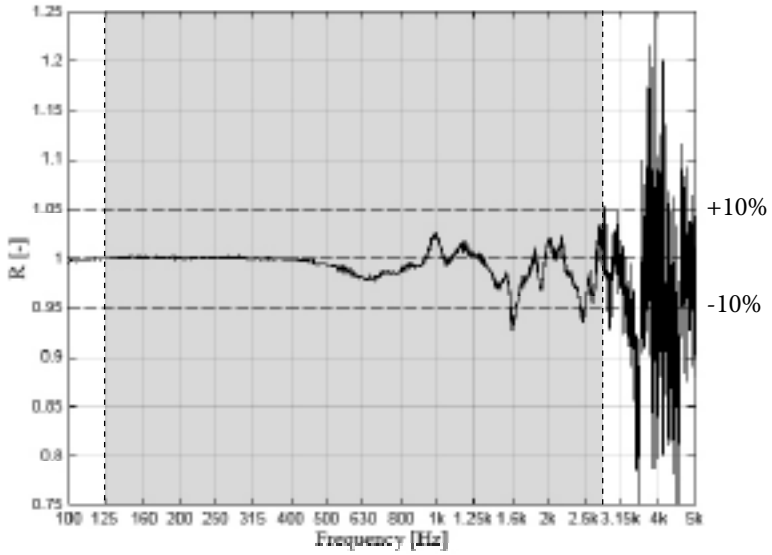

Figure 4.6: *Reflection factor for an empty tube.*

In Figure 4.7 an example is given of a measured normal incidence sound absorption curve for a WWCB-sample in the impedance tube. In this figure the ranges of the different frequency bands are given. It is shown that the sound absorption curve untill the 2800 Hz frequency band is accurate. It is for this reason that the SAA-value, the average value over the 200-2500 Hz 1/3 frequency bands, will be chosen to validate the impedance models. This single number value is chosen above the NRC-value because this value is rounded to 0.01, instead of 0.05 for the NRC-value. With the propagation model the sound absorption above and below this range can be predicted, but it will not be possible to validate these values.

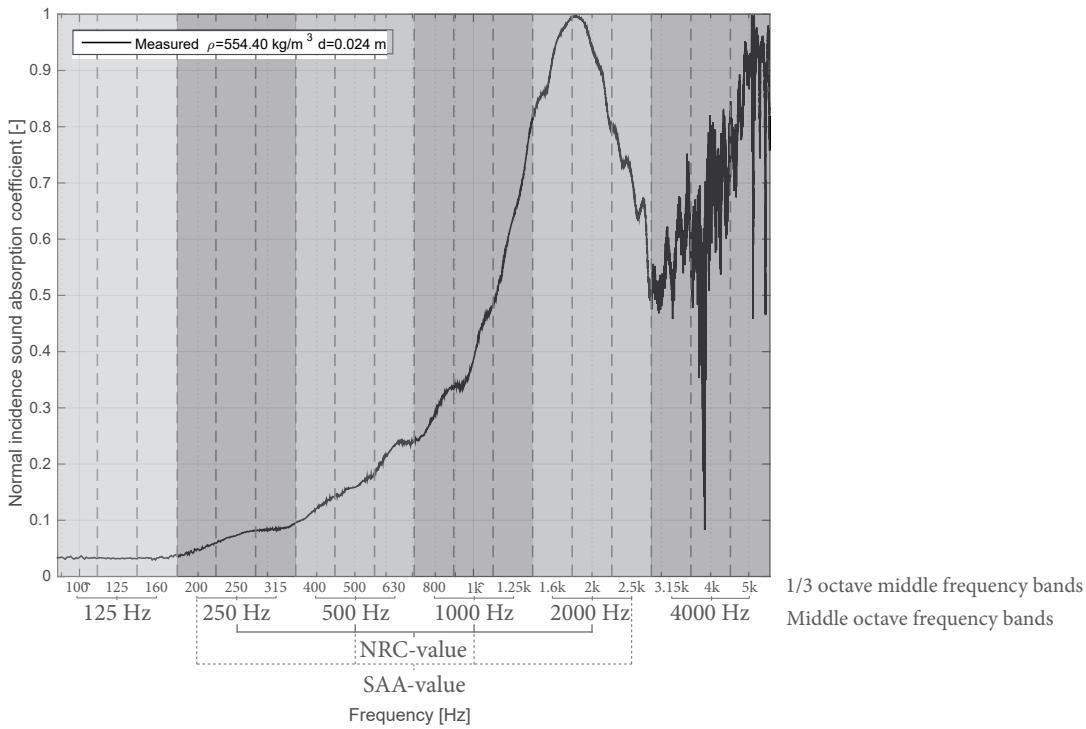

Figure 4.7: *Measured normal incidence sound absorption curve including the different frequency bands.*

4.5 INVERSE CALCULATION METHOD

As will be described in Chapter 5, the open porosity [-] and the flow resistivity [Ns/m^4] are directly measured. Where it is difficult to directly measure the parameters related to the internal pore structure (i.e. the tortuosity) for an inhomogeneous material like the WWCB, these input parameters will be determined by making use of the curve fitting approach, an inverse calculation method. This technique is often used in studies on the sound absorption of porous media (Johnson et al., 1987, Olny et al. 2002, Panneton et al. 2006). Impedance models are able to model the sound absorption curve based on the normal sound absorption coefficient curve measured in the impedance tube, applying the inverse calculation method. When some parameters are unknown, for example the tortuosity or a shape factor, these values can be obtained by making use of the Curve Fitting Toolbox in Matlab (R2014b). In this tool the equations, defined by the impedance model and the initial values need to be filled in together with the lower and upper limit of the specific parameter. These ranges, given in Table 4.3, are based on literature. These ranges are important to assure the obtained values are realistic and physically correct.

Table 4.5: *Input parameters for the curve fitting*

Parameter	Initial value	Lower limit	Upper limit
Tortuosity [-]	2	1	5
Porosity [-]	0.7	0.5	1.0
Shape factor [-]	0.8	0	2
Viscous characteristic length [μm]	150	50	350
Thermal characteristic length [μm]	150	50	350
Static thermal permeability [m^2]	10^{-10}	10^{-10}	10^{-8}

Understanding of these ranges for the different parameters is essential to get reliable results. Finally, it needs to be verified if the results obtained from the curve fitting approach are unique, which means that if the initial value, lower or upper limit is changed the outcome is still the same.

4.6 MODEL COMPARISON

For the model comparison, the following models were evaluated:
- Miki (1 parameter),
- Zwikker and Kosten (3 parameters),
- Attenborough (4 parameters),
- Johnson-Champoux-Allard (JCA) (5 parameters),
- Johnson-Champoux-Allard-Lafarge (JCAL) (6 parameters).

For all these models the unknown parameters are determined by making use of the curve fitting approach, which will be described in more detail in Chapter 5. An overview of the obtained values for the different input parameters for 25 mm thick WWCB (1.0 mm strand width and a density of 448 kg/m^3) is given in Table 4.6.

Table 4.6: *Obtained values for the input parameters.*

	Miki	Zwikker and Kosten	Attenborough	JCA	JCAL
Measured parameter					
Flow resistivity [Ns/m⁴]	4067	4067	4067	4067	4067
Fitted parameters					
Open porosity [-]	-	0.72	0.67	0.62	0.72
Shape factor [-]	-	0.19	0.74	-	-
Tortuosity [-]	-	-	3.61	2.17	2.22
Viscous characteristic length [10^{-6}m]	-	-	-	165.9	151.3
Thermal characteristic length [10^{-6}m]	-	-	-	210.6	196.2
Static thermal permeability [m²]	-	-	-	-	$5.73*10^{-9}$

Due to the material morphology, the Miki and Zwikker and Kosten model are not able to fit the measured values in the impedance tube and even the values obtained for the Zwikker & Kosten model are even unrealistic, which is shown in Figure 4.8 and Table 4.6. Also the real and imaginary part of the normalised surface impedance are not close to the measured values.

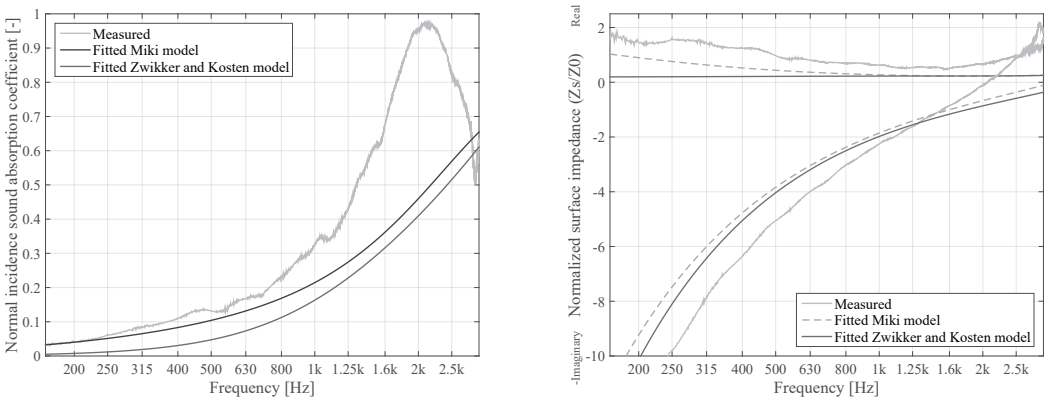

Figure 4.8: *Predicted values by the Miki and Zwikker and Kosten model compared to the measured values for (a) normal incidence sound absorption and (b) real and imaginary normalised surface impedance.*

A more detailed model, taking into account the complex internal pore structure of the WWCB, is therefore expected to give more accurate results. In Figure 4.9 a comparison is shown of the Attenborough, JCA and JCAL-model. The last mentioned model is able to fit the measured values, but the obtained values for the unknown values, are not unique. It is expected this is due to the higher number of unknown input parameters for this model in comparison to the Attenborough and JCA-model.

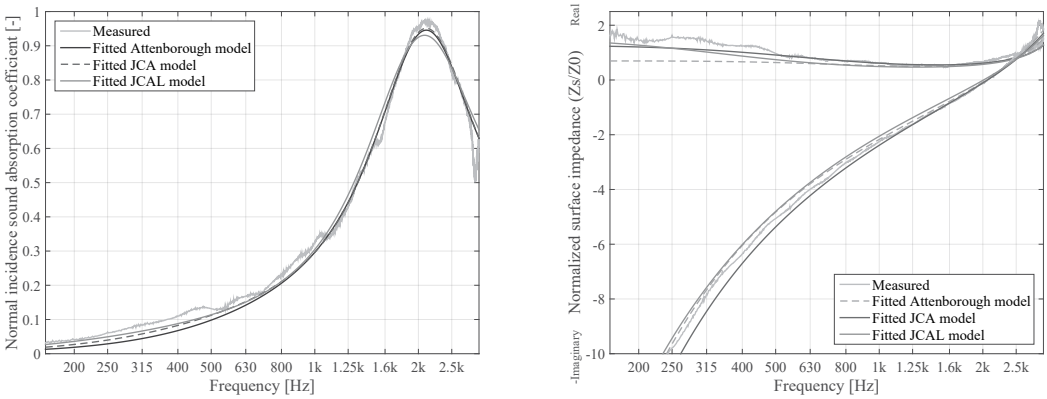

(a) *(b)*

Figure 4.9: *Fitted values by the Attenborough, JCA and JCAL models compared to the measured values for (a) normal incidence sound absorption and (b) real and imaginary normalized surface impedance.*

Finally, only the Attenborough and JCA-model are compared to each other. The graphs of the two models are very close to each other. To validate which model is able to predict the sound absorption of the WWCB the best, for every strand width, 10 samples varying in density, are measured. For the 1/3 octave bands in the frequency range 200-2500 Hz the relative deviation is calculated by making use of equation 4.13.

$$\varepsilon_{1/3octaveband} = \frac{\alpha_{\text{model,1/3octaveband}} - \alpha_{\text{measured,1/3octaveband}}}{\alpha_{\text{measured,1/3octaveband}}} \qquad [4.13]$$

where: ε is the relative error [-], $\alpha_{model,1/3octaveband}$ is the sound absorption for the specific 1/3 octave band calculated by the model [-] and $\alpha_{measured,1/3octaveband}$ is the sound absorption for the specific 1/3 octave band calculated by the model [-].

The dots in Figure 4.10 represent the calculated relative error and the error bars describe the standard deviation over the different samples. The two dashed horizontal lines are representing an error of plus and minus 10%. From the three graphs it can be seen that the relative value ε for both models is around the 0% above 1000 Hz, but increases below the 500 Hz. The errors seem to be high, but it needs to be noted that this are relative errors (i.e. if the absorption value for the 200 Hz 1/3 octave band is 0.01 and the predicted value is rounded of to 0.02, the error will be 100%).

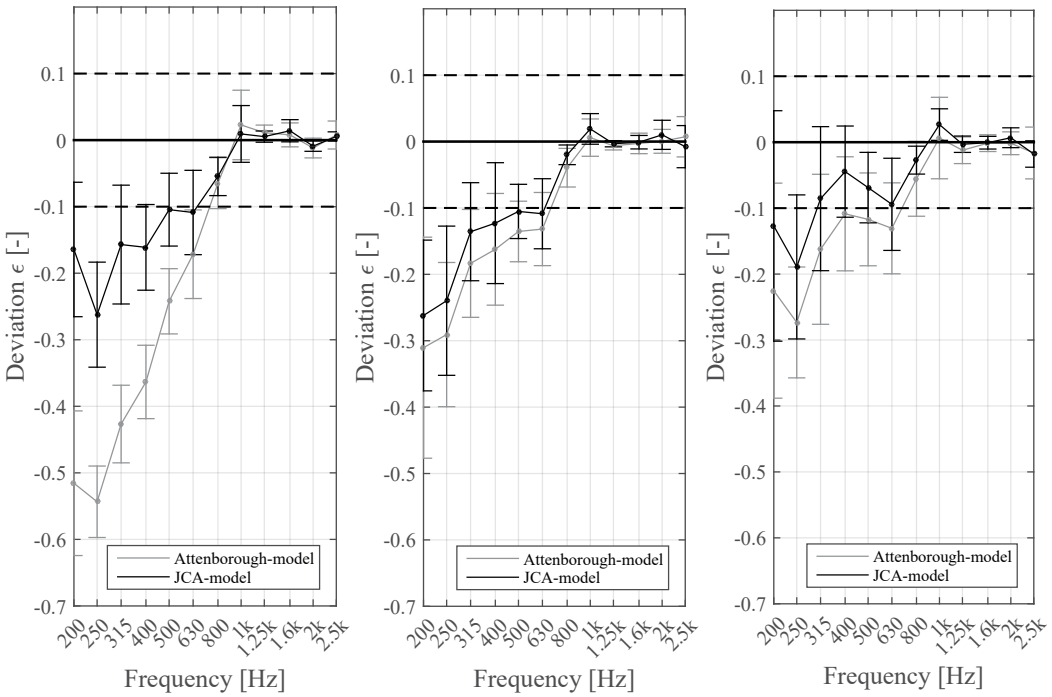

Figure 4.10: *Deviation for the Attenborough and JCA-model; (a) 1.0 mm, (b) 1.5 mm and (c) 2.0 mm fibre width.*

It can be concluded that the obtained deviation for the measured normal incidence sound absorption for the JCA-model is lower, especially for the lower frequencies, in comparison to the Attenborough model. Therefore, the JCA model is more appropriate able to predict the sound absorption of the WWCB and will be used hereafter. Moreover, the values, especially the tortuosity, obtained for the Attenborough model are higher than expected based on literature. It is therefore questionable if the values are realistic.

4.7 MODELLING DIFFERENT LAYERS AND AN AIR-CAVITY

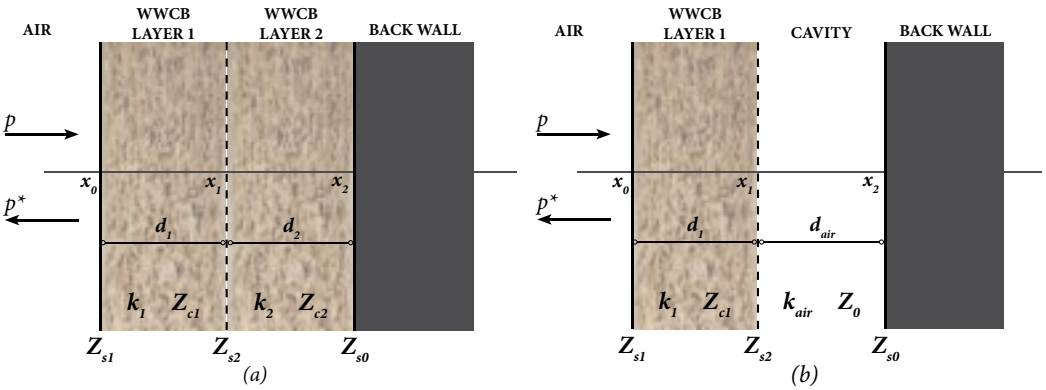

Figure 4.11: *Schematic overview of a multi-layer system with (a) two different WWCB-layers and (b) a WWCB-layer combined with an air-cavity.*

$$Z_{s,\text{total}} = \frac{-iZ_{s2}Z_{c1}\cot(k_1 d_1) + Z_{c1}^2}{Z_{s2} - iZ_{c1}\cot(k_1 d_1)} \qquad [4.14]$$

where $Z_{s,total}$ is the surface impedance of the total construction [Pa·s/m], Z_{s2} is the surface impedance of layer 2, Z_{c1} is the characteristic impedance of layer 1 [Pa·s/m], k_1 is the propagation wave number of layer 1 [s^{-1}] and d_1 is the thickness of layer 1 [m].

To model the surface impedance of a multi-layered construction, the different layers need to be evaluated individually (Cox D'Antonio, 2009). In case of the two-layered construction as presented in Figure 4.11, first the surface impedance of layer 2 needs to be calculated to be able to evaluate the surface impedance of the total construction.

In this example layer 2 can be considered as a rigid backed porous absorber and the surface impedance can be determined as presented in equation 4.5. To evaluate the surface impedance of the total construction equation 4.14 needs to be used.

In this way not only different WWCB layers can be combined and simulated, also the influence of an air-cavity or another porous material behind a WWCB can be evaluated. An example how to evaluate an air-cavity is given in Figure 4.11 in combination with equation 4.14. In case of another porous media behind the WWCB layer, the surface impedance of air should be changed into the surface impedance of that specific porous media.

4.8 FROM NORMAL INCIDENCE TO DIFFUSE INCIDENCE

The normal incidence sound absorption will be used to validate the outcomes of the impedance tube measurements. From the normal incidence sound absorption values it is possible to calculate the random incidence sound absorption. Which equation needs to be used depends if the WWCB is a locally reacting material or not. A locally reacting material is a material where the velocity inside the porous material is much smaller than that in air. The velocity component perpendicular to the surface then only depends on the pressure at the point and not upon the angle of incidence. This results in the assumption that the wave transmitted into the porous material it propagates effectively only propagates perpendicular to the surface (Attenborough, 1982). The speed of sound in air compared to the speed of sound in the WWCB, defined by the real part of the complex speed of sound following equation 4.15 is shown in Figure 4.12.

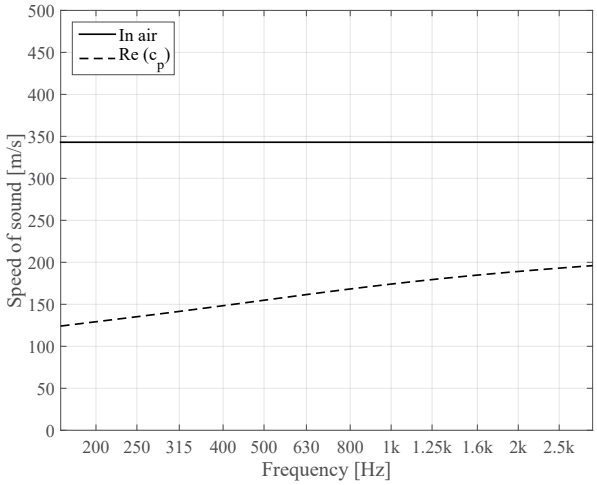

$$c_p = \frac{\omega}{k_c} \qquad [4.15]$$

where c_p is the complex speed of sound [m/s], ω the angular frequency [Hz] and k_c the complex wavenumber [m^{-1}].

Figure 4.12: *Comparison of the speed of sound in air and the speed of sound in the WWCB (25 mm WWCB).*

To be able to predict the diffuse sound absorption coefficient, first the reflection factor should be calculated for the different angles of incidences and the diffuse sound absorption can be determined, following equation 4.8 and 4.11.

$$R(\theta) = \frac{Z_n \cos(\theta) - 1}{Z_n \cos(\theta) + 1} \qquad [4.16]$$

$$\alpha_{diffuse} = \int_0^{\pi/2} \alpha(\theta) \sin 2\theta d\theta \qquad [4.17]$$

Where θ is the angle of incidence [rad] and $\alpha_{diffuse}$ the diffuse sound absorption coefficient [-].

5. ACOUSTIC CHARACTERIZATION OF THE WWCB

5.1 INTRODUCTION

Fundamental understanding of the composition and internal structure of the WWCB is essential in this study. Therefore first a detailed description will be given of the existing knowledge about the WWCBs.

Three different WWCBs with a thickness of 25 mm, which differ in fibre width (1.0, 1.5 and 2.0 mm), form the basis for this study. The difference between the 1.0 mm WWCB and the other two is the recipe. The 1.0 mm WWCB has a higher fibre surface area compared to the 1.5 and 2.0 mm WWCB and therefore the manufacturer decided to make use of more binder (+18%) for this board compared to the other boards.

Figure 5.1: *From left to right: WWCB-samples with 1.0, 1.5 and 2.0 mm fibres.*

At the end of the production process, the WWCB has maximum dimensions of 2,4 by 0.6 meter. From these boards, samples are taken all over the board. The bulk density is calculated by measuring the mass and the volume. The results show that the range in density over the samples is very large, which means the WWCB are highly inhomogeneous, making it relatively difficult to characterise and model the sound absorption. An overview of the measured densities for the three different fibre widths is given in Figure 5.2. This difference in density has a great influence on the other input parameters, e.g. the porosity, flow resistivity and the tortuosity.

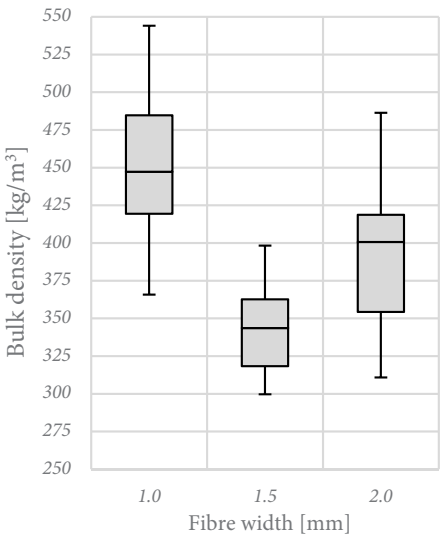

Figure 5.2: *Density ranges for the three different fibre widths.*

5.2 COMPOUND OF THE SAMPLES

The recipes of the boards are known and to determine the compound of the samples described as the wood-to-binder ratio, the following technique is used. It is expected that the compounds will differ because the binder is not equally distributed over the wood fibres. Next to this it is also expected that the wood fibres are not equally divided over the sample. This is a result of the production process and nature of the board as described in Chapter 2. The differences are visible when measuring the densities, amount of wood, binder and water content. For example; the amount of wood or binder varies over the board. This means another wood-to-binder ratio which may influences the sound absorption.

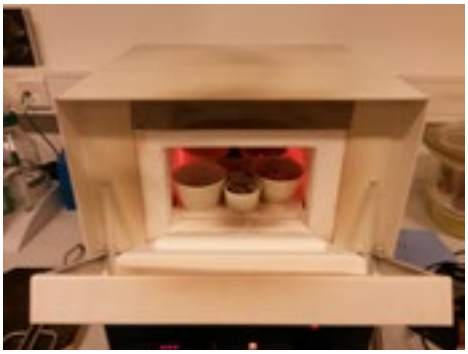

Figure 5.3: *Combustion of the WWCB-samples.*

First the samples are measured and put in an oven at 105 ^{0}C for 24 h, to remove the moisture. After that the samples are cooled down for at least 1 h in a desiccator with silica gel to remove the moisture. Before and after the mass is measured to determine the moisture content of the samples. After this the samples are transferred into an oven at 750 ^{0}C for 1 h to burn the wood fibres and remove the chemical moisture. The mass is again determined and the difference in mass lead to the wood-binder ratio.

In Figure 5.4 the indicative values for the wood-to-binder ratios are presented. It can be concluded from this figure that, because of the increased binder amount, the 1.0 mm fibre width is indeed showing lower wood-to-binder ratios. The 1.5 and 2.0 mm fibre width WWCB are showing similar results where the 2.0 mm is only showing higher and lower limits.

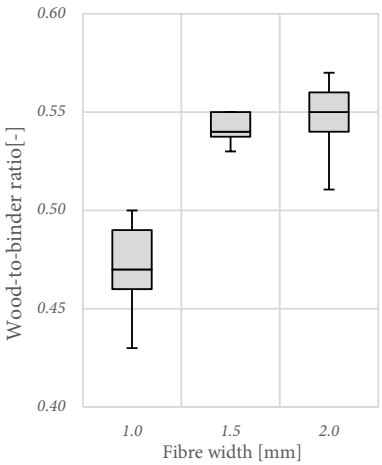

Fibre width [mm]	Average W/B ratio [-]
1.0	0.47
1.5	0.54
2.0	0.55

Figure 5.4: *Wood-to-binder ratios for the three different fibre widths.*

5.3 OPEN POROSITY

The open porosity is the ratio of the volume of the interconnected pores related to the total volume of the WWCB and can be defined using:

$$\phi = \frac{v_{interconnected pores}}{v_{total}} \quad [5.1]$$

Where $v_{interconnected\ pores}$ is the pore volume of the interconnected pores in [m³] and v_{total} is the total volume in [m³] of the WWCB.

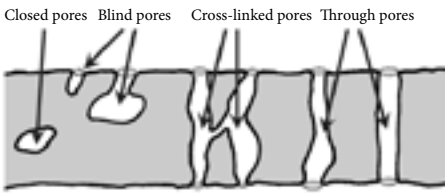

Figure 5.5: *Overview of the different pores within porous media (Giesche, 2006).*

This means that the closed pores, shown in Figure 5.5, are not taking into account. The open porosity can be measured in several ways. The first used method is to measure the open porosity with the Helium Pycnometer. A WWCB-sample, with a diameter of 46 mm, will be placed in a cup which will be placed into the pycnometer and then it will be filled up with gas (helium). The pycnometer compares the amount of helium that enters the cup including a WWCB-sample and an empty cup. In this way the skeleton volume can be determined and by knowing the total volume and mass of the sample the skeleton density and porosity can be calculated. The porosities are measured for a wide range of densities and for the three different fibre widths, which is presented in Figure 5.6. In this graph the measurements performed by Marco de Groot (2016) are included as well.

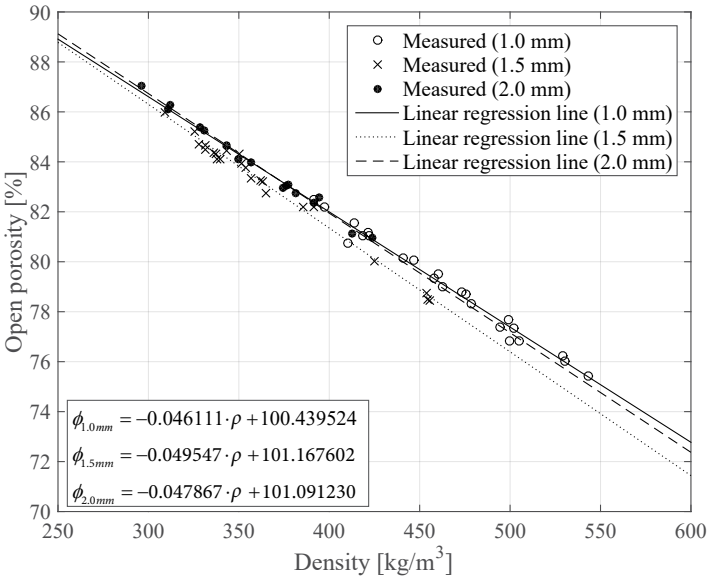

	300	350	400	450	500	550
1.0 mm	86.6	84.3	82.0	79.7	77.4	75.1
1.5 mm	86.3	83.8	81.3	78.9	76.4	73.9
2.0 mm	86.7	84.3	81.9	79.6	77.2	74.8

Figure 5.6: *Relation between the density [kg/m³] and the open porosity [%] measured with the helium pycnometer.*

The wood-cement ratio is lower for the 1 mm fibre width, which means it contains more binder and less wood for the same density compared to the 1.5 and 2.0 mm fibre width. Therefore a lower porosity is expected for 1 mm fibre width. This is not the case because the differences are very small, as presented in Figure 5.6. The linear relations for the 1.0 and 2.0 mm fibre width are similar.

In a previous study (Wassilief, 1996) the porosity of wood boards made of Pinus radiata wood was determined by measuring the resonance frequency of an oscillating column of water in a vertical glass tube connected to a volume of air with and without a sample. From the ratio of these resonance frequencies it was possible to calculate the porosity. The porosity measured by this method was much lower than the standard methods, like measurements done with the pycnometer. For example the helium pycnometer measures the total open porosity, including the porosity of the wood fibres that are open to the outside air (the air volume inside the hollow lumen), whereas this method (even at a slow compression rate of only 2 Hz) does not. It is thus expected that the air volume contained within the fibres does not take part in the acoustical process, like for example the sound absorption investigated in this study.

Applying Mercury porosimetry Autoporous IV 9500 from Micrometrics and a Phoenix Nantom CT-scan, the micro-structure and porosity of both the wood wool and WWCB-samples were investigated (Doudart de la Grée et al., 2014). The measured porosity inside these wood fibres (volume of the lumen) is approximately 63% and the pore diameter is in the range of 0-40 μm, which will be called the micro-porosity.

To determine the percentage of the total open porosity, measured by the helium pycnometer, located inside these wood fibres is difficult for a WWCB. During the production process the fibres are damaged and the cement is not equally divided over the wood fibres, as presented in Figures 5.7-5.9. Therefore it is not exactly known what amount of the porosity of the wood fibres is connected with the outside air and which is measured by the helium pycnometer.

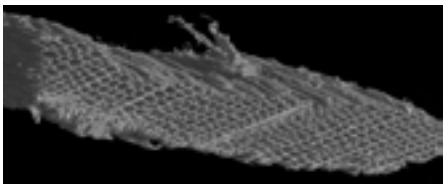

Figure 5.8: *3D scan of spruce wood wool using a Phoenix Nanotom© CT-scan: Cross-section of spruce wood wool.*

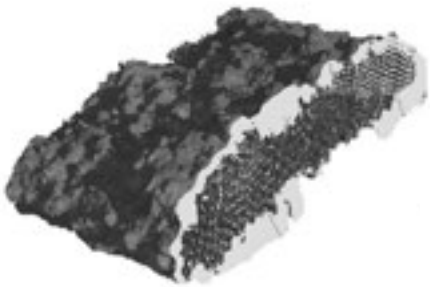

(a)

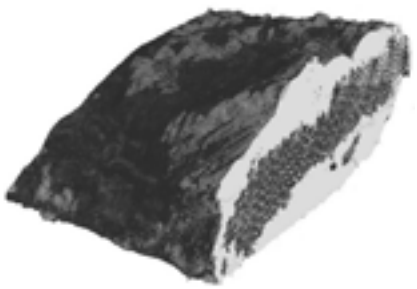

(b)

Figure 5.9: *3D scan of spruce wood wool using a Phoenix Nanotom© CT-scan: (a) Cross-section of not fully covered wood wool (b) Cross-section of fully covered wood wool by cement.*

Figure 5.7: *Microscopic picture of a WWCB using a Microscopic Keyence: Damage of the wood fibres during the production process.*

Moreover, in another study, it was proven that not all the porosity measured by the helium pycnometer takes part into the sound absorption of the wood based material wood-concrete. For the frequencies above the decoupling frequency the micro pores, about 10-15% of the total open porosity, do not absorb any sound and should be excluded from the propagation model (Glé et al. 2012).

For the WWCB this was tested in a more simplified way. Instead of filling in the value of the porosity into the propagation model, it was predicted by the curve fitting approach described in paragraph

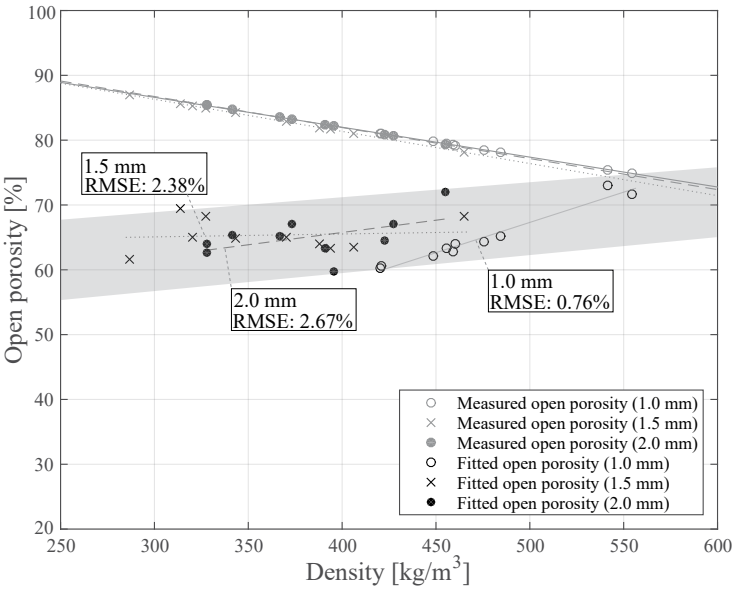

$$\phi_{1.0mm,\,fitted} = 0.093347 \cdot \rho + 20.637674 \quad [5.2]$$

$$\phi_{1.5mm,\,fitted} = 0.004521 \cdot \rho + 63.700232 \quad [5.3]$$

$$\phi_{2.0mm,\,fitted} = 0.037892 \cdot \rho + 50.601332 \quad [5.4]$$

Figure 5.10: *Relation between the density [kg/m³] and the acoustical effective open porosity [%] fitted with the JCA-model.*

4.5. The results were in all the cases lower, as presented in Figure 5.10.

In contrast to the measured open porosity in the helium pycnometer, Figure 5.10 shows that increasing the bulk density leads to an increase of the open porosity, which will be called the acoustically effective open porosity. Overall this acoustically effective open porosity is lower then the measured values, which can be explained by the fact the micro-pores are not all taken part in the acoustical process (Wassilief, 1996). This theory will be evaluated in Paragraph 6.7 by increasing the moisture content and measuring the influence on the sound absorption. It is assumed that for the lower densities the open pores are less effective, the pores are too big, which can be explained by the same principle as perforated panel absorbers having bigger openings, where the wall friction is less

efficient to damp the vibrations (Fuchs, 2013). This finally results in the regression lines presented in Figure 5.10, where the acoustically effective open porosity increases when the bulk density increases. The regression lines, and so the equations belonging to these lines, are for measured range assumed to be linear. It is known that the relation between the density and the open porosity cannot be completely linear, whereas at one stage the porosity will then drop below the 0% or excess the 100%. But as well for the measured values in the tube and the obtained values for the acoustical effective open porosity the values have the lowest root mean square error for the linear relations within the measured range.

Influence of the open porosity in the JCA-model

To evaluate the influence of the open porosity, different values are filled in the JCA-model (the other input parameters are kept constant) and the results are presented in Figure 5.11. The measured open porosity is for this sample 79% and from this graph it can be concluded this value is not able to fit the peak around the 2000 Hz. Decreasing the open porosity, results in a curve that is better able to fit it, which support the use of the acoustically effective open porosity. In contrast to this, the fit for the lower frequencies, especially between the 400 to 1000 Hz is worse. But as it is impossible in practice to only change the porosity without affecting the other input parameters, this case is not realistic. In Chapter 6 the optimum values for the different input parameters will be given.

The root mean square errors of the obtained values to the linear regression line are presented in Figure 5.10. Based on the presented influence of the open porosity, where the lines differ 10% in open porosity, it can be concluded that the RMSE-values of maximum 2.67% are relatively small.

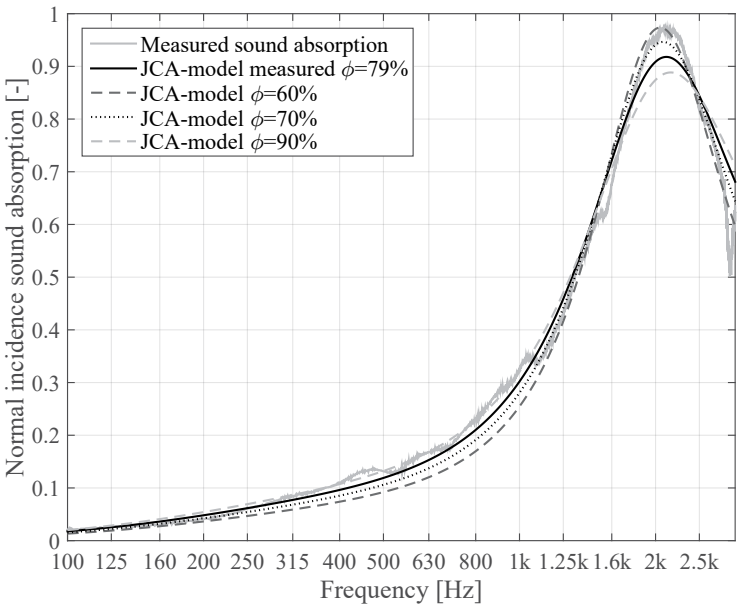

Figure 5.11: *Influence of the open porosity in the JCA-model compared to a 25 mm thick WWCB (1.0 mm strand width and density of 448 kg/m³).*

5.4 FLOW RESISTIVITY

The flow resistivity describes the resistance an airflow meets when passing a material. It thus describes how easily a sound wave is able to go through the WWCB. A higher value indicates that more sound energy may be lost through the WWCB due to the boundary layer effects within the material. It is directly related to other input parameters for the propagation models, i.e. a lower porosity leads to a higher flow resistivity. The most classical and simplified propagation models, Delany-Bazley model (Delany et al. 1970), only uses the flow resistivity and porosity to compute the absorption coefficient. To determine the flow resistivity according ISO 9053, equations 5.5, 5.6 and 5.7 are used.

A high flow resistivity means the sound wave will be rapidly attenuated inside the material and there will be little reflection at the back side of the material. The opposite will happen for a low flow resistivity; the sound wave will be reflected by the backing surface and, if the material has insufficient thickness, will leave the material again resulting in a lower sound absorption. If the flow resistivity is very high it can also mean that the surface has a relatively high impedance resulting in a lower sound absorption (Kleiner, 2011).

To determine the flow resistivity according ISO 9053, the flow resistivity meter at the Catholic University of Leuven is used. The flow resistivity σ [Ns/m^4] is measured by sending an air flow with a constant velocity through the WWCB-samples, and measuring the air velocity and pressure drop across the sample. The geometry of the WWCB-sample is cylindrical (diameter of 97 mm). With a valve the airflow through the sample can be changed. The pressure difference between the two faces of the samples is measured with a differential manometer connected to one of the multi-meters; the volume that flows per unit time is measured with a flow meter which is connected to the multimeter. In Figure 5.11 an overview of this principle is given.

$$\sigma = \frac{\Delta P}{\frac{Q}{\pi \cdot r^2} \cdot d} \qquad [5.8]$$

Where; Q is the mean flow of air per unit area of the sample [m^3/s], d is the thickness of the material sample [m], ΔP is the pressure difference over the material sample [Pa] and r is the sample radius [m].

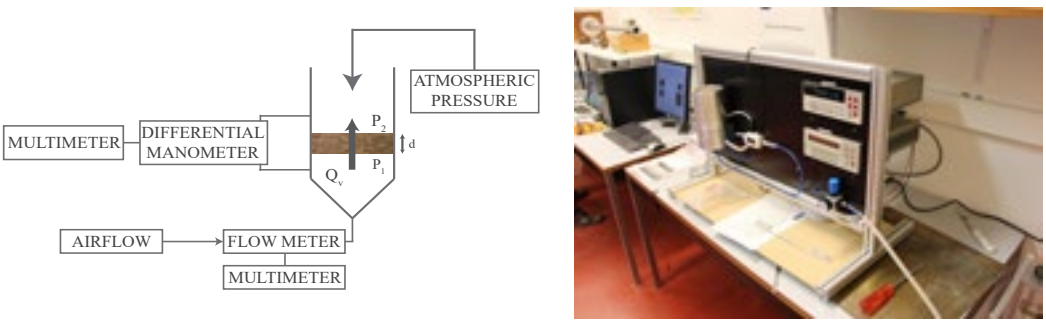

Figure 5.12: *Schematic overview (left) and a picture (right) of the flow resistivity measurements.*

For the three different fibre widths, the exponential relation between the density and the flow resistivity for the WWCB is given in Figure 5.13. As expected, if the density increases it will be more difficult for an airflow to pass through the material resulting in a high flow resistivity.

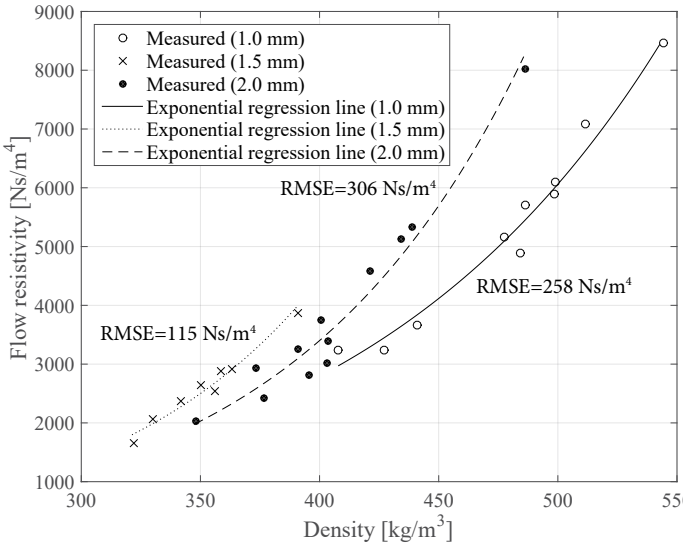

$$\sigma_{1.0mm} = 126.494842 \cdot e^{0.007739 \cdot \rho} \quad [5.9]$$

$$\sigma_{1.5mm} = 45.087750 \cdot e^{0.011472 \cdot \rho} \quad [5.10]$$

$$\sigma_{2.0mm} = 54.843703 \cdot e^{0.010318 \cdot \rho} \quad [5.11]$$

Figure 5.13: *Exponential relation between the bulk density [kg/m³] and the measured flow resistivity [Ns/m⁴].*

From Figure 5.13 it can be concluded that the influence of the strand width and the binder amount is great for the flow resistivity values. Regarding the binder amount, at the same porosity level, the flow resistivity is lower when having a higher binder amount. This indicates that the volume of wood fibres is a more influential with respect to the flow resistivity compared to the binder amount. The 1.0 mm strand width is showing the lowest flow resistivity values when comparing the strand widths for the same density. This is due to the higher binder amount, in case the recipe would be the same as for the 1.5 and 2.0 mm strand width, it is expected the curve would shift leftwards. The 1.5 mm strand width is showing higher values then the 2.0 mm one, because of the smaller strand width and the more refined grid. The 2.0 mm strand width WWCB is more rough and contains bigger openings, which results in a lower flow resistivity. It is for this reason that it is expected, when the 1.0 mm strand width WWCB would have the same recipe, this board will show the highest flow resistivity values.

Influence of the flow resistivity in the JCA-model

Analyzing the influence of the flow resistivity in the JCA-model in Figure 5.14, it can be concluded that the RMSE-values presented in Figure 5.13 are very low. From this graph it can be seen that an higher value than the value measured for this sample (4079 Ns/m^4), is slightly more accurate till the 2500 Hz. Where the used measurement method to determine the flow resistivity was very accurate and no literature was found to assume this would be incorrect it is decided to fit the flow resistivity, but to make use of the measured values.

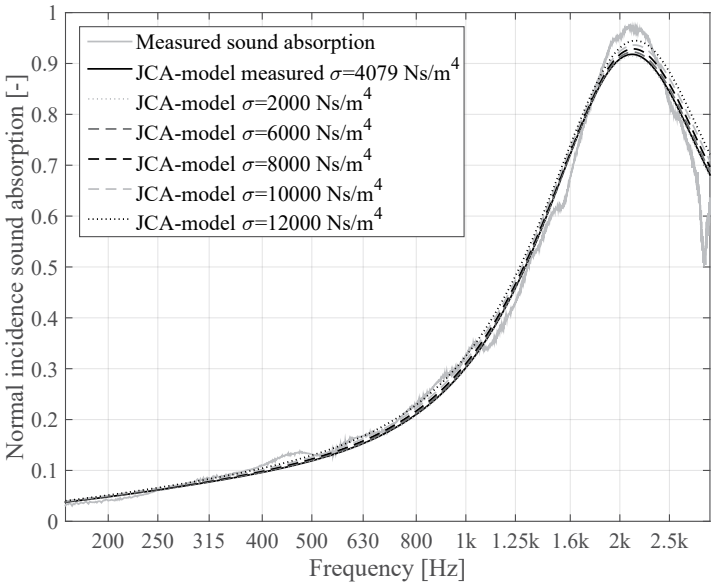

Figure 5.14: *Influence of the flow resistivity in the JCA-model compared to a 25 mm thick WWCB (1.0 mm strand width and density of 448 kg/m^3).*

5.5 TORTUOSITY

The tortuosity is the ratio between the path a sound wave travels through the WWCB and the direct path (thickness of the WWCB). In general, an increased complexity of the path leads to a higher sound absorption (Cox & D'Antonio, 2009).

For low- and medium flow resistivity materials, like the WWCB, the high-frequency limit appears to apply, the effect which shifts quarter wavelength resonance peaks in the normal incidence sound absorption spectrum to lower frequencies. In general, tortuosity mainly affects the location of the quarter-wavelength peaks (Wassilieff, 1996).

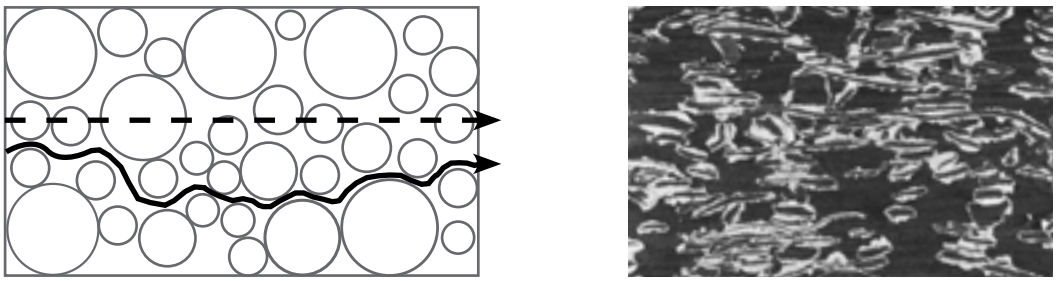

Figure 5.15: *Schematic overview of the tortuosity. dashed line is the direct path, solid line the path of the sound wave (Left). (Right) a cross-section of the WWCB, where the light parts represent the binder.*

In the acoustical lab at the KU Leuven an ultrasound tortuosity meter was present and schematically presented in Figure 5.15. The ultrasonic pulser creates an electrical pulse which is sent to the emitter. The emitter (transducer) converts the electrical pulse to an ultrasonic wave propagating in air. This wave crosses the sample and is detected by the other transducer (the receiver). The signal provided by the receiver is then captured by the oscilloscope. Two signals, one with and one without the sample between the transducers, are needed. Due to the presence of the sample, the microscopic fluid velocity undergoes changes in magnitude and direction.

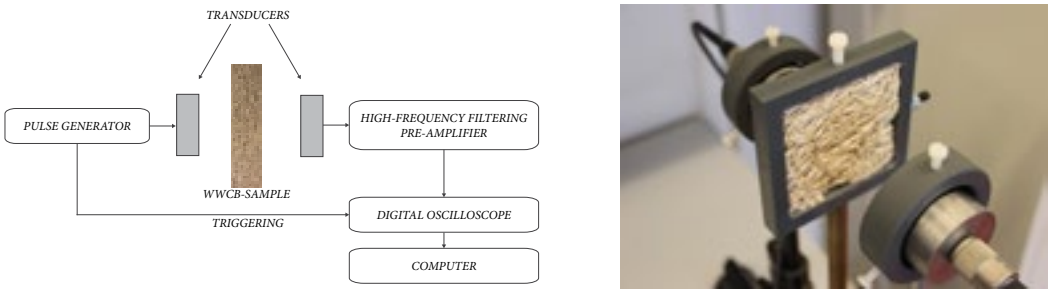

Figure 5.16: *A schematic overview of the experimental setup (left) and a picture of it (right).*

Unfortunately the tortuosity measurements were unsuccessful. Where measurements with materials with a higher porosity and a less complex path were successful, the reason that it did not work for the WWCB is that the electric pulse was not strong enough to pass the relatively rough WWCB with a complex path, resulting in a high tortuosity. Because the measurements were unsuccessful, the tortuosity will be fitted on the results of the impedance by making use of the JCA-model.

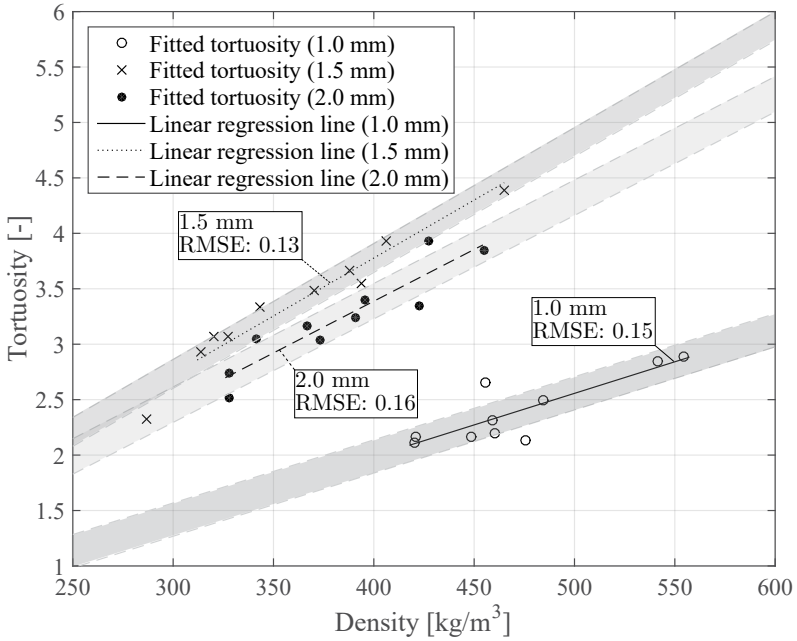

$$\alpha_{\infty,1.0mm} = 0.005693 \cdot \rho - 0.289734 \quad [5.12]$$

$$\alpha_{\infty,1.5mm} = 0.010454 \cdot \rho - 0.404240 \quad [5.13]$$

$$\alpha_{\infty,2.0mm} = 0.009334 \cdot \rho - 0.345694 \quad [5.14]$$

Figure 5.17: *Relation between the bulk density [kg/m³] and the fitted tortuosity [-].*

Influence of the tortuosity in the JCA-model

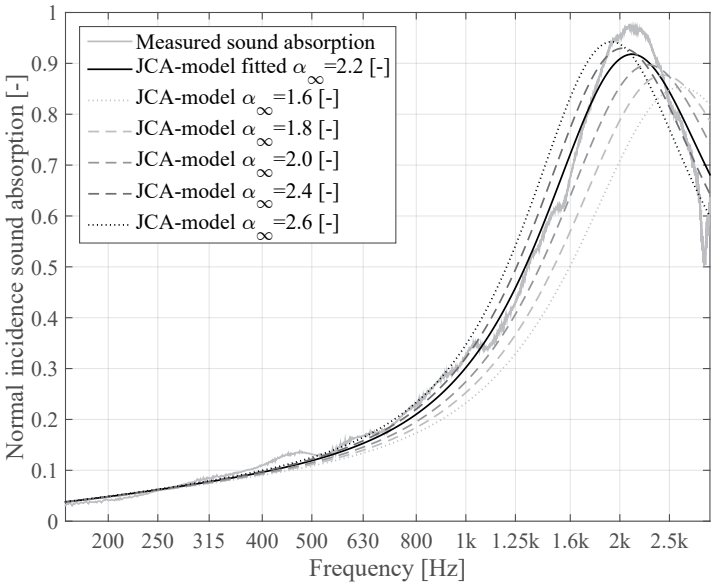

Figure 5.18: *Influence of the tortuosity in the JCA-model compared to a 25 mm thick WWCB (1.0 mm strand width and density of 448 kg/m³).*

A higher density leads to a more complex path for the sound wave to follow, resulting in a higher fitted tortuosity, which is visible in Figure 5.16 for the three different fibre widths. To make the WWCB acoustically thicker and make it more effective in the lower frequencies, a high value for the tortuosity is preferable. Therefore it is important to notice the difference in slope of the regression lines for the three fibres. This difference leads to a wider range in tortuosity values for the 1.5 mm fibre, which will have its influence on the sound absorption curves when comparing the fibre widths.

The 1.0 mm strand width values are lower due to the used recipe. When making use of the same recipe, it is expected this WWCB would show the highest values due to the increased amount of wood fibres compared to the other strand widths.

The presented RMSE-values, seem to be relatively high when analyzing the influence of the tortuosity in the JCA-model. The presented curves in Figure 5.17 are presented in steps of 0.2 for the tortuosity-value and this has a great influence on the normal incidence sound absorption, while the found RMSE-values are 0.15, 0.13 and 0.16 respectively for the different strand widths. While analyzing the prediction of the JCA-model to the measured values, this will be taken into account.

5.6 VISCOUS AND THERMAL CHARACTERISTIC LENGTHS

The inhomogeneous WWCB has all kind of different pores shapes due to the irregular distribution, orientation and placement of the wood fibres. Therefore it is almost impossible to define a general pore radius, shape factor or characteristic length and it will not be possible to measure these parameters in practice and and it is for this reason these parameters will be defined by making use of the curve fitting approach.

The effective density, describing the viscous effects, is more related to the narrow sections of the pores and the effective bulk modulus, describing the thermal effects which is more related to the wider sections of the pores (Champoux et al., 1991). Instead of making use of one pore shape factor Johnson et al. (1987) introduced two new parameters; the viscous and thermal characteristic length, defined by Λ and Λ' and having the unity 10^{-6} m, showing that the parameters are related to the pore micro-geometry. In this way the thermal and viscous effects related to the pore shape can be treated separately. A representation of a pore, with the characteristic lengths, is given in Figure 5.19. From this figure it is clear that the viscous characteristic length can never be larger than the thermal characteristic length.

$$\Lambda \leq \Lambda' \qquad [5.15]$$

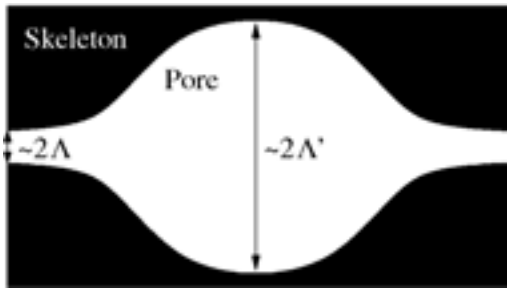

Figure 5.19: *Schematic representation of a pore (Matelys, 2016). Two characteristic lengths are related to the pore size.*

Viscous characteristic length (Λ)

The viscous characteristic length is the average of microscopic dimensions (10^{-6} m) of the pores. It mainly describes the viscous effects at medium and high frequencies (Matelys, 2016). The values presented in Figure 5.20 show values that are in line with the expectations. The fitted values are within the 50-500 μm range (Matetelys, 2016) and the values decrease with the increase of the density. The amount of material increases and therefore the characteristic length decreases. The RMSE-value is relatively low, but as is visible in Figure 5.21, it can lead to errors in the prediction of the sound absorption later on.

A decrease of the viscous characteristic length will increase the sound absorption, which is in line with the previous presented results for the acoustically effective open porosity. The smaller the pores, the more viscous effects can be effective.

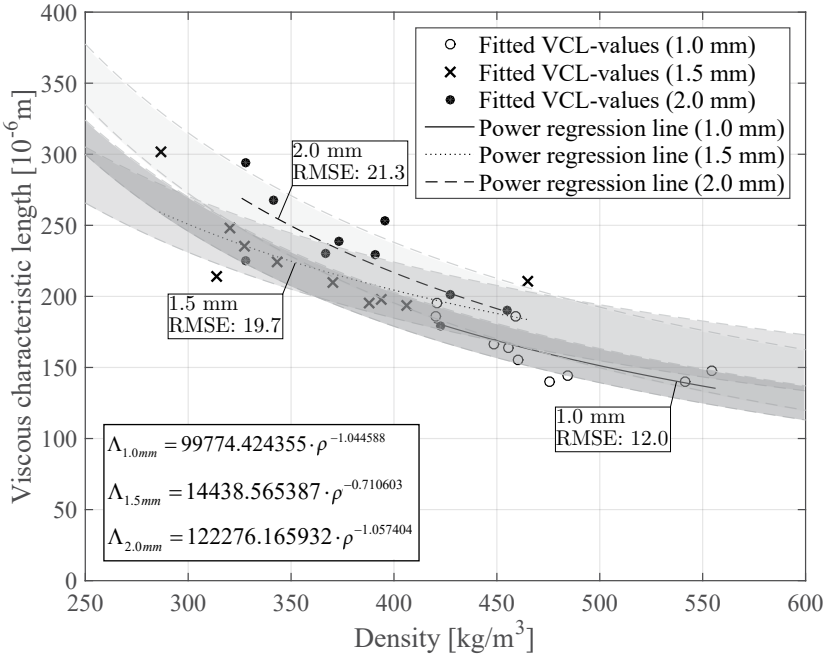

Figure 5.20: *Relation between the density [kg/m³] and the viscous characteristic length [10⁻⁶ m] fitted by the JCA-model.*

The found power relations is based on the comparison of the different relations (linear, exponential or power). The power regression line gave the lowest RMSE-value.

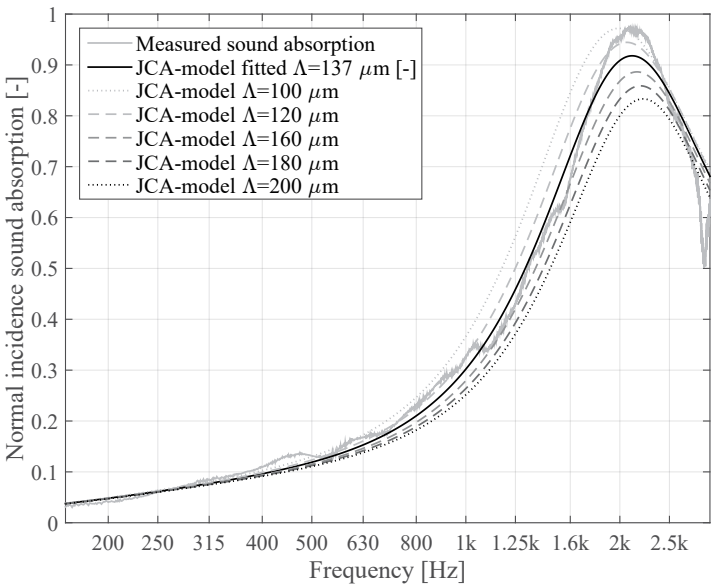

Figure 5.21: *Influence of the viscous characteristic length in the JCA-model compared to a 25 mm thick WWCB (1.0 mm strand width and density of 448 kg/m³).*

Thermal characteristic length (Λ')

The thermal characteristic length is the average of microscopic dimensions (10^{-6} m) of the pores that are related to the thermal losses. The thermal characteristic length is two times the average volume to surface ratio of the pores (Leclaire et al., 1996).

In Figure 5.21 a small decrease of the thermal characteristic length is visible for the 1.5 and 2.0 mm if the density increases. This is in line with the expectations, because of the amount of material increases and the pores shape will get smaller and therefore also the surface of the pores will decrease. The values are also within the range described by Matelys (2016). For the 1.0 mm, the values are also within the same range, only an increase is visible which cannot be explained. The influence of the thermal characteristic length in the JCA-model is very limited, as presented in Figure 5.22, so it is not expected this will lead to a prediction error later on.

The found power relations are based on the comparison of the different relations (linear, exponential or power). The power regression line gave the lowest RMSE-value.

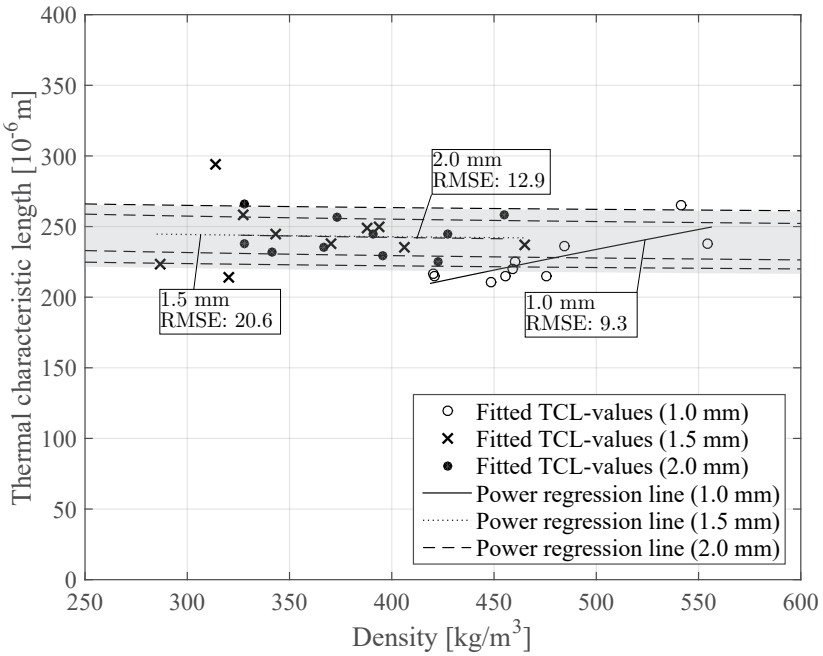

$$\Lambda'_{1.0mm} = 5.148369 \cdot \rho^{0.614019}$$

$$\Lambda'_{1.5mm} = 277.947695 \cdot \rho^{-0.02256}$$

$$\Lambda'_{2.0mm} = 291.929762 \cdot \rho^{-0.031082}$$

Figure 5.22: *Relation between the density [kg/m³] and the thermal characteristic length [10⁻⁶ m] fitted by the JCA-model.*

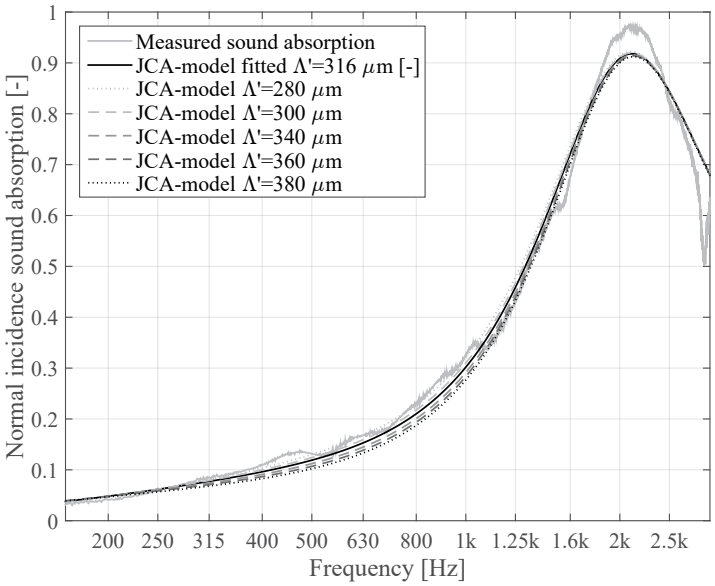

Figure 5.23: *Influence of the thermal characteristic length in the JCA-model compared to a 25 mm thick WWCB (1.0 mm strand width and density of 448 kg/m³).*

Although the influence is small, just as for the viscous characteristic length, it can be concluded that a decrease of the thermal characteristic length will increase the sound absorption.

5.7 SUMMARY

The input parameters are all related to each other. It is for example impossible to change the porosity, without affecting the flow resistivity. However, in the previous paragraphs, the influence of the different input parameters in the JCA-model is evaluated, to increase the understanding of the working of the model. From this, it can be concluded that the open porosity, tortuosity and the viscous characteristic length are the main influential parameters in the impedance model. Where the open porosity is only influencing the height of the peak, the tortuosity and viscous characteristic length are, next to influencing the height of the peak, also shifting the peak to the lower frequencies in case increased values. The influence of the flow resistivity and the thermal characteristic length is small and no errors are expected based on the found relations between these values and the bulk density.

5.8 RELATION BETWEEN INPUT PARAMETERS

A schematic overview of the relation between the density and the different input parameters is given in Figure 5.24. In this figure it is shown what happens when the density of a WWCB-sample is increased. Also the different input parameters are related to each other; it is for example impossible

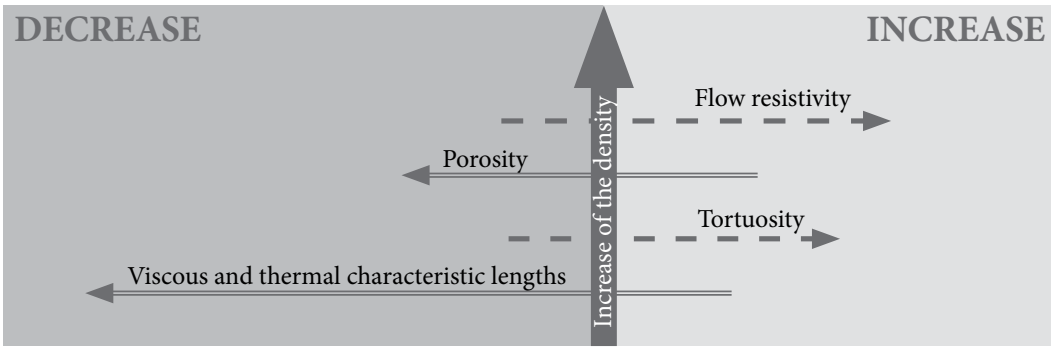

Figure 5.24: *Schematic overview of the relation between the input parameters and the density of the WWCB.*

to increase the porosity, without influencing the tortuosity. These relations, which are described in equations in the previous paragraphs, are of great importance to understand what happens if the density will be increased. Because a relation was found for all the input parameters and the density, only the density (in combination with the thickness) needs to be used as an input parameter for the impedance model, which is schematically shown in Figure 5.23. This increases the practical use of the model and also makes it possible to study how to optimize the sound absorption of the WWCB.

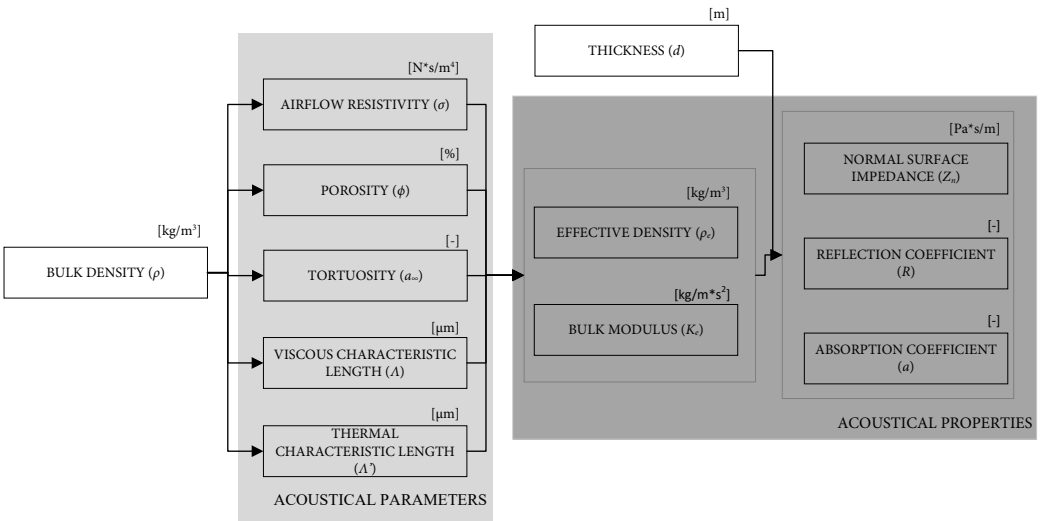

Figure 5.25: *Schematic overview of the propagation model.*

5.9 DENSIFICATION WITHIN THE WWCB

First the surface structure of boards with 1.0 and 2.0 mm strand widths is investigated. In Figure 5.26 it is visible that the surface structure of the 2.0 WWCB is showing larger openings and is more porous. In case the density for the two samples is exactly the same, this means that porosity in the other layers, behind the surface, needs to be lower in comparison to the 1.0 mm board, to get the same overall density. A grid difference between the 1 and 2 mm WWCB should therefore exist.

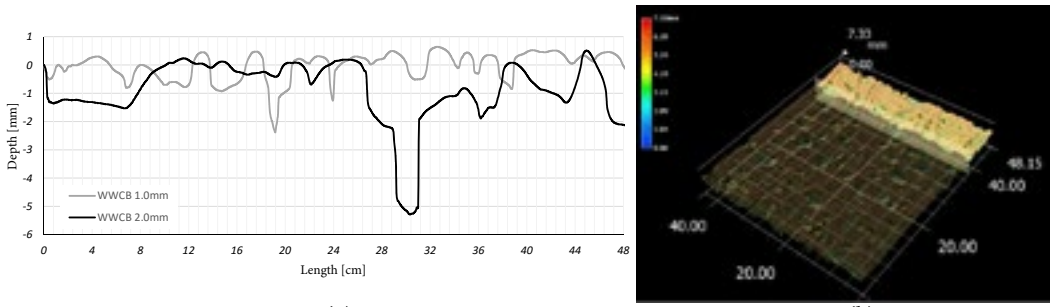

(a) *(b)*

Figure 5.26: *(a) Cross section of the surface of a 1.0 and 2.0 mm fibre WWCB; (b) visualisation how the picture is created (Made with a Keyence VHX500 microscope).*

The presented relations in this chapter between the bulk density and the input parameters are valid in case the wood fibres are equally divided over the thickness. Based on the Figure 5.26 it seems that a densification exists over the sample thickness. To evaluate this, 50 mm thick WWCBs (1.0 and 2.0 mm strand widths) are cut into three different layers and for each layer the density is measured seperately. The results are presented in Figure 5.27 and show a densification within the boards.

Layer 1 is the part of the board that is visible when mounted on a ceiling, layer 2 is the middle part and layer 3 the back of the board. The thickness of the layers is not for all the layers the same, as described in the caption of the figure. For the 1.0 mm WWCB the middle layer contains in almost all the cases more material than the 'surface'-layers. For the 2.0 mm WWCB the front layer is the

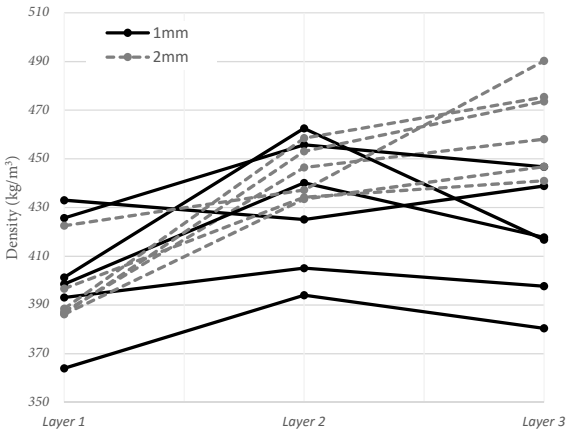

Figure 5.27: *Density distribution over twelve samples 50 mm WWCB (1 and 2 mm fibre widths) Layer 1 = 10.5 mm, Layer 2 = 25 mm Layer 3 = 10.5 mm.*

layer with the lowest density and highest porosity and the opposite is the case for the back layer. To evaluate the origin of this difference the wood to binder ratios are measured and the results are shown in Table 5.1.

A big difference is visible between the 1.0 and 2.0 mm strand width, meaning that amount of binder is higher for the back layer of the 2.0 mm WWCB. The binder is not well attached to the wood fibres in the top-layer and it is assumed that this is a result of the amount of water used in this recipe. It can be expected that too much water is used and the binder migrated down and finally attached to the wood fibres in the back-layer.

Table 5.1: *Wood to binder ratio for 50 mm WWCB*

Sample	Layer	Thickness [mm]	Density [kg/m³]	Wood-binder ratio [-]
50 mm [1.0 mm]	Top-layer	22.5	359	0.43
	Back-layer	23.2	404	0.44
50 mm [2.0 mm]	Top-layer	12.8	356	0.47
	Back-layer	13.2	449	0.36

As mentioned before, the relations between the bulk density and the input parameters are valid for WWCB-samples with a homogeneous distribution of the fibres over the thickness and for the wood-to-binder ratios presented in paragraph 5.2. Where this is not the case for the 2.0 mm strand width 50 mm thick WWCB, it is expected this will have an influence on the sound absorption because the input parameters will change. The open porosity will stay the same, but e.g. the flow resistivity will increase. In the next chapter this will be evaluated and the sample in Figure 5.28 will be modelled as a single layer, with the overall density and as a multi-layer, with the three different densities. In case the predicted values are too high, this can be explained by the fact that the back-layer can not be modelled by the created relations due to the high binder amount. This phenomenon is explained in section 6.5.

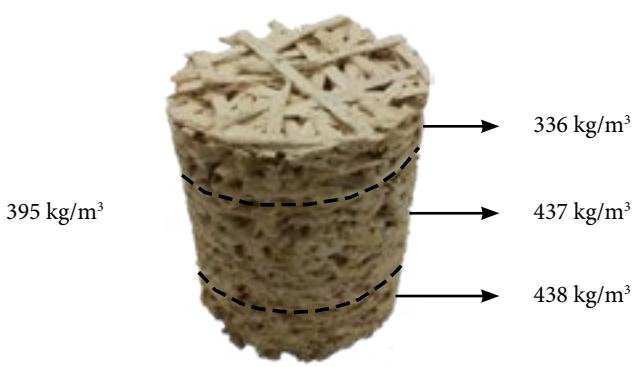

Figure 5.28: *Density distribution over a 50 mm thick WWCB-sample (2.0 mm strand width) Layer 1 = 10.5 mm, Layer 2 = 25 mm Layer 3 = 10.5 mm.*

6. RESULTS

6.1 INTRODUCTION

In Chapter 4 it is concluded that the Johnson-Champoux-Allard (JCA) model was found to be most appropriate to fit the measured normal incidence sound absorption values in the impedance tube. In Chapter 5 relations were found between the bulk density and the five input parameters. In this chapter first the applicability of these relations is evaluated and the relative errors from the measured values are given. This will not only be done for the 25 mm thick WWCB, but also for 15, 35 and 50 mm thick WWCBs, constructions with an air-cavity behind it and for multi-layers systems. Secondly the influence of the WWCB-properties, like the density, thickness and strand width and different constructions, for example with an air-cavity and other multi-layer systems, on the sound absorption will be evaluated. Finally the diffuse incidence sound absorption will be calculated and a comparison to the diffuse sound absorption measured in the reverberation room will be performed in this chapter.

6.2 VALIDATION STUDY

Out of the measured and predicted normal incidence sound absorption curves, the 1/3-octave and octave band values (250 - 2000 Hz) and the single number value for SAA are determined. The relative deviation is calculated with the following equation:

$$\varepsilon_{1/3octaveband} = \frac{\alpha_{\text{model,1/3octaveband}} - \alpha_{\text{measured,1/3octaveband}}}{\alpha_{\text{measured,1/3octaveband}}} \qquad [6.1]$$

Where; ε is the relative deviation [%], $\alpha_{measured}$ the measured sound absorption value [-] and $\alpha_{predicted}$ the predicted sound absorption value [-].

For each fibre strand width a comparison is given of the measured versus the predicted normal incidence sound absorption curve in Figure 6.1 till 6.3. Next to these figures a table is presented with the measured and predicted 1/3-octave band values, the deviation and the prediction error.

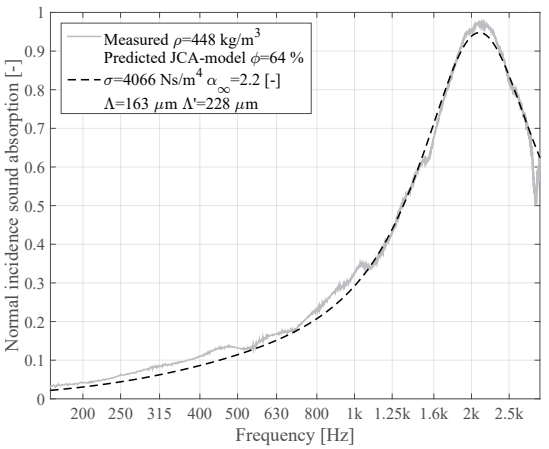

Figure 6.1: *Comparison of the measured and the predicted sound absorption curve for 25 mm WWCB with a 1.0 mm fibre strand width.*

Table 6.1: *25 mm WWCB (1.0 mm fibre strand width)*

	Measured	JCA-model	Deviation [-]	Error ε [%]
200 Hz	0.04	0.03	-0.01	26.2
250 Hz	0.06	0.04	-0.02	26.1
315 Hz	0.08	0.06	-0.02	25.5
400 Hz	0.11	0.09	-0.02	22.3
500 Hz	0.13	0.11	-0.02	13.3
630 Hz	0.17	0.15	-0.01	8.1
800 Hz	0.23	0.21	-0.02	9.9
1000 Hz	0.32	0.30	-0.02	7.6
1250 Hz	0.45	0.45	0.00	0.5
1600 Hz	0.69	0.71	0.02	3.0
2000 Hz	0.94	0.92	-0.02	1.8
2500 Hz	0.82	0.82	-0.00	0.4
SAA	*0.34*	0.32	-0.01	3.7

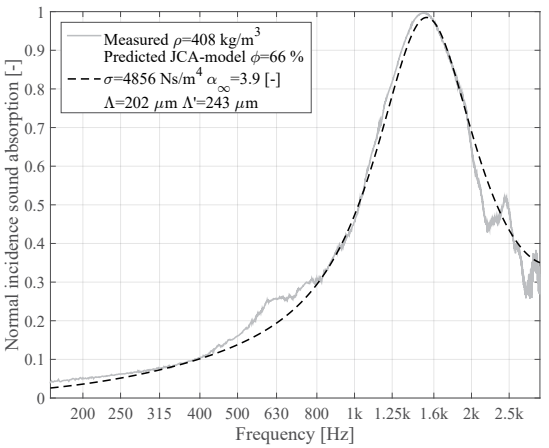

Figure 6.2: *Comparison of the measured and the predicted sound absorption curve for 25 mm WWCB with a 1.5 mm fibre strand width.*

Table 6.2: *25 mm WWCB (1.5 mm fibre strand width)*

	Measured	JCA-model	Deviation [-]	Error ε [%]
200 Hz	0.05	0.04	-0.01	28.8
250 Hz	0.06	0.05	-0.01	16.4
315 Hz	0.08	0.07	-0.00	5.2
400 Hz	0.11	0.10	-0.00	4.4
500 Hz	0.17	0.14	-0.03	16.0
630 Hz	0.25	0.20	-0.05	21.7
800 Hz	0.31	0.30	-0.02	5.5
1000 Hz	0.49	0.48	-0.00	0.4
1250 Hz	0.83	0.80	-0.03	4.2
1600 Hz	0.96	0.95	-0.00	0.5
2000 Hz	0.64	0.69	0.05	7.3
2500 Hz	0.41	0.43	0.02	5.2
SAA	*0.36*	0.35	-0.00	2.4

The deviations for all the examples are very small (maximum deviation is 0.05). Analysing the relative prediction error ε it can be seen above the 500/630 Hz this value is very low. In contrast to this the error values under this frequency are higher, which can be explained by the fact that the sound absorption values for the lower frequencies are small and a deviation of only 0.01 can already lead to an error of 28.8%. In the three graphs a peak is visible around the 500-630 Hz for the measured values and it is expected this peak is due to the resonances inside the impedance tube.

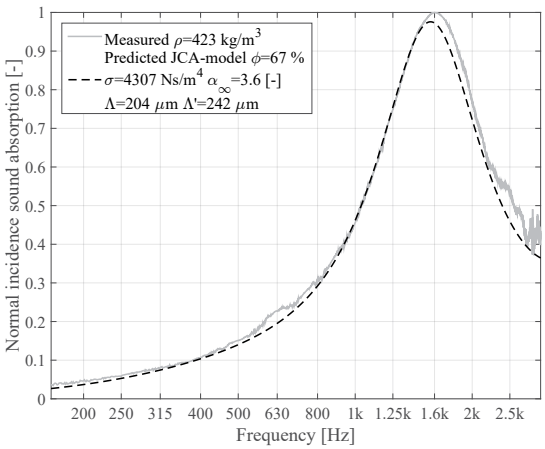

Figure 6.3: *Comparison of the measured and the predicted sound absorption curve for 25 mm WWCB with a 2.0 mm fibre strand width.*

Table 6.3: *25 mm WWCB (2.0 mm fibre strand width)*

	Measured	JCA-model	Deviation [-]	Error ε [%]
200 Hz	0.05	0.04	-0.01	18.9
250 Hz	0.06	0.05	-0.01	12.9
315 Hz	0.08	0.07	-0.01	6.7
400 Hz	0.11	0.10	-0.00	3.9
500 Hz	0.15	0.14	-0.01	7.0
630 Hz	0.22	0.20	-0.03	11.3
800 Hz	0.31	0.29	-0.02	4.9
1000 Hz	0.47	0.47	0.00	0.1
1250 Hz	0.77	0.77	0.00	0.6
1600 Hz	0.98	0.95	-0.03	2.7
2000 Hz	0.76	0.72	-0.04	5.8
2500 Hz	0.51	0.46	-0.05	10.3
SAA	*0.37*	0.36	-0.02	4.4

In Figure 6.4 the relative prediction error is given for the 10 different WWCB-samples for every fibre strand width in total. For all the strand widths it can be seen the average error from ± 500 Hz is within the 10% error range. The graphs, belonging to these prediction errors are presented in the Appendix H. Analysing the trend of the graphs, the deviation of the JCA-model from the measured values and the low error for the single number SAA-value, the errors are considered as acceptable, to predict the normal incidence sound absorption of the WWCB in this study.

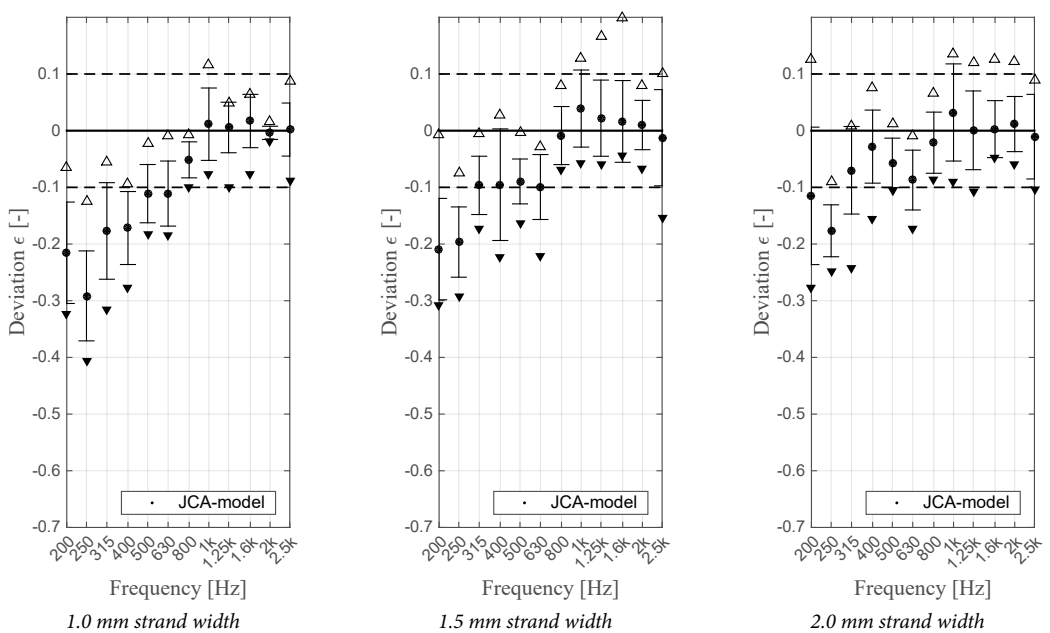

Figure 6.4: *Deviation of the predicted values using the JCA-model from the measured values. (25 mm thick WWCB).*

6.3 DEMONSTRATION OF THE MODEL

In this paragraph it will be demonstrated that the JCA-model, in combination with the obtained relations between the bulk density and the input parameters, is able to predict WWCBs with different thicknesses, combined with an air-cavity, multilayer systems and mineral wool. To demonstrate this, these constructions are also measured in the impedance tube and these outcomes are compared to the predicted values. It is important to notice no fitting of the input parameters took place for WWCB with other thicknesseses or for the different constructions.

6.3.1 Different thicknesses

For the 15 and 35 mm WWCB, presented in Figure 6.5a and 6.5b, it is possible to predict the normal sound absorption curves. Due to the densification inside the 50 mm WWCB the high amount of binder, as discussed in Paragraph 5.8, it is not possible to predict the sound absorption. In Figure 6.5c a 50 mm WWCB (2.0 mm strand width) is modelled as single- and multilayer. It can be seen especially the first peak of the curve is overestimated, which mainly can be explained by the lower wood-to-binder ratio for the 50 mm WWCB. It is expected a lower wood-to-binder ratio results in a lower sound absorption, which is in line with the results of Figure 6.5c. In Section 6.7 the influence of the wood-to-binder ratio is investigated.

For every comparison the SAA-value error is given, which is for all the cases acceptable (under the ±10%). More comparisons are given in Appendix I which are showing comparable results.

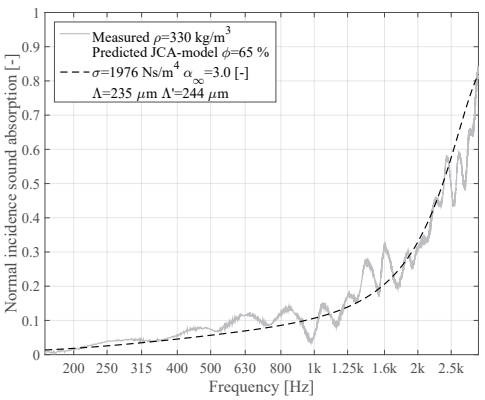

	Measured	JCA -model	Error ε [%]
SAA-value [-]	*0.15*	0.14	2.8

(a)

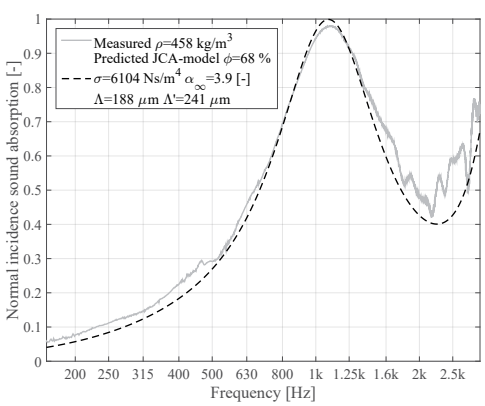

	Measured	JCA -model	Error ε [%]
SAA-value [-]	*0.46*	0.43	7.3

(b)

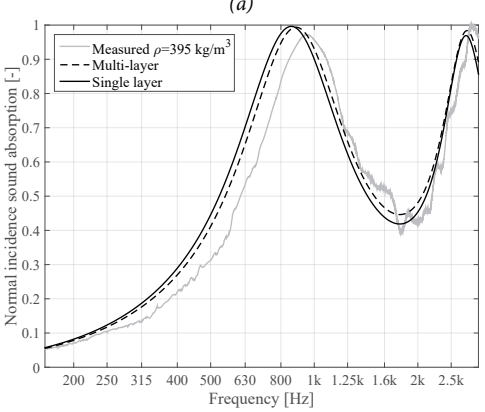

	Measured	JCA -model	Error ε [%]
SAA-value [-]	*0.46*	0.50	8.7

(c)

Figure 6.5: *Predicted values using the JCA-model compared to the measured values for (a) d = 15 mm (1.5 mm strand width), (b) d = 35 mm (2.0 mm strand width) and (c) d=50 mm (2.0 mm strand width).*

6.3.2 Different air-cavities

In Figure 6.6 the measured and predicted sound absorption curves for WWCB combined with air-cavities are compared. The predicted values are able to meet the measured values, but when the air-cavity is increased the error for the lower frequencies is increasing. As presented in Table 6.4, the relative error for the lower frequencies is indeed slightly higher.

From the three graphs it can be seen that increasing the air-cavity will increase the sound absorption. In the next chapter it will be evaluated the optimal thickness of the air-layer for the three strand widths.

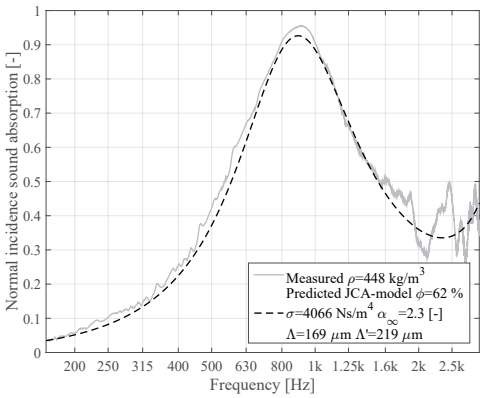

	Measured	JCA -model	Error ε [%]
SAA-value [-]	0.45	0.42	4.9

(a)

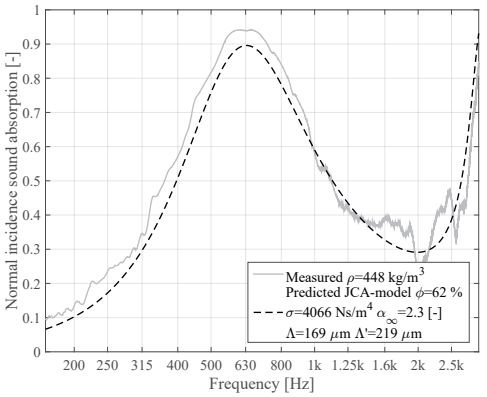

	Measured	JCA -model	Error ε [%]
SAA-value [-]	*0.50*	0.47	7.2

(b)

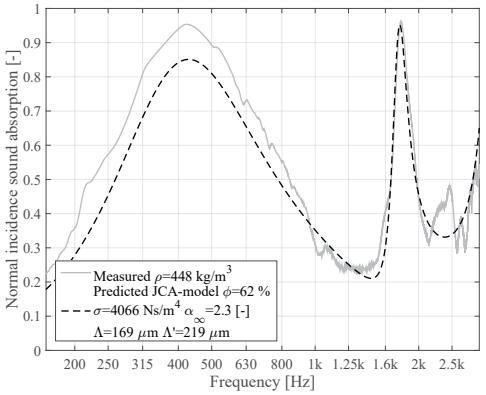

	Measured	JCA -model	Error ε [%]
SAA-value [-]	0.57	0.51	10.4

(c)

Table 6.4: *Prediction errors for the three different cavities*

	Error 25 mm cavity	Error 50 mm cavity	Error 100 mm cavity
200 Hz	12.6	23.9	25.2
250 Hz	20.3	24.6	20.4
315 Hz	11.1	15.6	14.3
400 Hz	9.6	12.5	10.6
500 Hz	10.8	8.3	10.3
630 Hz	6.9	5.6	10.5
800 Hz	2.4	6.2	11.4
1000 Hz	2.3	1.8	3.0

Figure 6.6: *Predicted values using the JCA-model compared to the measured values for a 25 mm WWCB with an air-cavity of (a) 25 mm, (b) 50 mm and (c) 100 mm.*

6.3.3 Multi-layer constructions

In Figure 6.7a the results for a multi-layer system of two 25 mm thick WWCB-layers is shown. Due to the difference in densities of the two layers, the sound wave propagates differently through the construction compared to a more homogeneous construction. It can be seen that the predicted values, based on the equations presented in paragraph 4.8, are not completely able to meet the measured ones. This can be explained by that the construction in theory is different from the construction in practice. Maybe a small air-gap existed between the samples, which makes the curve shift to the lower frequencies, due to the porous surface layers. The overall error for the SAA-value is low, which makes it possible to still study its influence in the next chapter.

in Figure 6.7b a multi-layer system with a 25 mm WWCB combined with a layer of mineral wool behind it is visualized. Due to the higher porosity (which is close to 1) and higher flow resistivity, it is possible to use the Miki model (Miki, 1990), as described in Chapter 4. The flow resistivity is much higher for the mineral wool (60000 Ns/m^4) and this value was assumed based on measurements done in another study with the almost the same material and the curve fitting approach (which both gave the same value (Hoekstra, 2016)). For this graph the Miki and JCA-model are combined and finally it meets the measured sound absorption values in the impedance tube, which shows the applicability of the model for the WWCB for all kinds of constructions. The MATLAB-script for this prediction can be found in Appendix F.

In Figure 6.7b also the absorption values for the different layers separately are given. It is clear to see that the sound absorption, especially for the lower frequency, is higher for the mineral wool sample. By combining the two samples the sound absorption is increased. Due to the increased thickness, the peak shifts to the left. Due to the combination with the WWCB-sample, the peak also shifts up, which can be explained by the increased tortuosity. As a result the path the sound wave has to travel is more complex.

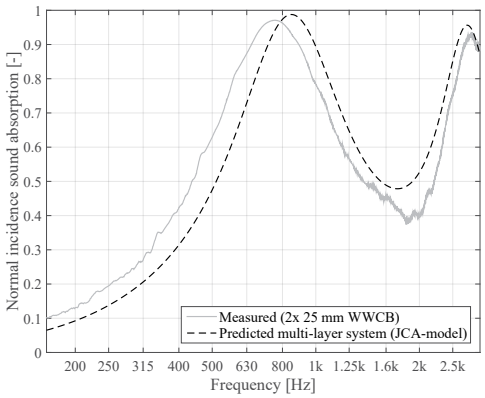

	Measured	JCA -model	Error ε [%]
SAA-value [-]	0.54	0.53	1.9

(a)

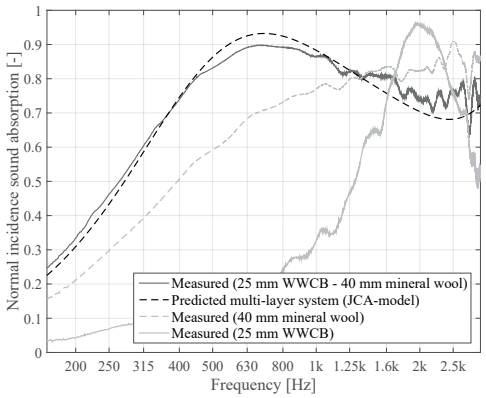

	Measured	JCA -model	Error ε [%]
SAA-value [-]	*0.73*	0.72	1.4

(b)

Figure 6.7: *Predicted values using the JCA-model compared to the measured values for (a) a multi-layer system with two WWCBs and (b) a 25 mm WWCB (1.0 mm strand width) combined with a 40 mm thick mineral wool sample.*

6.4 RANDOM INCIDENCE SOUND ABSORPTION

To measure the random incidence sound absorption coefficient of the WWCB, different boards, which differ in thickness and strand width are evaluated. The WWCBs were tested in the reverberation room of Peutz in Mook, the Netherlands. This reverberation has a volume of 214 m^3 and the tested WWCB had a surface area of 10.8 m^2.

The following boards were tested:

Table 6.5: *WWCBs tested in the reverberation room of Peutz.*

	Thickness [mm]			
Fibre width [mm]	**15**	**25**	**35**	**50**
1.0		X		
1.5	**X**	**X**	**X**	**X**
2.0		X		

Combining the JCA-model, making use of the found relations between the bulk density and the input parameters, and equation 4.16 and 4.17 the diffuse sound absorption values are calculated.

The samples measured in the impedance tube are relatively small (diameter of 40 mm) compared to the surface measured in the reverberation room (10.8 m^2). Where it is possible to measure the density of the small samples very accurately, this is more difficult for the big surface of 10.8 m^2. In the test reports only from one board, with the dimension of 2400 x 600 mm^2, the mass and thickness are measured. It is assumed that the other boards have exactly the same mass and same thickness. Based on the study done with the smaller samples it can be concluded this is not realistic. Therefore the densities for the big surfaces are sometimes over- or underestimated and this is corrected for the data presented in Figure 6.8 and 6.9. In the first figure an example is given of a 25 mm thick WWCB with a 1.0 mm fibre width and a density of 444 kg/m^3. Figure 6.9 shows the deviation of the predicted values to the measured 1/3-octave bands sound absorption.

The prediction error is relatively small, but as mentioned before, assumptions are made for the average density of the 10.8 m^2. Therefore, it can only be concluded that the calculated diffuse incidence sound absorption curve is following the trend of the measured curve.

Next to this, studies by Jeong (2013) show that it is not possible to directly compare the random incidence sound absorption measured in a reverberation room to the diffuse sound absorption values obtained from the results measured by the impedance tube method. Due to the fact the incidence in the reverberation rooms is never completely diffuse, a correction factor needs to be introduced. This correction factor is not known for the specific room and therefore the values cannot be validated.

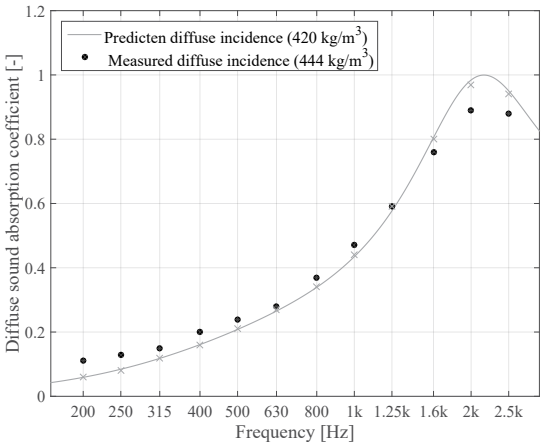

Figure 6.8: *Comparison of the measured and predicted diffuse sound absorption for a 25 mm thick WWCB with a 1.0 mm strand width.*

Table 6.6: *Comparison of the measured and predicted diffuse 1/3 octave bands sound absorption for a 25 mm WWCB with a 1.0 mm fibre*

	Measured	JCA-model	Deviation [-]	Error ε [%]
200 Hz	0.11	0.06	-0.05	45.5
250 Hz	0.13	0.08	-0.05	38.5
315 Hz	0.15	0.12	-0.03	20.0
400 Hz	0.20	0.16	-0.04	20.0
500 Hz	0.24	0.21	-0.03	12.5
630 Hz	0.28	0.27	-0.01	3.6
800 Hz	0.37	0.34	-0.03	8.1
1000 Hz	0.47	0.44	-0.03	6.4
1250 Hz	0.59	0.59	0.00	0.0
1600 Hz	0.76	0.80	0.04	5.3
2000 Hz	0.89	0.97	0.08	9.0
2500 Hz	0.88	0.94	0.06	6.8
SAA	*0.42*	*0.42*	*0.00*	*0.00*

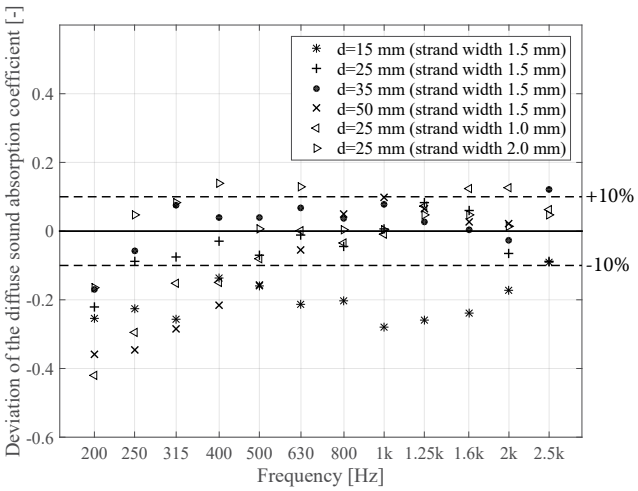

Figure 6.9: Deviation of the predicted to the measured diffuse 1/3 octave band sound absorption.

Figure 6.10: *WWCBs in the reverberation room of Peutz in Mook, the Netherlands.*

6.5 INFLUENCE OF THE STRAND WIDTH

WWCB with different strand widths (1.0, 1.5 and 2.0 mm) are compared in this study. To evaluate the influence of the strand width on the normal incidence sound absorption, WWCBs with the same density are predicted with the JCA-model and the results are presented in Figure 6.11. In table 6.7 the input parameters belonging to these curves are given. It needs to be noted that the wood-to-binder ratio for the three strand widths is different, due to the different recipes used per strand width. The presented comparison therefore only applies for these recipes and is not only a comparison of the strand widths.

The presented sound absorption curve for the 1.0 mm performs worse in comparison with the 1.5 and 2.0 mm and this can mainly be explained by the difference in recipe. Due to the higher binder amount, which leads to a lower total volume of material, the tortuosity and flow resistivity values are lower. Moreover, the smaller strand width leads to a more refined grid, but therefore also a higher acoustical effective open porosity and lower thermal and viscous characteristic lengths.

The 1.5 and 2.0 mm strand width WWCB are showing comparable results. The small difference can mainly be explained by the difference in flow resistivity and the tortuosity. The higher strand diameter leads to a WWCB with some bigger openings and leads on average to a lower flow resistivity and tortuosity. Although the difference in small, this finally results in a slightly lower sound absorption.

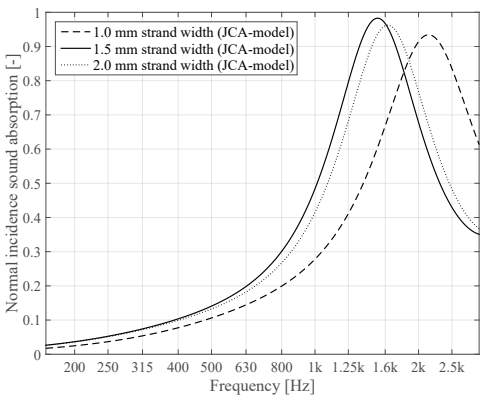

Strand width [mm]	SAA-value [-]
1.0	0.31
1.5	0.36
2.0	0.35

Figure 6.11: *Visualization of the influence of the three different strand widths (d=25 mm and ρ=400 kg/m³).*

Table 6.7: *WWCB parameters belonging to the normal incidence sound absorption curves of Figure 6.11.*

Strand width [mm]	Measured density range [kg/m³]	Acoustical effective open porosity [%]	Flow resistivity [Ns/m⁴]	Tortuosity [-]	Viscous characteristic length [µm]	Thermal characteristic length [µm]
1.0	400	58	2795	1.99	191	204
1.5	400	65	4436	3.78	204	242
2.0	400	65	3400	3.38	216	242

6.6 INFLUENCE OF THE DENSITY

To evaluate the influence of the density on the sound absorption, the normal incidence sound absorption curves are shown in Figure 6.12 for the three different strand widths. The range of the density is chosen on the measured density range of the samples.

Increasing the density results in a higher flow resistivity, tortuosity and effective acoustical porosity and will therefore result in a higher sound absorption. The WWCB is more efficient in damping the vibrations by viscous and thermal effects. In the observed range, the SAA-value is only increasing. At some stage, the density will become too high, which means that the sound wave will be reflected, and the sound absorption will be reduced. This 'optimum density' will be predicted and discussed in Chapter 7.

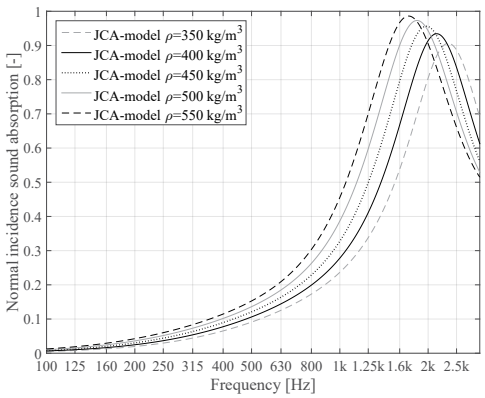

(a) 1.0 mm strand width

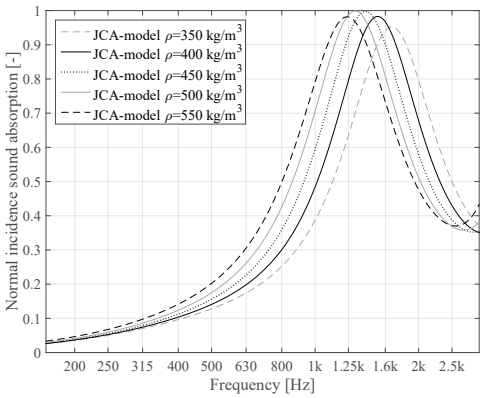

(b) 1.5 mm strand width

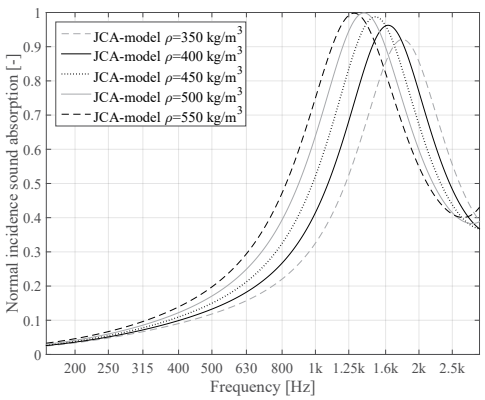

(c) 2.0 mm strand width

Figure 6.12: Influence of the bulk density on the normal incidence sound absorption.

Table 6.8: *SAA-values for different densities and strand widths.*

	Strand width [mm]		
Density [kg/m³]	**1.0**	**1.5**	**2.0**
350	0.27	0.34	0.32
400	0.31	0.36	0.35
450	0.34	0.37	0.37
500	0.36	0.38	0.39
550	0.39	0.39	0.40

6.7 INFLUENCE OF THE THICKNESS

As already mentioned in a previous study (Doudart de la Grée, 2014), the sound absorption will increase when increasing the thickness. This principle is explained in Chapter 2. The influence of the thickness (15, 25, 35, 50 and 100 mm) for the three strand widths is shown in Figure 6.13.

It is important to mention that in this comparison, it is assumed that the composition of the thicker WWCB is exactly the same as the validated 25 mm WWCB. In the demonstration of the model it is shown that this is the case for the 15 and 35 mm WWCB. But due to the densification within the thicker WWCB (> d= 50 mm), layers with different densities (see Section 5.8) are observed and the shown graphs do not take this into account. In case the production process is modified and the WWCBs are more homogeneous over the different layers, the presented values in Figure 6.13 are applicable.

While the boards characteristics are the same, changing the thickness will not influence the other input parameters for the JCA-model. Therefore, the input parameters are not given in the presented graphs.

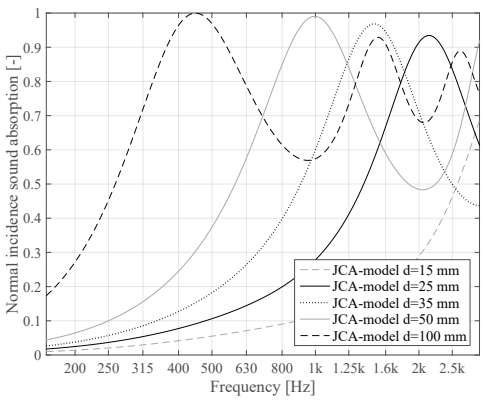

(a) 1.0 mm strand width

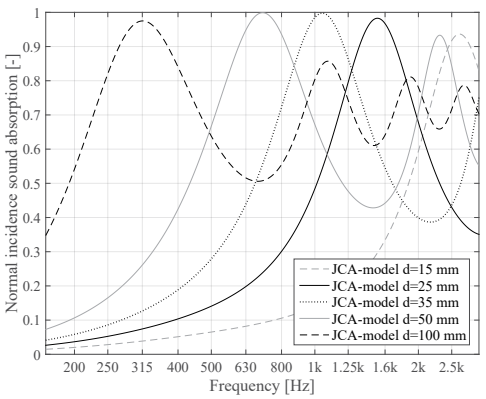

(b) 1.5 mm strand width

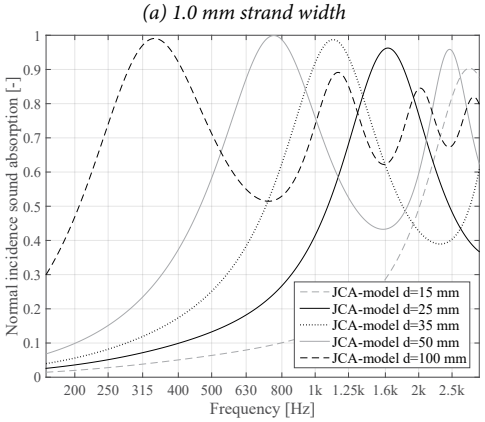

(c) 2.0 mm strand width

Table 6.9: *SAA-values for different thickness's and strand widths including the difference [%] to the 25 mm WWCB (ρ=400 kg/m³).*

	Strand width [mm]		
Thickness [mm]	**1.0**	**1.5**	**2.0**
15 (-40%)	0.13 (-58%)	0.21 (-42%)	0.19 (-46%)
25	0.31	0.36	0.35
35 (+40%)	0.40 (+29%)	0.43 (+19%)	0.42 (+20%)
50 (+100%)	0.49 (+58%)	0.55 (+53%)	0.54 (+54%)
100 (+200%)	0.71 (+129%)	0.71 (+97%)	0.72 (106%)

Figure 6.13: Influence of the thickness on the normal incidence sound absorption for three different strand widths.

6.8 INFLUENCE OF THE AIR-CAVITY

As discussed in Section 6.3.2 an air-cavity behind the WWCB will contribute to an increased sound absorption, due to standing waves inside the air-cavity and the resulting extra vibration in the construction. Increasing the air-cavity behind a 25 mm WWCB will have its optimum value between the 100 and 200 mm.

As is presented in the demonstration of the model in Section 6.3.2, the model was not able to predict the lower frequencies accurately. Therefore it needs to be noted that the presented influences in Figure 6.15 for e.g. the first quarter wavelength peak will therefore be slightly higher in practice.

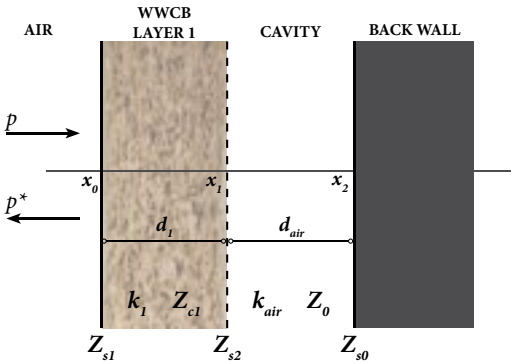

Figure 6.14: *Schematic overview of a multi-layer system with a WWCB-layer combined with an air-cavity.*

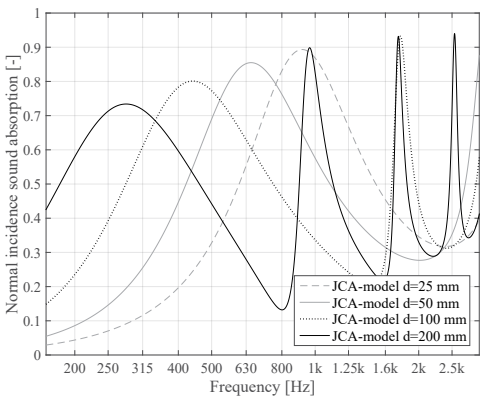

(a) 1.0 mm strand width

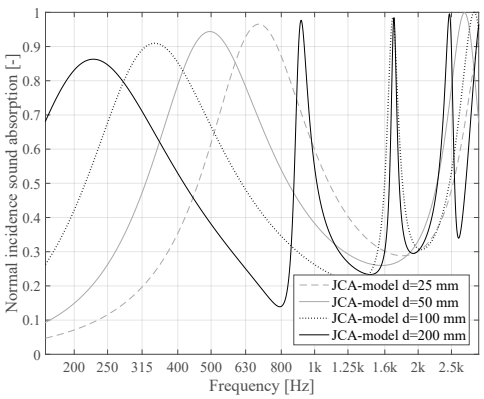

(b) 1.5 mm strand width

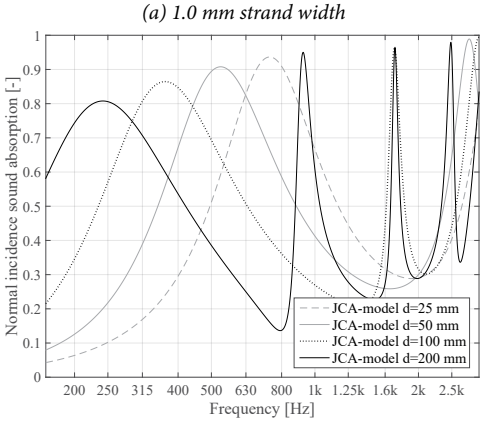

(c) 2.0 mm strand width

Table 6.10: *SAA-values for different air-cavities and strand widths (ρ=400 kg/m³)*

	Strand width [mm]		
Air-cavity [mm]	**1.0**	**1.5**	**2.0**
25	0.40	0.44	0.42
50	0.43	0.50	0.47
100	0.48	0.52	0.50
200	0.48	0.50	0.48

Figure 6.15: Influence of an air-cavity behind a 25 mm WWCB on the normal incidence sound absorption for three different strand widths.

6.9 INFLUENCE OF THE WOOD-TO-BINDER RATIO

6.9.1. Increased wood-to-binder ratio

In the study so far only regular WWCB is investigated, with the wood-to-binder ratio as mentioned in Section 5.2. Besides these boards, also boards with a higher binder amount, to increase the fire resisting properties, are evaluated (the so-called A2-boards). From these boards also samples are measured and the bulk properties are presented in Table 6.11.

Table 6.11: *Measured properties of the A2-WWCB.*

Strand width [mm]	Density range [kg/m³]	Thickness [mm]	Wood-to-binder ratio [-]
1.5	330-509	24	0.38-0.39

In Figure 6.16a the open porosity of the A2-boards, determined by the helium pycnometer, is presented and compared to the regular WWCB. Due the increased binder amount, the open porosity is lower for these WWCBs with the same density. This can be explained by the increased mass density of the binder compared to wood, which leads to less volume of material in the boards with an increased binder amount. Based on the comparison of the wood-to-binder ratio, it can be concluded that the 'standard' WWCB consists of ± 26.5% more wood that equals to a decrease of the porosity of ± 0.9%.

Not only does the porosity differ for these boards, but also the other input parameters for the JCA-model. It is for this reason that the derived relations between the bulk density and the input parameters cannot be used for the boards with an increased binder amount. Based on the results and analysis, presented in the previous chapters, it is expected that the increased binder amount will decrease the sound absorption compared to a regular WWCB with the same density. To test this, also A2-boards are measured in the impedance tube. The results are presented in Figure 6.15b and it can be concluded the sound absorption is indeed worse in comparison to the regular WWCB. The sound wave has less problems to go through the internal pore structure and therefore the viscous and thermal effects are reduced and less efficient for the A2-boards.

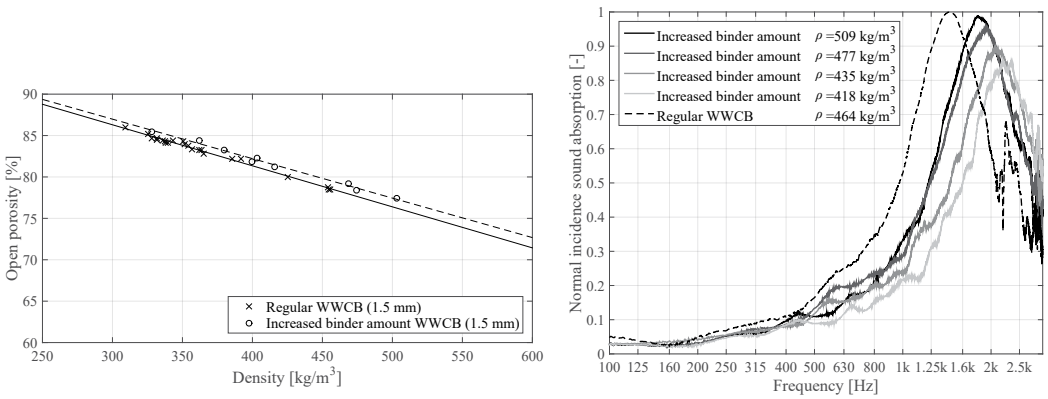

(a) *(b)*

Figure 6.16: *Measured (a) open porosity and (b) the normal incidence sound absorption of the regular WWCB and a board with an increased binder amount.*

For the boards containing of more binder, a correction factor needs to be introduced in order to predict the sound absorption of these boards. This is possible, as supported by the results presented in Figure 6.15b, where a same trend is visible when increasing the density, as it is for the regular WWCB.

6.9.2 Decreased wood-to-binder ratio

The previously described results for the regular WWCB shows an increased sound absorption if the density is higher. The main reason is the more complex path. Where in the study about the thermal insulation of the WWCB (De Groot, 2016) the boards with a decreased binder amount are showing better results, boards with an even lower binder amount were produced for these studies. From different samples, taken from these boards, also the open porosity and the normal incidence sound absorption are determined. The results are shown in Table 6.12 and Figure 6.17.

The produced boards consist of 2.0 mm strand width and show indeed a higher density. The expected decrease of the open porosity is visible, only the linear regression line is higher for the lower densities, which is shown in Figure 6.17a. Probably this is due to the limited number of samples measured in helium pycnometer. The sound absorption values are higher compared to the measured value for the a 'standard' WWCB, which support the found relations described before.

Table 6.12: *Measured properties of the WWCB with an decreased binder amount.*

Strand width [mm]	**Density range [kg/m³]**	**Thickness [mm]**	**Wood-to-binder ratio [-]**
2.0	436-529	25	-

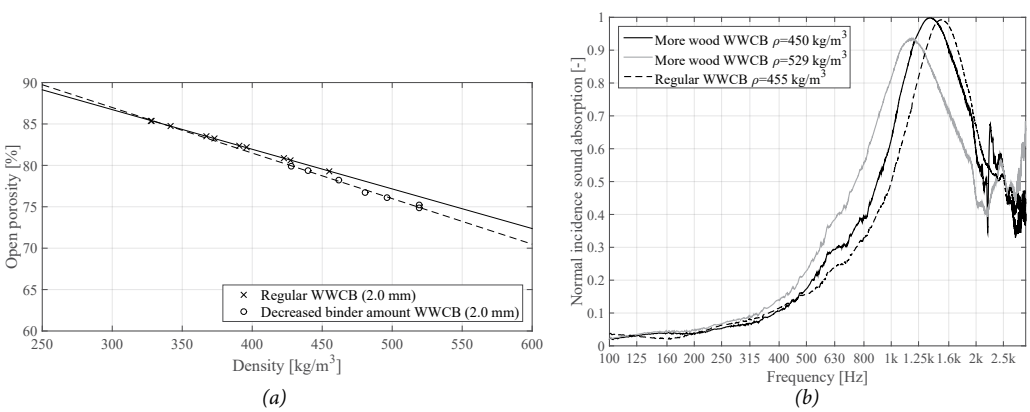

(a) *(b)*

Figure 6.17: *Measured (a) open porosity and (b) the normal incidence sound absorption of the regular WWCB and a board with an decreased binder amount.*

6.10 INFLUENCE OF THE MOISTURE CONTENT

The influence of the moisture content on the sound absorption is measured and shown in Figure 6.18.

To study this influence, firstly, the samples are measured in the impedance tube (under normal conditions containing ± 0.5-0.6 gram of moisture). Secondly, the same samples are dipped into a cup of water for a couple of minutes to make it saturated. This sample is put into a desiccator, where a relative humidity of 100% is created, for 24 hours to remove the excessive moisture and to only fill the cell walls and lumen of the wood fibres. Thirdly, the mass of the saturated sample is determined and its normal incidence sound absorption is measured. After that the sample it dried, the mass and the normal incidence sound absorption are measured again. Finally, at the moment the sample was back in its original state (more or less the same density) it is measured again in the impedance tube.

In theory, the cell walls and lumen of the wood fibres are able to take up water up to 220% (Norway spruce) of their own mass. Where it is not possible to exactly determine how much volume of wood is present in a WWCB-sample and, at the moment, it is also not known what the influence of the binder is on the amount of water that can be taken up by the wood fibres.

It can be seen a saturated sample show lower sound absorption values. But if the WWCB-sample is not completely saturated, but is still having a higher moisture content, the difference with the original sample is small.

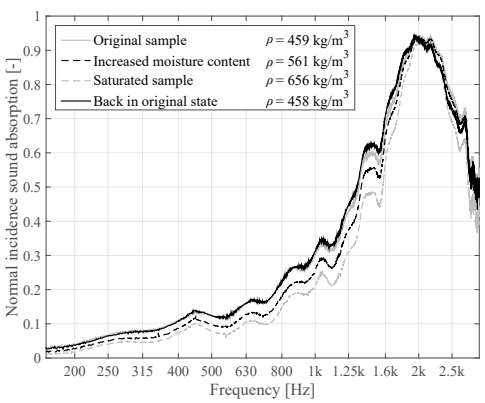

Sample	Density [kg/m³]	Assumed mass of wood [gr]	Moisture [gr]	Percentage [%]
Original	459	± 4.40	± 0.68	± 15.45
Increased	561	± 4.40	± 3.89	± 88.41
Saturated	656	± 4.40	± 6.76	±153.63

(a) 1.0 mm strand width (d=25 mm) - sample 1

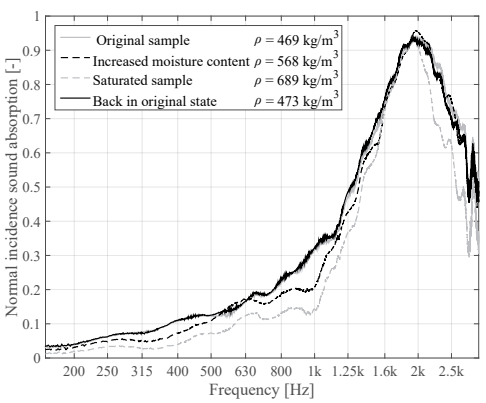

Sample	Density [kg/m³]	Assumed mass of wood [gr]	Moisture [gr]	Percentage [%]
Original	469	± 4.48	± 0.69	± 15.40
Increased	568	± 4.48	± 3.75	± 83.71
Saturated	689	± 4.48	± 7.47	± 167.74

(b) 1.0 mm strand width (d=25 mm) - sample 2

Figure 6.18: *Absorption curves for a WWCB-sample with different moisture contents.*

Table 6.13: *Measured 1/3-octave band values for a WWCB-sample having different moisture contents (belonging to Figure 6.17b).*

	Original sample	Increased moisture content	Saturated sample	Back in original state
200 Hz	0.04	0.03 (-25%)	0.02 (-50%)	0.04 (0%)
250 Hz	0.07	0.05 (-29%)	0.04 (-43%)	0.06 (-14%)
315 Hz	0.08	0.06 (-25%)	0.05 (-38%)	0.08 (0%)
400 Hz	0.11	0.09 (-18%)	0.07 (-36%)	0.11 (0%)
500 Hz	0.13	0.10 (-23%)	0.08 (-38%)	0.13 (0%)
630 Hz	0.15	0.12 (-20%)	0.10 (-33%)	0.15 (0%)
800 Hz	0.22	0.18 (-18%)	0.14 (-26%)	0.22 (0%)
1000 Hz	0.30	0.25 (-17%)	0.21 (-30%)	0.31 (3%)
1250 Hz	0.44	0.39 (-11%)	0.33 (-25%)	0.46 (5%)
1600 Hz	0.68	0.64 (6%)	0.57 (-16%)	0.71 (4%)
2000 Hz	0.91	0.91 (0%)	0.89 (-9%)	0.91 (0%)
2500 Hz	0.76	0.75 (-1%)	0.69 (-2%)	0.72 (-5%)
SAA	*0.32*	0.30 (6%)	0.27 (-16%)	0.33 (3%)

From these figures it seems like the influence of the moisture content is relatively small. But looking at the absorption values for the 1/3-octave bands presented in Table 6.13, relatively big errors are presented. For the higher frequencies, above 1600 Hz, there is almost no influence, but under this frequency a decrease of the normal incidence sound absorption is shown.

It does not completely confirm the theory described in Section 5.3, that increasing the moisture content of different samples, which leads to a decrease of the micro-porosity (cell walls and the lumen of the wood fibres are filled with moisture), does not significantly influence the sound absorption. But evaluating the increase of the density (+42.9%) it can be assumed that not all the micro pores take part in the acoustical process, which supports the decision to not make use of the open porosity measured by the helium pycnometer and instead the values obtained by the inverse calculation method. But due to the high error, it is questionable if it is correct to state none of the micro-pores are taken part in the acoustical process. Currently, not enough knowledge is available to draw conclusions what exactly happens when the moisture content is increased.

A conclusion that can be drawn is that the WWCB can be used for outdoor purposes and, the sound absorption properties, after getting wet, remain the same.

7. OPTIMIZING THE SOUND ABSORPTION OF WWCB

7.1 INTRODUCTION

Based on the results presented in the previous chapter, an optimization study can be performed. First of all it needs to be noted that the found relations between the bulk density and the input parameters for the JCA-model are determined within a specific range. It is possible to extrapolate these relations, e.g. to analyze higher densities, but it is unknown how accurate these values will be. Therefore, the presented optimization study in this chapter can only be used as an indication. Specific values will be given, but only trends will be used for discussion. To validate these outcomes is out of the scope of this study.

For the three different strand widths, first the density range and thickness will be evaluated. Secondly, the different air-cavities, with a WWCB-sample varying in density and thickness are investigated. Finally, the multi-layer construction is studied (an optimum construction for two WWCBs with varying densities).

Although the wood-to-binder ratio was considered in this study, no correction factors were created for the JCA-model. The influence of the wood-to-binder ratio has been measured in Section 6.9 and 6.10, but cannot be optimized in this study because currently it can not be modelled. From this study it can only be concluded that the wood-to-binder ratio needs to be as low as possible, while considering that it fulfils the stated requirements for the strength and fire resisting properties.

7.2 THICKNESS AND DENSITY

For a 25 mm thick WWCB the density is investigated in Figure 7.1 for the three strand widths. For the single number SAA-value, different optimum values are visible. Where the 1.5 mm strand width shows a peak around the 650 kg/m^3, the peaks of the 2.0 mm (700 kg/m^3) and 1.0 mm (800 kg/m^3) are at higher densities. These values follow the relations created between the bulk density and the input parameters and, as discussed earlier, it is unknown how accurate these values are. From the results presented in the previous chapter it was already expected the peak would be at a higher density and this is supported by the present results. WWCB with higher densities should be produced with the same wood-to-binder ratio, to validate if the predicted values are indeed correct.

In Figure 7.2 the density is evaluated for different thicknesses. From these contour-plot it can be concluded that at one stage the density will get too high, so that the thickness does not have a infuence on the sound absorption anymore. The influence of the thickness is greater for the lower densities, which can be explained by the fact that at a certain stage the flow resistivity will get too high and the path the sound wave has to travel will become too complex.

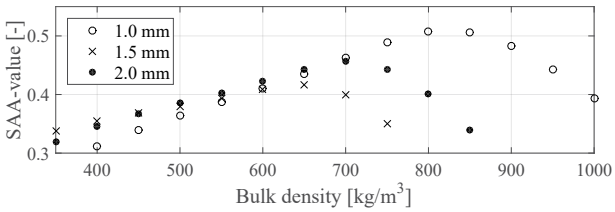

Figure 7.1: *SAA-values for different densities for the three different strand widths (d=25 mm).*

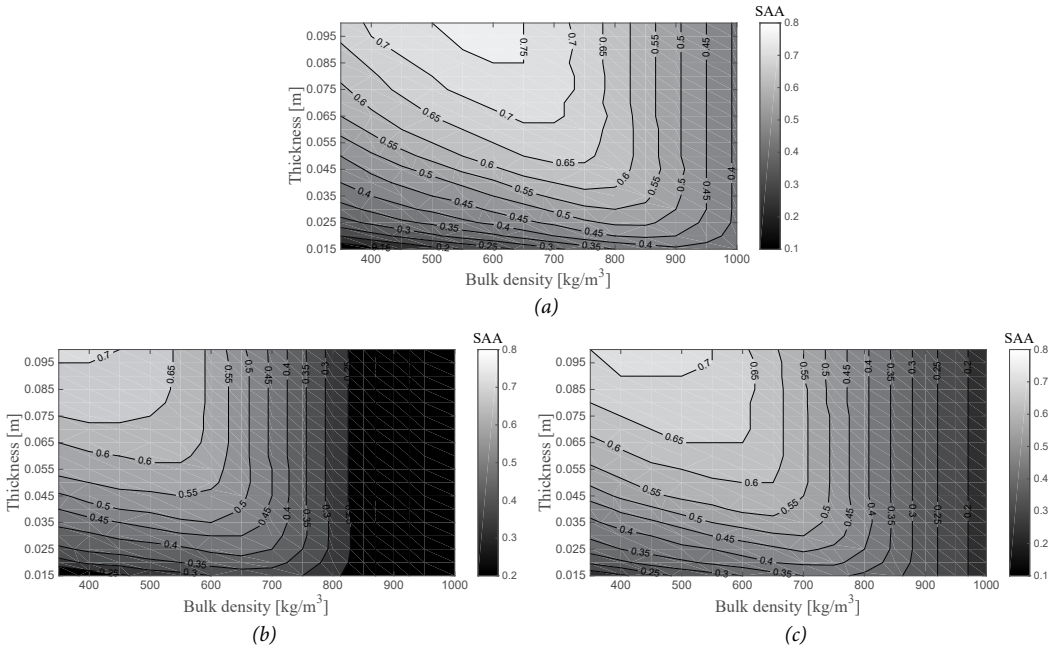

Figure 7.2: *SAA-values presented in a contour-plot for different densities and thickness's: (a) 1.0 mm strand width,(b) 1.5 mm strand width and (c) 2.0 mm strand width.*

7.3 AIR-CAVITY THICKNESS AND DENSITY

Based on the results of the influence of the air-cavity in Section 6.4, it can be concluded that an air-cavity will increase the sound absorption of WWCBs. To study the optimal thickness of this air-cavity, different air-cavity thicknesses (25-200 mm) are simulated with the WWCB using a wide range of densities (350 - 950 kg/m^3) and different thickness's (15, 25, 35 and 50) for the three different strand widths. The results, presented in contour-plots, are presented in Figure 7.4, 7.5 and 7.6 respectively.

From Figures 7.4-7.6 it can be concluded that the optimum construction is to apply a 15 mm thick WWCB (1.0 mm strand width) with a density of ±750 kg/m^3 and an air-cavity of ± 125 mm thick. For thicker WWCBs, the optimum value shifts to a lower density and a smaller air-cavity. For all the strand widths, the optimum thickness of the air-cavity is around the 100-150 mm.

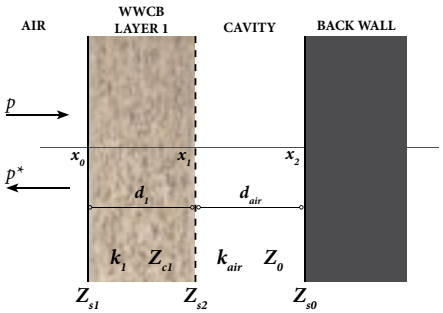

Figure 7.3: *Schematic representation of a construction with a WWCB combined with an air-cavity.*

1.0 mm strand width

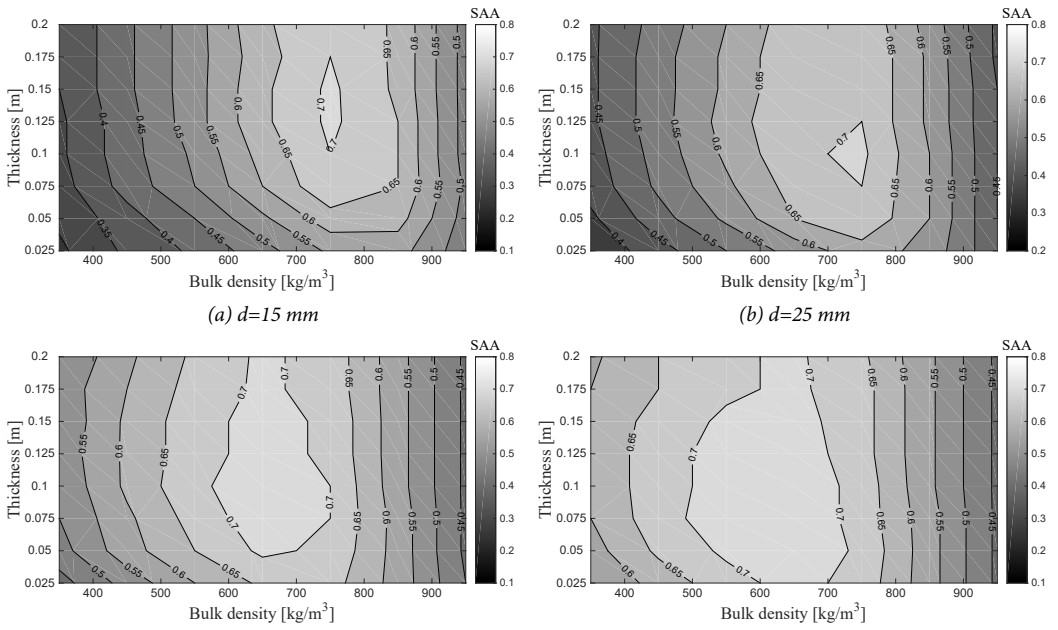

(a) d=15 mm *(b) d=25 mm*

(c) d=35 mm *(d) d=50 mm*

Figure 7.4: *SAA-values presented in a contourplot for different densities and air-cavities (1.0 mm strand width).*

1.5 mm strand width

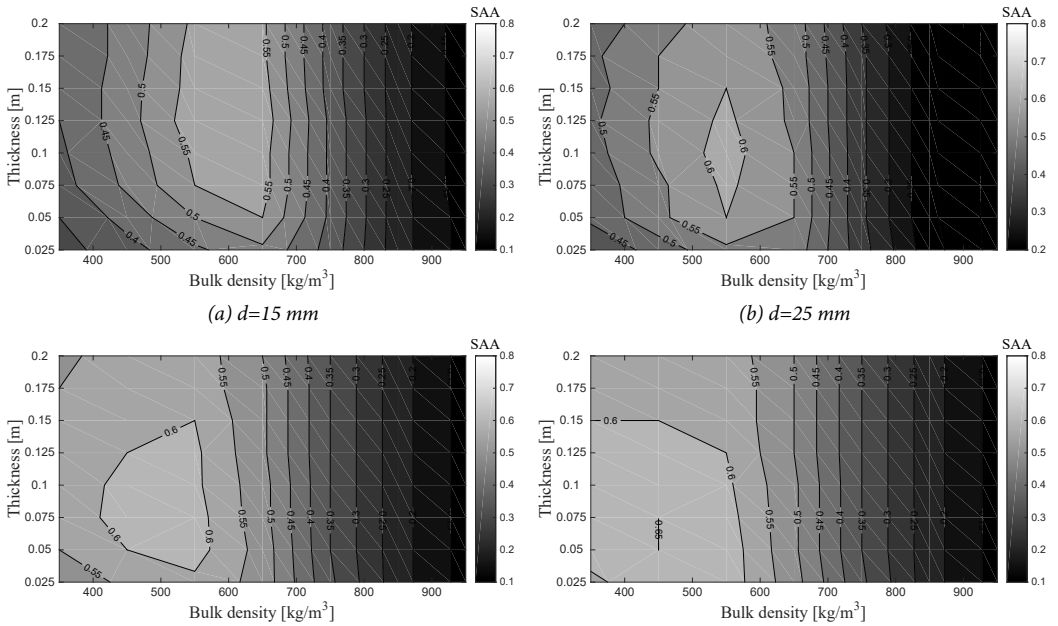

(a) d=15 mm *(b) d=25 mm*

(c) d=35 mm *(d) d=50 mm*

Figure 7.5: *SAA-values presented in a contourplot for different densities and air-cavities (1.5 mm strand width).*

2.0 mm strand width

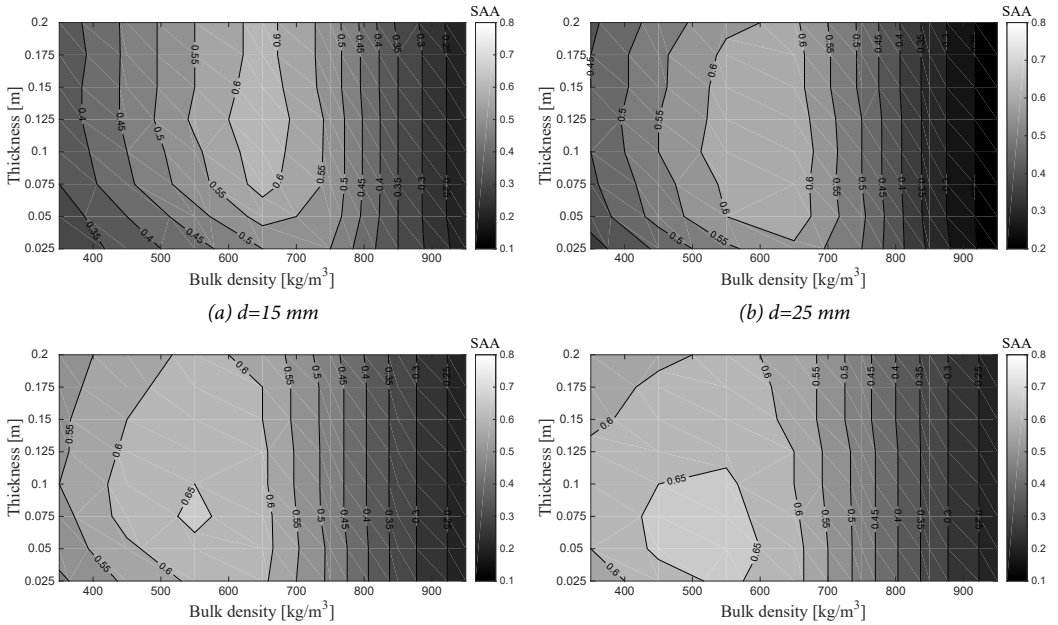

(a) d=15 mm *(b) d=25 mm*

(c) d=35 mm *(d) d=50 mm*

Figure 7.6: *SAA-values presented in a contourplot for different densities and air-cavities (2.0 mm strand width).*

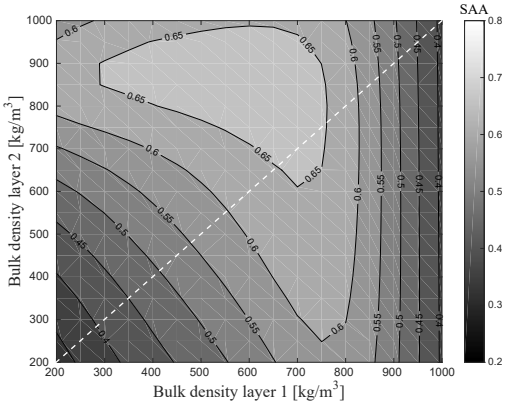

(a) 1.0 mm strand width (2x 25 mm thick WWCB)

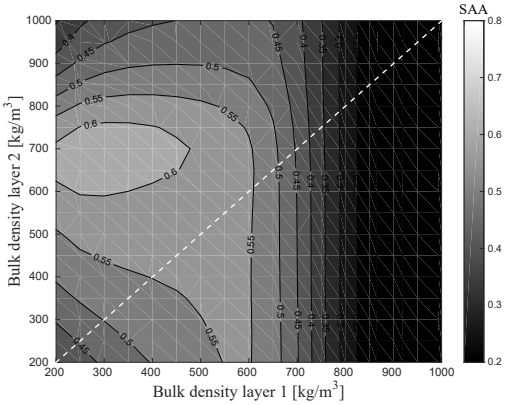

(a) 1.5 mm strand width (2x 25 mm thick WWCB)

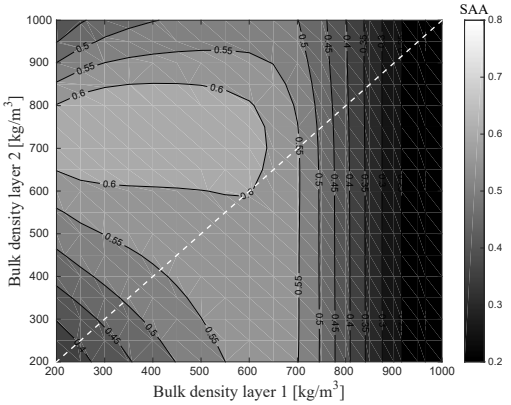

(c) 2.0 mm strand width (2x 25 mm thick WWCB)

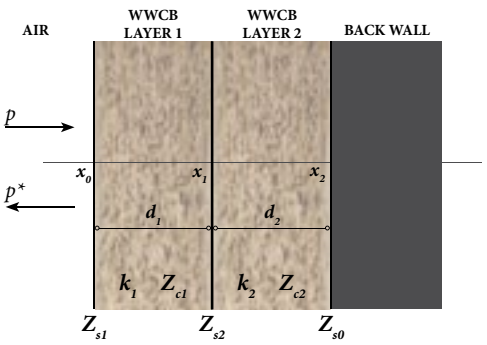

Figure 7.7: *SAA-values presented in a contourplot for different densities and air-cavities (1.0 mm strand width).*

7.4 MULTI-LAYER CONSTRUCTION (2X 25 MM WWCB)

In Figure 7.7 the influence is of a multi-layer construction is evaluated. Two WWCB-samples, both with a thickness of 25 mm, with variating densities are presented. The white dashed line represents a WWCB with a homogeneous density over the thickness. The main conclusion is that the first layer should contain a much lower density in comparison with the second layer. From the presented values it can be concluded that this will increase the sound absorption significantly.

This principle can be explained by the fact that the sound wave will be able to enter the construction relatively easily but will experience more resistance along the travelling path. For this study only two layers with a constant thickness are evaluated. For the manufacturer and for further research it will be interesting to study the combination of different thicknesses and multi-layers. It is expected this will increase the sound absorption even more.

7.5 INFLUENCE ON OTHER WWCB PROPERTIES

The overall conclusion is that increasing the density of the currently produced WWCBs will increase the sound absorption. An optimum value of the density for the sound absorption is presented in this chapter. A higher density will also increase the bending strength, but will negatively influence the thermal properties. Another outcome is that a decreased binder amount will have a positive influence on the sound absorption. This will be negative for the bending strength, as well as for the fire resistance. But it will positively influence the thermal properties. The outcomes of this study therefore need to be evaluated for the other properties to find an overall optimum.

8. DISCUSSION

Methodology

At the moment this study was started, no systematic study was performed on the sound absorption of WWCBs. In the chosen methodology first the WWCB was characterized and the production process was analysed to understand the results, secondly the possibility to model the acoustical properties was investigated and finally the sound absorption was optimized. The methodology was systematic and step-by-step more knowledge was gained on the sound absorption of WWCBs. The values obtained for the unknown parameters in the impedance model, by the inverse calculation method, are in line with the expectations, and a certain range was found when relating it to the bulk density of the WWCB. The comparison of the models gave a clear insight in the working of the different impedance and finally a suitable model was found for the WWCB. An indication how to optimize the sound absorption of the WWCB is given in the optimization study. Due to the uncertainty of the extrapolation of the found relations between the bulk density and the different parameters no exact numbers can be given. A validation study with the optimum values should be performed to evaluate how accurate these results are. It is demonstrated that the model is working for WWCBs with different thicknesses, densities and combined with an air-cavity measured for this study.

Limited frequency range

In this study the evaluated frequency range is limited (250-2000 Hz), which is due to the limited accuracy of the impedance tube. It would have been better to have a impedance tube with reliable results in the range of 125-4000 Hz, which would make it possible to increase the optimize number α_{ω}.

Acoustical effective open porosity

In the present study an indication was found that not all the measured open porosity in the helium pycnometer takes part in the acoustical process. It was not studied in more detail what the exact micro-pores are and if indeed some pores are too big to take part in the acoustical process.

Relations between the bulk density and the input parameters

In this study it is demonstrated that by making use of the found relations between the bulk density and the input parameters, the sound absorption of regular WWCB can be predicted. It only works for this specific wood-to-binder ratio range and the used recipe for the tested boards. In case the recipe is changed (like the boards with the increased fire resisting properties), a correction factor needs to be introduced.

9. CONCLUSIONS

The WWCBs are able to absorb sound due to the high open porosity, complex internal pore structure and irregular surface structure. The main influential parameters of the WWCB are the density, thickness, strand width and the wood-to-binder ratio.

The first conclusion is that the boards are highly inhomogeneous, which make them more difficult to characterize in comparison to homogeneous porous materials. Mainly due to the production process, the wood fibres are not equally divided over the surface (and for thicker boards also not over the thickness). Furthermore, the binder is not equally divided over the wood fibres, resulting in some fully and partly covered wood fibres.

Impedance model

The impedance models evaluated in this study are the Miki, Zwikker and Kosten, Attenborough, Johnson-Champoux-Allard (JCA) and Johnson-Champoux-Allard-Lafarge (JCAL) models. The Miki and Zwikker and Kosten models are suitable for porous materials having straight cylindrical pores and it was found these models are not working for the WWCB. The JCAL-model was able to meet the measured sound absorption values in the impedance tube, but it has too many unknown input parameters to be able to get unique results for these parameters during the inverse calculation method. The Attenborough and JCA model are able to meet the measured sound absorption and

unique values were found for the input parameters. Comparing these models, the error for the JCA-model is lower for the lower frequencies and almost the same for the higher frequencies. It is finally concluded that the Johnson-Champoux-Allard (JCA) model was found to be most appropriate to fit the normal incidence sound absorption values in the impedance tube.

The JCA-model requires five input parameters; the open porosity, flow resistivity, tortuosity and viscous and thermal characteristic lengths. The flow resistivity was directly measured. Where it is difficult to measure the tortuosity and the characteristic lengths (especially for the WWCB), it was decided to determine these values by the inverse calculation method, by making use of the curve fitting approach based on the measured sound absorption curve in the impedance tube.

Acoustical effective open porosity

Sensitivity analysis for the porosity in the JCA-model and based on literature shows that the measured open porosity in the helium pycnometer was too high. Therefore, instead of making use the measured open porosity, this value was determined by the inverse calculation method. The fitted results are indeed showing lower values, which means that not all the porosity measured by the helium pycnometer is contributing to sound absorption. This can be explained by the fact that some pores are too big and some parts are too small to take part in the acoustical process.

Sensitivity of the input parameters in the JCA-model

The input parameters are not only related to the bulk density, but also to each other. So in practice it is not possible to analyze the influence of the input parameters separately. However, for the impedance model, a sensitivity analysis is performed for the different input parameters to evaluate its influence in the JCA-model. It can be concluded that the acoustical effective open porosity and the flow resistivity are mainly influencing the quarter wave length peaks. The tortuosity and the viscous characteristic length are also influencing both the height and peak location of the peak. It was found that changing the thermal characteristic length does not have a significant influence on the sound absorption curve.

Relations between the bulk density and the input parameters

To increase the practical use of the impedance model, the five input parameters for the JCA-model are related to the bulk density. Relations are created for every strand width. It can be concluded that the JCA-model, making use of the relations between the bulk density and the input parameters, is able to predict the sound absorption of the inhomogeneous WWCB with a root mean square error between the 0.01 and 0.03 for the 1/3-octave bands in the 200-2500 Hz frequency range for all the evaluated WWCBs. This validation study is performed for three different strand widths, different thicknesses (15, 25, 35 and 50 mm), applying an air-cavity or combining different WWCB-layers and for making use of another porous material behind it.

Influence of the WWCB parameters on the sound absorption

Increasing the thickness will improve the overall sound absorption, especially due to the fact a thicker WWCB will be more efficient in the lower frequencies. Increasing the thickness of a 1.0 mm strand width with a density of 400 kg/m^3 from 25 mm to 50 mm will increase the SAA-value with 58% (SAA-value from 0.31 to 0.49).

Increasing the bulk density leads to an improved sound absorption. In the optimization study it was found was the at a certain point the bulk density will get too high and since then the sound absorption will decrease. For the 1.0 mm strand the found optimum density is ± 825 kg/m^3 and the SAA-value will be 0.51.

In this study, the influence of the strand width cannot be seen separately from the recipe. Evaluating the whole density range, it can be concluded that the 1.0 mm strand width is showing the best results. In the lower density range, due to the higher binder amount of the 1.0 mm strand width, the 1.5 mm strand width is showing better results, as presented in Figure 6.11.

Considering the same bulk density, increasing the wood-to-binder ratio will negatively influence the sound absorption. This is due to the higher mass content of cement and therefore total volume is lower, which for example decreases the flow resistivity and tortuosity. Next to this also WWCB with a higher amount of wood fibres are evaluated. The opposite counts for the above described analysis for a WWCB with a higher binder amount. Which means a WWCB with a higher amount of wood fibres results in a higher sound absorption, compared to a regular WWCB.

Applying an air-cavity increases the sound absorption. In case only the sound absorption properties are important, less material can be used and the same or even higher absorption values can be achieved compared to a WWCB fixed directly to a solid wall or ceiling. An optimum air-cavity thickness is found between 100 and 150 mm.

Different samples, which differ in density, can be applied in a multi-layer system. Also combinations with mineral wool, which increases the sound absorption significantly, are validated by combining the JCA-model (for the WWCB-sample) and the Miki-model (for the mineral wool sample).

10. RECOMMENDATIONS FOR FURTHER RESEARCH

Based on the outcomes of the present study, the following parts are interesting for further research.

Production process
Mainly due to the production process, the WWCBs are inhomogeneous. In order to be able to control and to optimize the final sound absorption of the WWCB it is interesting to study the possibilities to optimize the production process. In this way there will be more control of the bulk properties of the produced WWCB and the optimization study can be performed in practice.

Extend the found relations between bulk density and to the input parameters to different recipes
All over the world WWCB are produced, with different recipes and different wood-to-binder ratios. The present study focuses on the commercial WWCB from one manufacturer. And the created model is only suitable for the composition of these WWCB. In case the binder amount is significantly changed the created relation between the bulk density and the input parameters do not likely work anymore. Therefore it is interesting to study if it possible to create a model where the density and the wood-to-binder ratio can be used as input parameter, to make the impedance more universally usable.

Extrapolation of the created relations between the bulk density and the input parameters
Measured density ranges are used to create relations to predict values outside these measured ranges. How accurate the results are outside these ranges, is still unknown. Therefore, it will be interesting to study this (i.e. produce WWCB with a density outside the measured range and to study if the predicted values are correct).

Influence of the micro-porosity
In this study a start is made to investigate the influence of the micro-porosity. It has been proven that not all the micro-porosity takes part in the acoustical process, but it is not known how much the micro-porosity exactly is and what its influence is on the sound absorption.

Low frequency analysis
It is still of main interest to study the possibilities to change the WWCB in such a way it can be applied as a low frequency absorber. In this study the main focus was on the material WWCB itself, but by applying a porous sheet, plate or membrane, which will work as a resonant absorbers, in front of the WWCB, will increase the low frequency sound absorption.

Different shape of the board
In this study the main focus was on modelling the sound absorption in 1-D. To increase the applicability of WWCB in practice it also of interest to evaluate the sound absorption in 2-D and 3-D. This can be done by e.g. modelling the WWCB in COMSOL and evaluate the effect on the sound absorbing properties of different shapes and different surface structures (Like the boards produced by Baux or Troldtekt).

(a) *(b)*

Figure 10.1: WWCB produced by (a) Troldtekt and (b) Baux.

11. ACKNOWLEDGEMENTS

First of all I would like to thank my parents, Joop and Greet, and my sister, Lisanne for supporting me to reach my goals, for letting me do my own thing and letting me take my time without putting any pressure on me. I am sure without the freedom that I had I would not be able to stand where I am now.

Next to that, I would like to thank Niels Hoekstra for his help in the acoustical lab and Marco de Groot and Veronica Caprai for their help in the Building Physics lab.

Finally, I would like to acknowledge the STW-foundation, Dr. Jan van Dam (Wageningen UR), Knauf Insulation, ENCI B.V., Eltomation, and van Gansewinkel minerals for their provision of material and technology. Furthermore, I would like to thank the Building Acoustics and Building Materials group for their support, supervision and help when it was necessary.

BIBLIOGRAPHY

Allard, J. F., & Atalla, N. (1993). *Propagation of sound in porous media: Modelling sound absorbing materials* (First edit.). New York: Wiley and Sons. Ltd.

Aro, M. (2008). Wood strand cement board. *In 11th International Inorganic-Bonded Fiber Composites Conference* (pp. 169–179). Madrid, Spain.

Atak, O., Huijssen, J., Rychtarikova, M., Pluymers, B., & Desmet, W. (2010). Application of the wave based method for mid-frequency analysis on a room acoustics case. P*roceedings of ISMA: International Conference on Noise and Vibration Engineering,* 1969–1984.

Attenborough, K. (1983). Acoustical characteristics of rigid fibrous absorbents and granular materials. *The Journal of the Acoustical Society of America*, 73(3), 785. doi:10.1121/1.389045

Baux. (2016). *Baux acoustic panels*. Retrieved from http://www.baux.se/

Bécot, F.-X., Chevillotte, F., Gauthier, M., Jaouen, L., & Rodenas, J. (2016). *Matelys*. Retrieved from www.matelys.com

Beekman, T. (2012). *Geluidsabsorptie van sedumdaken*. Hogeschool Fontys.

Beranek, L. L. (1942). Acoustic impedance of porous materials. *The Journal of the Acoustical Society of America,* 13(3), 248–260. doi:10.1121/1.1916172

Biot, M. A. (1956). Theory of propagation of elastic waves in a fluid-saturated porous solid. I. Low-frequency range. *The Journal of the Acoustical Society of America*, 28(2), 168–178. doi:10.1121/1.1908239

Bodén, H., Carlsson, U., Glav, R., Wallin, H.-P., & Åbom, M. (2005). *Sound and vibration*. Stockholm: KTH - Royal Institute of Technology.

Caprai, V., Doudart de la Grée, G. C. H., Yu, Q. L., & Brouwers, H. J. H. (2015). *Application of an innovative binder in wood wool cement board.* Eindhoven University of Technology. Retrieved from http://alexandria.tue.nl/extra2/afstversl/bwk/Caprai_2015.pdf

Champoux, Y. (1992). On acoustical models for sound propagation in rigid frame porous materials and the influence of shape factors. *The Journal of the Acoustical Society of America,* 92(2), 1120. doi:10.1121/1.405281

Champoux, Y., & Allard, J. F. (1991). Dynamic tortuosity and bulk modulus in air-saturated porous media. *Journal of Applied Physics,* 70(4), 1975–1979. doi:10.1063/1.349482

Champoux, Y., Stinson, M. R., & Daigle, G. A. (1991). Air-based system for the measurement of porosity, *The Journal of the Acoustical Society of America,* 89(2), 910–916. doi:10.1121/1.1894653

Cox, T. J., & D'Antonio, P. (2009). *Acoustic Absorbers and Diffusers: Theory, design and application* (2nd editio.). Oxon: Taylor & Francis.

de Groot, M. C. (2016). *An optimization of the thermal conductivity of wood-wool composites*. Eindhoven University of Technology. Thesis in progress.

Delany, M. E., & Bazley, E. N. (1970). Acoustical properties of fibrous absorbent materials. *Applied Acoustics*, 3(2), 105–116.

Doudart de la Grée, G. C. H., Yu, Q. L., & Brouwers, H. J. H. (2014a). Wood-wool cement board : Optimized inorganic coating, 154–164. In H. V. T. Huong & H. M. Thygesen (Eds.), *International Inorganic-Bonded Fiber Composites Conference (IIBCC)*, 154–164, Da Nang, Vietnam. Retrieved from https://pure.tue.nl/ws/files/3856782/572985535976567.pdf

Doudart de la Grée, G. C. H., Yu, Q. L., & Brouwers, H. J. H. (2014b). Wood-wool cement board: potential and challenges. *In Proceedings of the 5th International Conference Non-Traditional Cement and Concrete (NTCC2014),* 279–282. Brno, Czech Republic. Retrieved from https://pure.tue.nl/ws/files/3841378/449247297565249.pdf

Fuchs, H. V. (2013). A*pplied Acoustics: Concepts, Absorbers, and Silencers for Acoustical Comfort and Noise Control*. Statewide Agricultural Land Use Baseline 2015 (Vol. 1). doi:10.1017/CBO9781107415324.004

Giesche, H. (2006), Mercury porosimetry: A general (practical) overview. Particle and Particle Systems Characterization, *Particle & Particle Systems Characterization*, 23(1), 9–19. doi:10.1002/ppsc.200601009

Glé, P., Gourdon, E., & Arnaud, L. (2011). Acoustical properties of materials made of vegetable particles with several scales of porosity. *Applied Acoustics,* 72(5), 249–259. doi:10.1016/j.apacoust.2010.11.003

Glé, P., Gourdon, E., & Arnaud, L. (2012). Modelling of the acoustical properties of hemp particles. *Construction and Building Materials,* 37, 801–811. doi:10.1016/j.conbuildmat.2012.06.008

Hoekstra, N. (2016) *Sound absorption of periodically spaced baffles.* Eindhoven University of Technology. Thesis in progress.

Horoshenkov, K. V., & Swift, M. J. (2001). The effect of consolidation on the acoustic properties of loose rubber granulates. *Applied Acoustics*, 62, 665–690. doi:10.1016/S0003-682X(00)00069-4

Hucheng, Q., & Martin, R. (2014). Characterizing the sound absorption of wood concrete. *In International Inorganic-Bonded Fiber Composites Conference* , 176–184, Da Nang, Vietnam.

Jeong, C.-H. (2013). Converting Sabine absorption coefficients to random incidence absorption coefficients. *The Journal of the Acoustical Society of America*, 133(6), 3951–3962. doi:10.1121/1.4802647

Johnson, D. L., Koplik, J., & Dashen, R. (1987). Theory of dynamic permeability and tortuosity in fluid-saturated porous media. *Journal of Fluid Mechanics*, 176(1), 379. doi:10.1017/S0022112087000727

Kirchhoff, G. (1868). On the influence of heat conduction in a gas on the motion of sound. *Annalen Der Physik*, 134, 177–193.

Kleiner, M. (2011). *Acoustics and Audio Technology.* (J. Ross Publishing, Ed.) (Third edit.).

Kollmann, F., & Schneider, A. (1963). On the Sorption Behaviour of Heat Stabilized Wood. *Holz Als Roh - Und Werkstoff*, 3, 77–85.

Kuttruff, H. (2007). *Acoustics: An introduction.* Statewide Agricultural Land Use Baseline 2015 (Vol. 1). Abingdon, Oxon: Taylor & Francis. doi:10.1017/CBO9781107415324.004

Kuzniarz, J. J. (1973). Hearing loss and speech intelligibility in noise. *In Proceedings of the international congress on noise as a public health problem* (pp. 57–71). Dubrovnik, Yugoslavia.

Lafarge, D., Lemarinier, P., Allard, J. F., & Tarnow, V. (1997). Dynamic compressibility of air in porous structures at audible frequencies. *The Journal of the Acoustical Society of America*, 102(4), 1995–2006. doi:10.1121/1.419690

Leclaire, P. (2012). Characterization of porous absorbent materials. *In Proceedings of the Acoustics,* 25-27 April (pp. 1883–1888). Nantes, France.

Martin, R., & Hucheng, Q. (2008). The practice of manufacturing durisol noise barrier panels. *In 11th International Inorganic-Bonded Fiber Composites Conference (IIBCC)* (pp. 198–202). Madrid, Spain. Retrieved from http://iibcc.net/media/9796/Rohn-the-practice-of-manufacturing.pdf

Miki, Y. (1990). Acoustical properties of porous materials. Modifications of Delany-Bazley models. *Journal of the Acoustical Society of Japan (E)*.

Morse, P. M., & Ingard, K. U. (1968). *Theoretical Acoustics.* New York: McGraw-Hill.

Oliva, D., & Hongisto, V. (2013). Sound absorption of porous materials – Accuracy of prediction methods. *Applied Acoustics,* 74(12), 1473–1479. doi:10.1016/j.apacoust.2013.06.004

Olny, X., & Panneton, R. (2008a). Acoustical determination of the parameters governing thermal dissipation in porous media. *The Journal of the Acoustical Society of America*, 123(April 2006), 814–824. doi:10.1121/1.2828066

Olny, X., & Panneton, R. (2008b). Acoustical determination of the parameters governing viscous dissipation in porous media. *The Journal of the Acoustical Society of America*, 123(April 2006), 814–824. doi:10.1121/1.2828066

Olny, X., Panneton, R., & Tran-Van, J. (2002). An indirect acoustical method for determining intrinsic parameters of porous materials. *In Proceedings of the 2nd Biot conference*, Grenoble, France.

Peerlings, L. (2015). *Methods and techniques for precise and accurate in-duct aero-acoustic measurements: Application to the area expansion.* Statewide Agricultural Land Use Baseline 2015 (Vol. 1). doi:10.1017/CBO9781107415324.0 04

Pereira, C., Caldeira Jorge, F., Irle, M., & Ferreira, J. M. (2006). Characterizing the setting of cement when mixed with cork, blue gum, or maritime pine, grown in Portugal II: X-ray diffraction and differential thermal analyzes. *Journal of Wood Science,* 52(4), 318–324. doi:10.1007/s10086-005-0775-y

Rayleigh, Lord. (1945). *Theory of sound.* New York: Dover publications.

Seddeq, H. S. (2009). Factors Influencing Acoustic Performance of Sound Absorptive Materials. *Australian Journal of Basic and Applied Sciences,* 3(4), 4610–4617.

Tijsma, T. W. (2014). *Impedance tube Measurement protocol*, Eindhoven University of Technology

van Elten, G. J. (2006). Production of wood wool cement board and wood strand cement board (Eltoboard) on one plant and applications of the products. *In 10th International Inorganic-Bonded Fiber Composites Conference* (pp. 1–12). Sao Paulo, Brazil. Retrieved from http://eltomation.nl/Eng/Publications/Lecture IIBCC WWCB.pdf

Wassilieff, C. (1996). Sound absorption of wood-based materials. *Applied Acoustics*, 48(4), 339–356.

Zwikker, C., & Kosten, C. W. (1949). *Sound absorbing materials.* New York: Elsevier.

APPENDIX A

MATLAB-SCRIPT FOR THE DIFFERENT IMPEDANCE MODELS

DELANY-BAZLEY-MIKI MODEL

```
d          =;              %Thickness of the sample
density    =;              %Bulk density of the sample
fvector    =;              %Frequency range
rho0       =1.204;         %Denotes value in air where ambiguity might otherwise arise [kg/m3]
c0         =;              %Speed of sound (m/s)
z0         =rho0*c0;       %Specific acoustic impedance of air (Kg/m2*s)
sigma      =;              %Airflow resistivity [Ns/m4]
omega      =2*pi*fvector;  %Angular frequency [s^-1]


%% Compute variable X and print frequency limits of validity for the two models
X = fvector/sigma;
f_min = 0.01*sigma
```

```
f_max = 1.00*sigma

%% Revised expressions of Delany and Bazley model by Miki

Z_Miki = rho0*c0*( 1 + 5.50*(X*1000).^(-0.632)- i*8.43*(X*1000).^(-0.632) );

k_Miki = omega/c0 .* (-i) .* ( 11.41*(X*1000).^(-0.618)+ i* (1 + 7.81*(X*1000).^(-0.618) ) );

%% Compute sound absorption for a sample of thickness d backed by a rigid and impervious wall under at room
temperature and pressure conditions

Z_s = -j.*Z_Miki./tan(k_Miki*d);
a= 1 - ( abs( (Z-rho0*c0)./(Z+rho0*c0) ) ).^2;
```

ATTENBOROUGH MODEL

```
%Input parameters
d           =;          %Thickness of the sample
density     =;          %Bulk density of the sample
fvector     =;          %Frequency range
rho0        =1.204;     %Denotes value in air where ambiguity might otherwise arise [kg/m3]
c0          =;          %Speed of sound (m/s)
z0          =rho0*c0;   %Specific acoustic impedance of air (Kg/m2*s)
tort        =;          %Tortuosity [-] range[1-3]
sigma       =;          %Airflow resistivity [Ns/m4]
epsilon     =;          %Porosity [-]
omega       =2*pi*fvector;  %Angular frequency [s^-1]
eta         =18.27e-6;  %Visocity of air [Poiseuille] 1.84*10^-5
P0          =101320;    %Atmospheric pressure [N/m2]
gamma       =1.4;       %Ratio of the specific heat capacity [-]
Cp          =1.01;      %Specific heat capacity of air at constant pressure [J/kg/K]
kappa       =2.41*10^-2;%Thermal conductivity of air [Wm/K]
Npr         =0.71;      %Prandtl number (0.77 at 20*C)
s_b         =;          %Shape factor

% Effective (/dynamic) Density
% Accounts for the viscous losses
%-----------------------------------------------------------------

lambda=(1/2*s_b)*((8*tort*rho_0*omega)./(sigma*epsilon)).^0.5;
T_bes=besselj(1,lambda*sqrt(-i))./besselj(0,lambda*sqrt(-i));
rho_c=((tort*rho0)/epsilon)*(1-(2./lambda*sqrt(-i)).*T_bes).^-1;
```

```
% Effective (/dynamic) bulk modulus
% Accounts for the thermal losses
%-----------------------------------------------------------------

T_bes2=besselj(1,Npr^0.5*lambda*sqrt(-i))./besselj(0,Npr^0.5*lambda*sqrt(-i));
K_w=((gamma*P0)/epsilon)*(1+((2*(gamma-1))./(Npr^0.5*lambda*sqrt(-i))).*T_bes2).^-1;

%Characteristic Impedance
Zc=(K_w.*rho_c).^0.5;

%Complex wave number
k_c=omega.*sqrt(rho_c./K_w);

%Surface impedance of sample
Zs=-1i*Zc.*cot(k_c*d);

%Normalised impedance
Zn=Zs/z0;

%Reflection coefficient
R=(Zs-z0)./(Zs+z0);

%Absorption coefficent
a=1-(abs(R)).^2;
```

JOHNSON-CHAMPOUX-ALLARD (JCA) MODEL

```
%Input parameters:
density         =;
fvector         =;          %Frequency range
d               =;          %Thickness of the sample
rho0            =1.204;     %Denotes value in air where ambiguity might otherwise arise [kg/m3]
c0              =;          %Speed of sound (m/s)
z0              =rho0*c0;   %Specific acoustic impedance of air (kg/m²*s)
alpha_inf       =;          %Tortuosity [-]
sigma           =;          %Airflow resistivity [Ns/m⁴]
epsilon         =;          %Porosity [-] range [0-1]
omega           =2*pi*fvector;  %Angular frequency [s^-1]
eta             =1.84*10^-5;    %Visocity of air [Poiseuille] (1.84*10^-5 )
viscous         =;          %Viscous characteristic dimension [m] [range 10-1000 10^-6m]
thermal         =;          %Thermal characteristic dimension [m] [range 10-1000 10^-6m]
P0              =101320;    %Atmospheric pressure [N/m²]
```

```
gamma          =1.4;          %Ratio of the specific heat capacity [-]
Npr            =0.71;         %Prandtl number (0.77 at 20*C)

% Effective (/dynamic) Density
% Accounts for the viscous losses
%-----------------------------------------------------------------
rho_eq=(tort*rho0/epsilon).*(1+((sigma*epsilon)./(1i*omega*rho0*tort)).*sqrt(1+((1i*4*(tort^2)*eta*rho0*omega)/
((sigma^2)*((viscous*10^-6)^2)*(epsilon^2)))));

% Effective (/dynamic) bulk modulus
% Accounts for the thermal losses
%-----------------------------------------------------------------
K_eq=(gamma*P0/epsilon)./(gamma-(gamma-1).*(1+(((8*eta)./((((thermal*10^-6)^2)*Npr*rho0*omega*1i)).*sqrt(1+(1i*
(((thermal*10^-6)^2)*Npr*rho0*omega)/(16*eta))))).^-1);

%Characteristic Impedance
Zc=(K_eq.*rho_eq).^0.5;

%Complex wave number
k_c=omega.*sqrt(rho_eq./K_eq);

%Surface impedance of sample
Zs=-1i*Zc.*cot(k_c*d);

%Normalised specific acoustic impedance
Zn=Zs./z0;

%Reflection coefficient
R=(Zs-z0)./(Zs+z0);

%Absorption coefficent
a=1-(abs(R)).^2;
```

APPENDIX B

MATLAB-SCRIPT FOR THE IMPEDANCE TUBE MEASUREMENTS

```
clear all       % Clears all previously defined variables in matlab
close all       % Closes all open figure windows

%_____________________________________________________________________
% DATA INPUT & INPUT PARAMTERS
% _____________________________________________________________________

load IRmic1.txt                 % Loads the impulse responses measured at mic. pos. 1, 2, 3,
load IRmic2.txt                 % 5 and 6 into matlab. In order to be able to do so, the
load IRmic3.txt                 % filenames of the impulse response text files should
load IRmic4.txt                 % should be the same as the file names in the load
load IRmic5.txt                 % command and the header should be removed
load IRmic6.txt

fs = 192000;                    % sample frequency [Hz] The number of samples
                                % taken per second by the audio device (sampler)
```

```
z1 = 1.188;                          % Distance from mic1 to the specimen surface [m]
z2 = 0.8480;                         % Distance from mic2 to the specimen surface [m]
z3 = 0.550;                          % Distance from mic3 to the specimen surface [m]
z4 = 0.310;                          % Distance from mic4 to the specimen surface [m]
z5 = 0.1890;                         % Distance from mic5 to the specimen surface [m]
z6 = 0.0596;                         % Distance from mic6 to the specimen surface [m]
z_values = [z1; z2; z3; z4; z5; z6]; % Vector with all z values for convenience

fvector = [150:2800];                % Frequency vector [Hz] Defines the frequency range
                                     % of interest. For this frequency range the
                                     % absorption factor of the material will be calculated

zt = 1.3690;                         % Distance from the source to the specimen surface [m]
                                     % The distance is used to determine the amount of
                                     % samples used for cross correlation of the signals
                                     % and can be measured using for example a tapemeasure

%_____________________________________________________________________________
% CALCULATED PARAMETERS
%_____________________________________________________________________________
IR1 = IRmic1(1:fs,1);                % Impulse response measured by microphone 1
IR2 = IRmic2(1:fs,1);                % Impulse response measured by microphone 2
IR3 = IRmic3(1:fs,1);                % Impulse response measured by microphone 3
IR4 = IRmic4(1:fs,1);                % Impulse response measured by microphone 4
IR5 = IRmic5(1:fs,1);                % Impulse response measured by microphone 5
IR6 = IRmic6(1:fs,1);                % Impulse response measured by microphone 6
IR = [IR1 IR2 IR3 IR4 IR5 IR6];      % Matrix with all IRs for convenience

% Defines the location of the data for the first second of the impulse
% response. For example the first second of the impulse response measured
% by microphone 1 is located in the file IRmic1 (IRmic1.txt was loaded
% previously), the data is located in rows 1 to fs, column 1

% % Find reference peak to determine the sample ranges for peak 1 and peak 2
% % for all Impulse Responses
% [ref_peak,~]=find(IR5(1:1000)==max(IR5(1:1000)));
% ref_peak = ref_peak+100;
%
% % Calculate the number of samples between the peak of the direct wave and
% % the peak of the reflected wave. Subsequently calculate sound speed from
```

```
% % the differences in all Impulse Responses
% peak = zeros(4,2);                          % Pre-allocation
% c_values = zeros(4,1);                      % Pre-allocation
%
% for pp = (1:4)                              % pp = IR1, IR2, IR3, IR4, IR5 and IR6
% [peak(pp,1),~]=find(IR(1:ref_peak,pp)==max(IR(1:ref_peak,pp)));
% [peak(pp,2),~]=find(IR(ref_peak:2000,pp)==max(IR(ref_peak:2000,pp)));
%
% c_values(pp,1) = (2*z_values(pp,1))/((peak(pp,2)+ref_peak)-peak(pp,1))*fs;
% end

piek1 = 8.5;                                %1st peak
piek2 = 1330;                               %2nd peak
dpiek = piek2-piek1;                        %Difference in peaks
tpiek = dpiek/192000;                       %Time between peaks
c = (1/tpiek)*(2*1.188);                    %Speed of sound


ki_emp = -0.02*sqrt(fvector)./(c.*0.04);    % Calculate the attenuation
                                            % constant for correcting plane
                                            % wave attenuation by the
                                            % impedance tube according to
                                            % ISO 10534-2

L = z1;                                     %  Relevant tube lenght [m]

x1 = 0;                                      %  Distance between mic1 and mic1 [m]
x2 = L-z2;                                  %  Distance between mic2 and mic1 [m]
x3 = L-z3;                                  %  Distance between mic3 and mic1 [m]
x4 = L-z4;                                  %  Distance between mic4 and mic1 [m]
x5 = L-z5;                                  %  Distance between mic5 and mic1 [m]
x6 = L-z6;                                  %  Distance between mic6 and mic1 [m]

N = round((zt/c)*fs)*2;                     % The number of samples before the direct sound
                                            %  reaches the back wall of the tube. This number is used for the
                                            %  cross correlation of the signals in which only the direct sound is taken
                                            %  into account

%_____________________________________________________________________
% CROSS CORRELATION
%_____________________________________________________________________
```

```
% The impulse responses are measured seperately, this may cause a phase
% difference. To correct this, the difference in sample number of the first
% peak in the impulse response is compared to the expected difference in
% sample number caused by the increase in distance from the source.

% Cross correlation for IR2 with IR1 as reference
C2 = xcorr(IR1(1:N+1),IR2(1:N+1));      %  Crosscorrelation function of IR2
                                        %  with IR1 as reference over samples 1
                                        %  to N+1
M2 = max(C2,[],1);                      %  Maximum value in cross correlation
                                        %  C2
                                        % The maximum value in the cross correlation is the
                                        % amount of samples the highest peak in IR1 differs
                                        % from the highest peak in IR2
for n = 1:2*N;                          % The function finds the row number in wich M2 occurs
  if C2(n) == M2;                       % "If row n in the range 1 to 2N in C2 equals M2
  A2 = n;                               % than A2 = n"

  end
end

% Cross correlation for IR3 with IR1 as reference
C3 = xcorr(IR1(1:N+1),IR3(1:N+1));      %  Cross correlation function of IR3
                                        %  with IR1 as reference over samples 1
                                        %  to N+1
M3 = max(C3,[],1);                      %  Maximum value in cross correlation
                                        %  C3
                                        % The maximum value in the cross correlation is the
                                        % amount of samples the highest peak in IR1 differs
                                        % from the highest peak in IR3
for n = 1:2*N;                          % The function finds the row number in wich M3 occurs
  if C3(n) == M3;                       % "If row n in the range 1 to 2N in C3 equals M3
  A3 = n;                               % than A3 = n"
  end
end

% Cross correlation for IR4 with IR1 as reference
C4 = xcorr(IR1(1:N+1),IR4(1:N+1));      %  Crosscorrelation function of IR4
                                        %  with IR1 as reference over samples 1
                                        %  to N+1
M4 = max(C4,[],1);                      %  Maximum value in cross correlation
```

```
                                    %  C4
                                    % The maximum value in the cross correlation is the
                                    % amount of samples the highest peak in IR1 differs
                                    % from the highest peak in IR4

for n = 1:2*N;                      % The function finds the row number in wich M4 occurs
  if C4(n) == M4;                   % "If row n in the range 1 to 2N in C4 equals M4
  A4 = n;                           % than A4 = n"
  end
end

% Cross correlation for IR5 with IR1 as reference
C5 = xcorr(IR1(1:N+1),IR5(1:N+1));  %  Crosscorrelation function of IR5
                                    %  with IR1 as reference over samples 1
                                    %  to N+1
M5 = max(C5,[],1);                  %  Maximum value in cross correlation
                                    %  C5
                                    % The maximum value in the cross correlation is the
                                    % amount of samples the highest peak in IR1 differs
                                     % from the highest peak in IR5

for n = 1:2*N;                      % The function finds the row number in wich M5 occurs
  if C5(n) == M5;                   % "If row n in the range 1 to 2N in C5 equals M5
  A5 = n;                           % than A5 = n"
  end
end

% Cross correlation for IR6 with IR1 as reference
C6 = xcorr(IR1(1:N+1),IR6(1:N+1));  %  Crosscorrelation function of IR6
                                    %  with IR1 as reference over samples 1
                                    %  to N+1
M6 = max(C6,[],1);                  %  Maximum value in cross correlation
                                    %  C6
                                    % The maximum value in the cross correlation is the
                                    % amount of samples the highest peak in IR1 differs
                                    % from the highest peak in IR6

for n = 1:2*N;                      % The function finds the row number in wich M6 occurs
  if C6(n) == M6;                   % "If row n in the range 1 to 2N in C6 equals M6
  A6 = n;                           % than A6 = n"
  end
```

```
end

S2 = N+1-A2;                    % Number of samples the first peak in the impulse
S3 = N+1-A3;                    % response differs from the first peak in IR1
S4 = N+1-A4;
S5 = N+1-A5;
S6 = N+1-A6;

D2 = round((x2/c)*fs);          %  Number of samples the first peak in the
D3 = round((x3/c)*fs);          %  impulse response should differ from the
D4 = round((x4/c)*fs);          %  first peak in IR1
D5 = round((x5/c)*fs);
D6 = round((x6/c)*fs);

T1 = 0;                         % Number of samples the impulse response should be
T2 = D2 - S2;                   % shifted forward to correlate with microphone 1
T3 = D3 - S3;                   % (negative means it should be shifted backwards)
T4 = D4 - S4;
T5 = D5 - S5;
T6 = D6 - S6;

% IR1 is taken as a reference and all other IRs are shifted a number of
% samples as calculated above

IR11 = IR1;
IR22 = zeros(length(IR1),1);
IR33 = zeros(length(IR1),1);
IR44 = zeros(length(IR1),1);
IR55 = zeros(length(IR1),1);
IR66 = zeros(length(IR1),1);

if T2 >= 0
   IR22(T2+1:end) = IR2(1:end-T2);
else
   IR22(1:end+T2) = IR2(-T2+1:end);
end
if T3 >= 0
   IR33(T3+1:end) = IR3(1:end-T3);
else
   IR33(1:end+T3) = IR3(-T3+1:end);
end
```

```
if T4 >= 0
    IR44(T4+1:end) = IR4(1:end-T4);
else
    IR44(1:end+T4) = IR4(-T4+1:end);
end
if T5 >= 0
    IR55(T5+1:end) = IR5(1:end-T5);
else
    IR55(1:end+T5) = IR5(-T5+1:end);
end
if T6 >= 0
    IR66(T6+1:end) = IR6(1:end-T6);
else
    IR66(1:end+T6) = IR6(-T6+1:end);
end
%_____________________________________________________________________
% FAST FOURIER TRANSFORM
%_____________________________________________________________________

FFT1 = fft(IR11);                    % Fourier Transform of the correlated impulse
FFT2 = fft(IR22);                    % response
FFT3 = fft(IR33);
FFT4 = fft(IR44);
FFT5 = fft(IR55);
FFT6 = fft(IR66);
%_____________________________________________________________________
% COMPUTATIONS
%_____________________________________________________________________
% The function is repeated for each frequency whitin the range of interest
% The plane wave propagating trough the tube is modeled. The ideal
% propagation of the wave over the length traveled without obstructions is
% modeled and compared to the wave reflected by the specimen and back wall
for ff = 1:length(fvector)
k = (2*pi*fvector(ff)./c)+(1i*ki_emp(ff));
e11= exp(-1i*k*x1);
e12= exp(-1i*k*(2*L-x1));
e21= exp(-1i*k*x2);
e22= exp(-1i*k*(2*L-x2));
e31= exp(-1i*k*x3);
e32= exp(-1i*k*(2*L-x3));
e41= exp(-1i*k*x4);
```

```
e42= exp(-1i*k*(2*L-x4));
e51= exp(-1i*k*x5);
e52= exp(-1i*k*(2*L-x5));
e61= exp(-1i*k*x6);
e62= exp(-1i*k*(2*L-x6));
M = [e11 e12;e21 e22;e31 e32;e41 e42;e51 e52;e61 e62];
Pmeas=[FFT1(fvector(ff)+1);FFT2(fvector(ff)+1);FFT3(fvector(ff)+1);
    FFT4(fvector(ff)+1);FFT5(fvector(ff)+1);FFT6(fvector(ff)+1)];
Ptemp = M\Pmeas;
R(ff) = Ptemp(2,1)./Ptemp(1,1);
end

Z = -(R+1)./(R-1);                          %  Surface impedance

a = 1-abs(R).^2;                            %  Absorption coefficient
%_____________________________________________________________________________
% TABLE
%_____________________________________________________________________________
Mimped = [fvector;real(Z);imag(Z);abs(Z)]';
%save 'RESULT_table_Impedance'.txt Mimped /ascii

alpha = [fvector;a]';
save('absorption.txt','alpha','-ascii')

% Matrix contaning frequency [Hz] in column 1, the real part of the
% impedance in column 2, the imaginary part of the impedance in column 3
% and the absulute part of the impedance in column 4.

% saves Mimped as a text file named: RESULT_table_Impedance.txt

% Mabsorp = [fvector;abs(a)]';
% save 'RESULT_table_absorption'.txt Mabsorp /ascii

% Matrix contaning the frequency in column 1 and absorption in column 2
% Saves Mabsorb (absorption) as a text file named:
% RESULT_table_absorption.txt
%_____________________________________________________________________________
% FIGURE
%_____________________________________________________________________________
figure(1)
  semilogx(fvector,real(Z))
```

```
    hold on;semilogx(fvector,imag(Z))
    hold on;semilogx(fvector,abs(Z))
    legend('real(Z)','imag(Z)','abs(Z)')
    axis([10 5000 -25 25])
    xlabel('Frequency [Hz]')
    ylabel('Surface impedance [-]')
    grid
    saveas( gcf,'RESULT_graph_impedance','jpg');

figure(2)
    semilogx(fvector,a)
    axis([10 5000 0 1])
    xlabel('Frequency [Hz]')
    ylabel('Absorption coefficient [-]');
    grid
    saveas( gcf,'RESULT_graph_absorption','jpg');

figure(3)
    semilogx(fvector,real(R))
    legend('real(R)')
    axis([10 5000 -1 2])
    xlabel('Frequency [Hz]')
    ylabel('Reflection factor [-]')
    grid

figure(4)
    plot(IR11(1:3000,:))
    hold all; plot(IR22(1:3000,:))
    hold all; plot(IR33(1:3000,:))
    hold all; plot(IR44(1:3000,:))
    hold all; plot(IR55(1:3000,:))
    hold all; plot(IR66(1:3000,:))
```

APPENDIX C

CURVE FITTING SCRIPT

```
%% Fit: 'Curve fitting WWCB'.

%% Load measured absorption (a) and define frequency range (fvector)
[xData, yData] = prepareCurveData( fvector, a );

%% Set up fittype and options.
%% Define script and the unknown parameters
ft = fittype( 'JCA(fvector,alpha_inf,epsilon,viscous,thermal)', 'independent', 'fvector', 'dependent', 'y' );
opts = fitoptions( 'Method', 'NonlinearLeastSquares' );
opts.Display = 'Off';
opts.Lower      = [0    0.5    50    50    ];
opts.StartPoint = [2    0.7    150   150   ];
opts.Upper      = [5    1.0    350   350   ];

% Fit model to data.
[fitresult, gof] = fit( xData, yData, ft, opts );

% Plot fit with data.
figure( 'Name', 'Curve fitting WWCB' );
h = plot( fitresult, xData, yData );
legend( h, 'a vs. fvector', 'untitled fit 1', 'Location', 'NorthEast' );
% Label axes
xlabel fvector
ylabel a
grid on
```

APPENDIX D

STRAND WIDTH COMPARISON SCRIPT

```
close all
clear all

fvector    =[0:5656];
density    =400;
d          =0.025;

%% JCA - model - 1.0 mm
% Defining the input parameters
```

```
sigma           =126.494842*exp(0.007739*density);
epsilon         =(0.093347*density+20.637674)/100;
tort            =0.005693*density-0.289734;
viscous         =99774.424355*density^(-1.044588);
thermal         =5.148369*density^(0.614019);

% Call JCA-function for the 1.0 mm strand width
a_JCA           =JCA(fvector,d,tort,sigma,epsilon,viscous,thermal);
a_JCA_10mm      =a_JCA;

%% JCA - model - 1.5mm
% Defining the input parameters
sigma           =45.08775*exp(0.011472*density);
epsilon         =(0.004521*density+63.700232)/100;
tort            =0.010454*density-0.404240;
viscous         =14438.565387*density^(-0.710603);
thermal         =277.947695*density^(-0.02256);

% Call JCA-function for the 1.5 mm strand width
a_JCA           =JCA(fvector,d,tort,sigma,epsilon,viscous,thermal);
a_JCA_15mm      =a_JCA;

%% JCA - model - 2.0mm
% Defining the input parameters
sigma           =54.844*exp(0.0103*density) ;
epsilon         =(0.037892*density+50.601332)/100;
tort            =0.009334*density-0.345694;
viscous         =122276.165932*density^(-1.057404);
thermal         =291.929762*density^(-0.031082);


% Call JCA-function for the 2.0 mm strand width
a_JCA           =JCA(fvector,d,tort,sigma,epsilon,viscous,thermal);
a_JCA_20mm      =a_JCA;

%% FIGURES
  h1=figure(6)
  h= semilogx(fvector,a_JCA_10mm,'k--',fvector,a_JCA_15mm,'k',fvector,a_JCA_20mm,'k:','Linewidth',1.2)
  axis([165 3000 0 1])
  xlabel('Frequency [Hz]','FontName','Times New Roman','Fontsize',17)
  ylabel('Normal incidence sound absorption [-]','FontName','Times New Roman','Fontsize',17);
```

```
id=[100 125 160 200 250 315 400 500 630 800 1000 1250 1600 2000 2500]
idtext = {100 125 160 200 250 315 400 500 630 800 '1k' '1.25k' '1.6k' '2k' '2.5k'};
set(gca, 'XTick',id,'XTickLabel',idtext,'Fontsize',15)
lngd=legend('1.0 mm strand width (JCA-model)","1.5 mm strand width (JCA-model)","2.0 mm strand width (JCA-model)","location","northwest')
set(lngd,'fontsize',15)
set(gca,'FontName","Times New Roman');
grid
box on
print(h1,'-dpdf","-r600","FibreComparison_JCA')
```

APPENDIX E

MATLAB SCRIPT AIR-CAVITY

```
clear all
close all

lair1          =[0.025:0.025:0.2];
for ii         = 1:length(lair1)

%% Air-layer (Layer 1)
lair           = lair1(ii);        %Depth of air layer
rho0           =1.204;             %Denotes value in air where ambiguity might otherwise arise [kg/m3]
c0             =343.2;             %Speed of sound (m/s)
z0             =rho0*c0;

fvector        =[0:5656];          %Frequency range
kair=2*pi*fvector./c0;
```

```
%Impedance at top of air layer
Zs2 = -j*z0.*cot(kair.*lair);

density         =;
d               =;          %Thickness of the sample
sigma           =;          %Airflow resistivity [Ns/m4]

%% JCA - model
epsilon         =;          %Porosity
tort            =;          %Tortuosity
viscous         =;          % Viscous characteristic length
thermal         =;          % Thermal characteristic length

%% Call functions for the characteristic impedance and wavenumber
Zc_JCA=JCAZc(fvector,d,tort,sigma,epsilon,viscous,thermal);
k_JCA=JCAk(fvector,d,tort,sigma,epsilon,viscous,thermal);
tortJCADP=tort;

Zstot_JCA=(-j*Zs2.*Zc_JCA*cot(k_JCA.*d)+((Zc_JCA).^2))./(Zs2-j*Zc_JCA.*cot(k_JCA.*d));

%Reflection coefficient
R=(Zstot_JCA-z0)./(Zstot_JCA+z0);

%Absorption coefficent
a_JCA(ii,:)=1-(abs(R)).^2;
```

APPENDIX F

MULTI-LAYER SYSTEM SCRIPT FOR WWCB COMBINED WITH MINERAL WOOL

```
close all
clear all

%Calculation layer 2 (MINERAL WOOL)
%-------------------------------------------------------------------------------------------------------------------
------
f = [0:1:5656];
omega = 2*pi*f;

rho0=           1.213;     % [Kg.m-3] density at rest of air at 18C, 1atm
c_0=            344.7;     % [m.s-1] speed of sound in air at 18C, 1atm
P_0=            1.0132e+05; % [N.m-2] atmospheric pressure at 18C, 1atm
sigma=          60000      % [N.s.m-4] static air flow resistivity of material
h=              0.040      % [m] thickness of materia
```

```
X = f/sigma;
f_min = 0.01*sigma
f_max = 1.00*sigma


%%%%%
%%%%% Delany and Bazley model
%%%%% (NB: gamma = alpha + j beta = j k )
%%%%%
Z_DB70 = rho_0*c_0*( 1 + 9.08*(X*1000).^(-0.75) ...
            - i*11.9*(X*1000).^(-0.73) );

k_DB70 = omega/c_0 .* (-i) .* ( 10.3*(X*1000).^(-0.59) ...
                    + i* ( 1 + 10.8*(X*1000).^(-0.70) ) );

K_DB70 = Z_DB70.*omega./k_DB70;
rho_DB70 = k_DB70.*Z_DB70./omega;


%%%%%
%%%%% Revised expressions of Delany and Bazley model by Miki
%%%%% (NB: gamma = alpha + j beta = j k )
%%%%%

Z_DB70_Mik90 = rho_0*c_0*( 1 + 5.50*(X*1000).^(-0.632) ...
                - i*8.43*(X*1000).^(-0.632) );

k_DB70_Mik90 = omega/c_0 .* (-i) .* ( 11.41*(X*1000).^(-0.618) ...
                        + i* (1 + 7.81*(X*1000).^(-0.618) ) );

K_DB70_Mik90 = Z_DB70_Mik90.*omega./k_DB70_Mik90;
rho_DB70_Mik90 = k_DB70_Mik90.*Z_DB70_Mik90./omega;


%%%%%
%%%%% Compute sound absorption using the two models
%%%%% for a sample of thickness d backed by a rigid
%%%%% and impervious wall under at room temperature
%%%%% and pressure conditions
%%%%%
```

```
Z = -j.*Z_DB70./tan(k_DB70*h);
alpha_DB70 = 1 - ( abs( (Z-rho_0*c_0)./(Z+rho_0*c_0) ) ).^2;


Zs2 = -j.*Z_DB70_Mik90./tan(k_DB70_Mik90*h);
%Calculation layer 1
%-------------------------------------------------------------------------------------------------------------

density=458.4;
fvector=        0:5656;          %Frequency range
d1=           0.0255;            %Thickness of the sample
rho0=          1.204;            %Denotes value in air where ambiguity might otherwise arise [kg/m3]
c0=           344.7;             %Speed of sound (m/s)
z0=             rho0*c0;                  %Specific acoustic impedance of air (Kg/m2*s)

%% 1.0 mm JCA (fitted porosity)
epsilon=(0.093347*density+20.637674)/100;
tort=0.005693*density-0.289734;
viscous=99774.424355*density^(-1.044588);
thermal=5.148369*density^(0.614019);
sigma2=126.494842*exp(0.007739*density);

P0=             101320;             %Atmospheric pressure [N/m2]
gamma=          1.4;                %Ratio of the specific heat capacity [-]
Npr=            0.71;               %Prandtl number (0.77 at 20*C) Cox
omega=          2*pi*fvector;       %Angular frequency [s^-1]
eta=            1.84*10^-5;         %Visocity of air [Poiseuille] 1.84*10^-5
P0=             101320;             %Atmospheric pressure [N/m2]
gamma=          1.4;                %Ratio of the specific heat capacity [-]
Npr=            0.71;               %Prandtl number (0.77 at 20*C)

% Effective (/dynamic) Density
% Accounts for the viscous losses
%-----------------------------------------------------------------
rho_eq=(tort*rho0/epsilon).*(1+((sigma2*epsilon)./(1i*omega*rho0*tort)).*sqrt(1+((1i*4*(tort^2)*eta*rho0*omega)/
((sigma2^2)*((viscous*10^-6)^2)*(epsilon^2)))));

% Effective (/dynamic) bulk modulus
% Accounts for the thermal losses
%-----------------------------------------------------------------
K_eq=(gamma*P0/epsilon)./(gamma-(gamma-1).*(1+(((8*eta)./(((thermal*10^-6)^2)*Npr*rho0*omega*1i)).*sqrt(1+(1i*
```

```
(((thermal*10^-6)^2)*Npr*rho0*omega)/(16*eta))))).^-1);

%Characteristic Impedance
Zc1=(K_eq.*rho_eq).^0.5;

%Complex wave number
k1=omega.*sqrt(rho_eq./K_eq);

%-------------------------------------------------------------------------------------------------------------
Zstot=(-j*Zs2.*Zc1.*cot(k1.*d1)+((Zc1).^2))./(Zs2-j*Zc1.*cot(k1.*d1));

%Reflection coefficient
R=(Zstot-z0)./(Zstot+z0);

% %Absorption coefficent
% %a(ii,:)=1-(abs(R)).^2;
a=1-(abs(R)).^2;

% %LOAD MEASURED VALUES IN THE IMPEDANCE TUBE
% %-------------------------------------------------------------------------------------------------------------
load absorption.txt;
ameas=absorption(:,2);

% %FIGURES
% %-------------------------------------------------------------------------------------------------------------

h1=figure(1)
        h=semilogx(fvector,ameas,'k',fvector,a,'k--','Linewidth',1.2)
        axis([165 3000 0 1])
        set(h(1),'Color',[0.7 0.7 0.7]);
        xlabel('Frequency [Hz]','FontName','Times New Roman','Fontsize',17)
        ylabel('Normal incidence sound absorption [-]','FontName','Times New Roman','Fontsize',17);
        id=[100 125 160 200 250 315 400 500 630 800 1000 1250 1600 2000 2500]
        idtext = {100 125 160 200 250 315 400 500 630 800 '1k' '1.25k' '1.6k' '2k' '2.5k'};
        set(gca, 'XTick',id,'XTickLabel',idtext,'Fontsize',15)
        lngd=legend('Measured (25 mm WWCB - 40 mm mineral wool)','Predicted multi-layer system (JCA-model)','lo
        cation','southeast')
        set(lngd,'fontsize',15)
        set(gca,'FontName','Times New Roman');
        grid
        box on
        print(h1,'-dpdf','-r600','WWCB-MINERALWOOL')
```

APPENDIX G

VALIDATION STUDY FOR THE ATTENBOROUGH AND JCA-MODEL
1.0 mm strand width (Belonging to Figure 4.10)

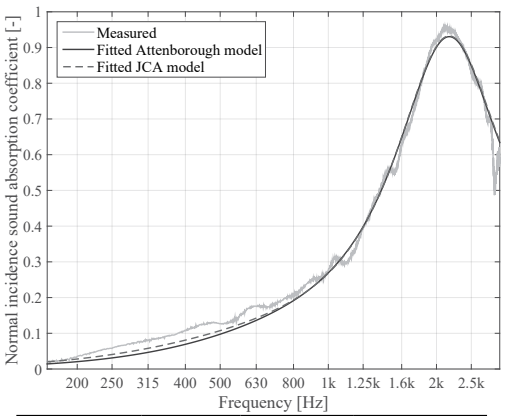

	Measured	JCA-model	Attenborough
SAA-value [-]	0.32	0.31	0.30

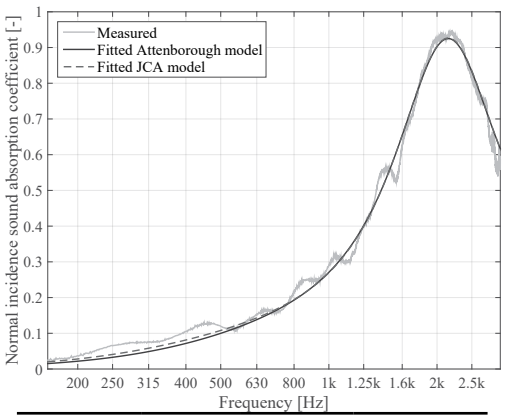

	Measured	JCA-model	Attenborough
SAA-value [-]	0.32	0.31	0.30

Figure G.1: Validation study of 25 mm thick WWCB 1.0 mm strand width (left) ρ=420.4 kg/m^3 and (right) ρ=421.0 kg/m^3

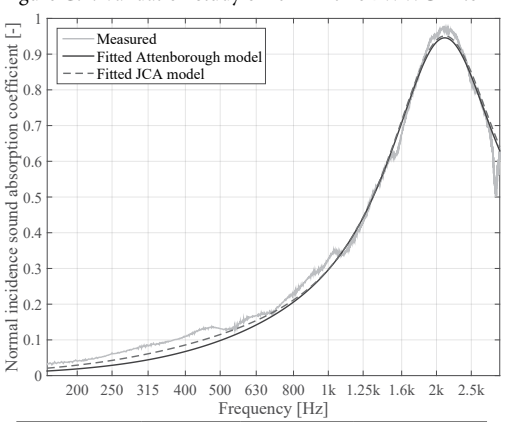

	Measured	JCA-model	Attenborough
SAA-value [-]	0.34	0.33	0.32

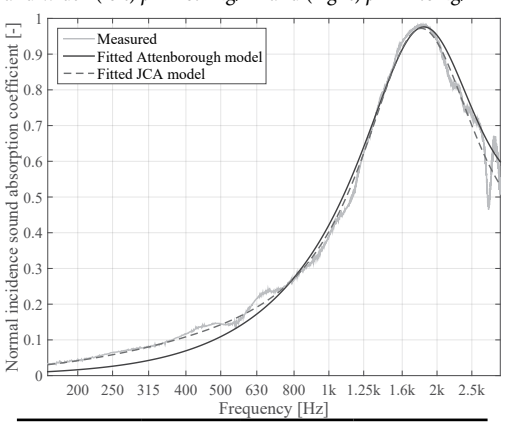

	Measured	JCA-model	Attenborough
SAA-value [-]	0.37	0.37	0.36

Figure G.2: Validation study of 25 mm thick WWCB 1.0 mm strand width (left) ρ=448.4 kg/m^3 and (right) ρ=541.4 kg/m^3

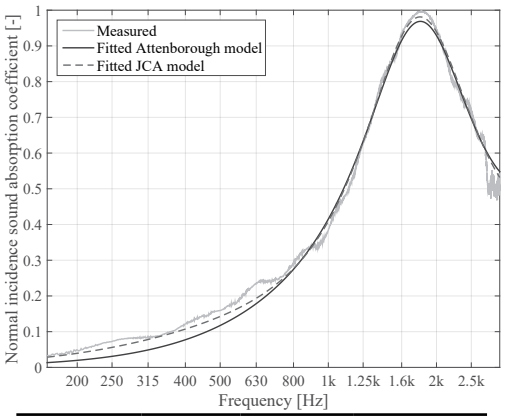

	Measured	JCA-model	Attenborough
SAA-value [-]	0.38	0.37	0.36

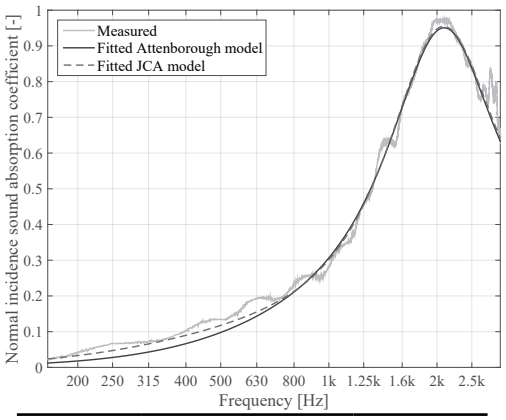

	Measured	JCA-model	Attenborough
SAA-value [-]	0.34	0.33	0.32

Figure G.3: Validation study of 25 mm thick WWCB 1.0 mm strand width (left) ρ=554.4 kg/m^3 and (right) ρ=460.3 kg/m^3

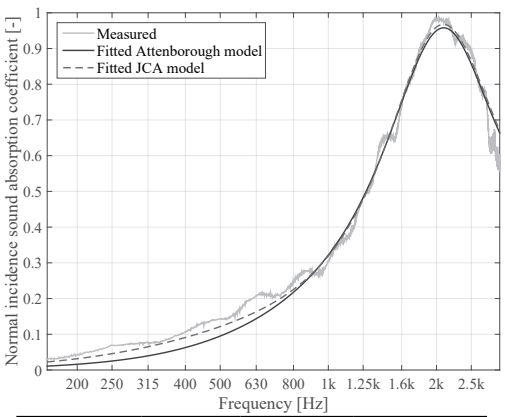

	Measured	JCA-model	Attenborough
SAA-value [-]	0.35	0.34	0.33

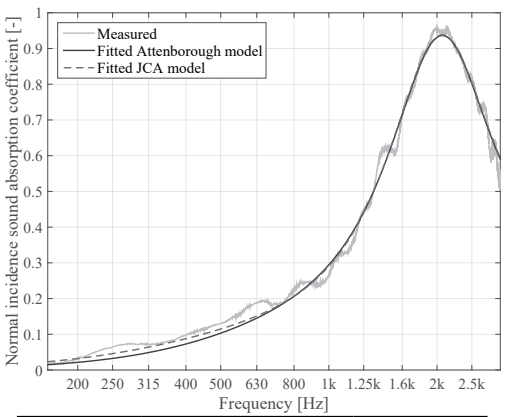

	Measured	JCA-model	Attenborough
SAA-value [-]	0.33	0.32	0.32

Figure G.4: Validation study of 25 mm thick WWCB 1.0 mm strand width (left) ρ=475.7 kg/m^3 and (right) ρ=459.4 kg/m^3

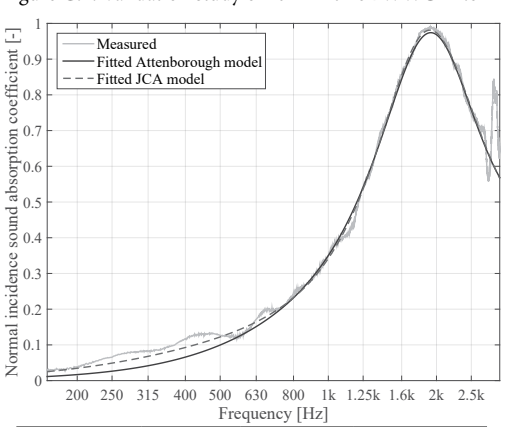

	Measured	JCA-model	Attenborough
SAA-value [-]	0.36	0.35	0.34

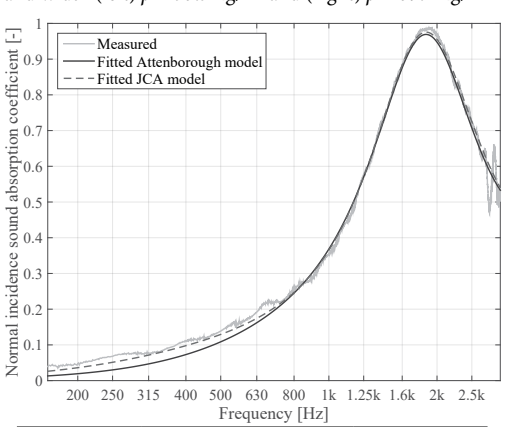

	Measured	JCA-model	Attenborough
SAA-value [-]	0.36	0.36	0.35

Figure G.5: Validation study of 25 mm thick WWCB 1.0 mm strand width (left) ρ=484.4 kg/m^3 and (right) ρ=483.6 kg/m^3

VALIDATION STUDY FOR THE ATTENBOROUGH AND JCA-MODEL
1.5 mm strand width (Belonging to Figure 4.10)

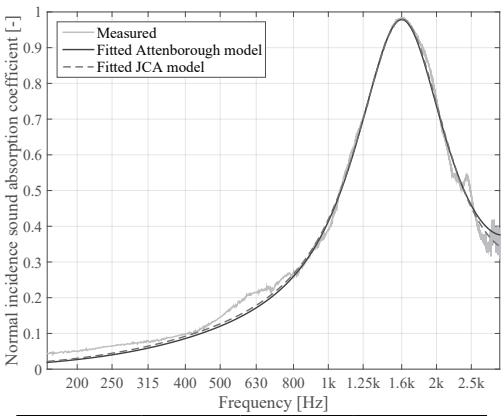

	Measured	JCA-model	Attenborough
SAA-value [-]	0.35	0.34	0.34

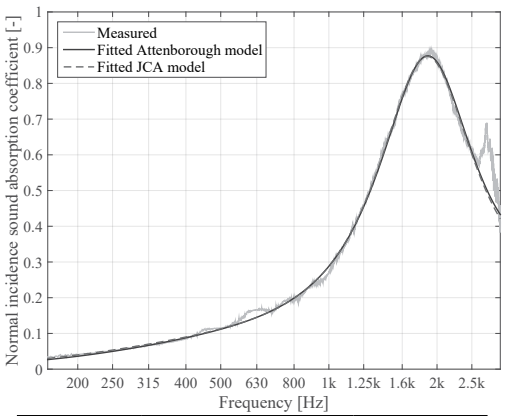

	Measured	JCA-model	Attenborough
SAA-value [-]	0.31	0.31	0.30

Figure G.6: Validation study of 25 mm thick WWCB 1.5 mm strand width (left) ρ=393.7 kg/m^3 and (right) ρ=315.5 kg/m^3

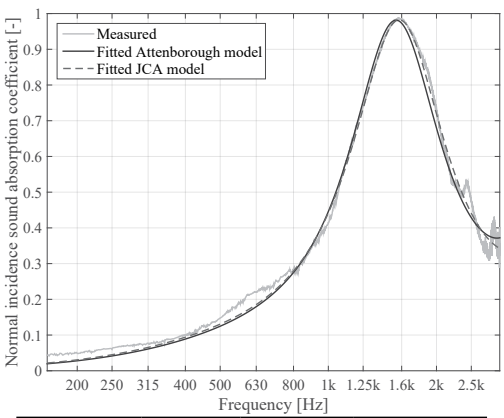

	Measured	JCA-model	Attenborough
SAA-value [-]	0.35	0.35	0.34

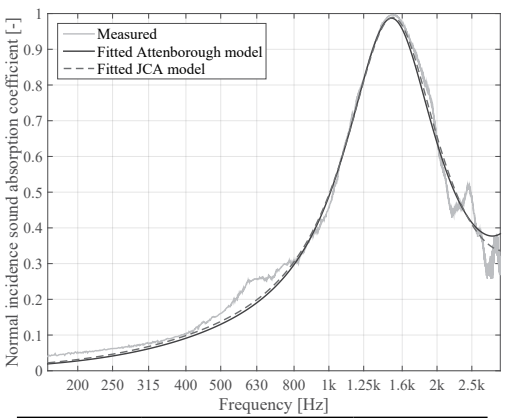

	Measured	JCA-model	Attenborough
SAA-value [-]	0.36	0.35	0.35

Figure G.7: Validation study of 25 mm thick WWCB 1.5 mm strand width (left) ρ=388.1 kg/m^3 and (right) ρ=406.3 kg/m^3

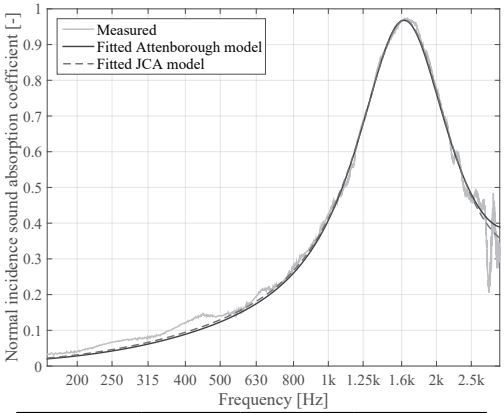

	Measured	JCA-model	Attenborough
SAA-value [-]	0.35	0.34	0.34

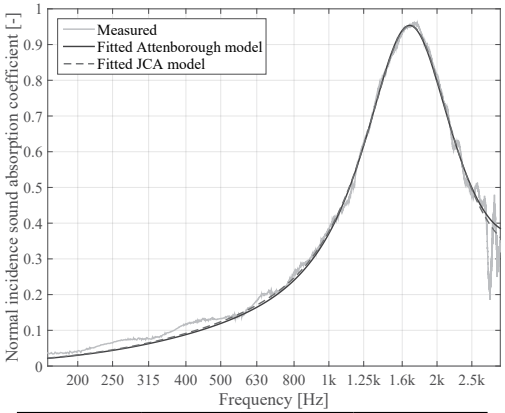

	Measured	JCA-model	Attenborough
SAA-value [-]	0.34	0.33	0.33

Figure G.8: Validation study of 25 mm thick WWCB 1.5 mm strand width (left) ρ=370.2 kg/m^3 and (right) ρ=343.0 kg/m^3

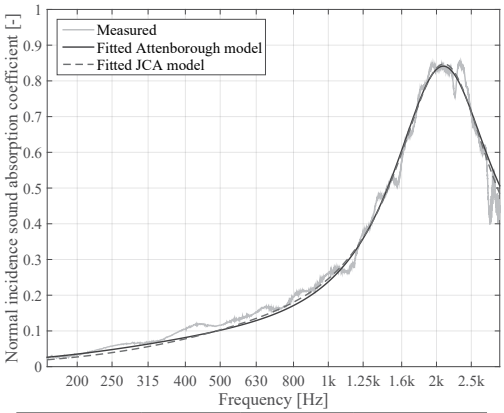

	Measured	JCA-model	Attenborough
SAA-value [-]	0.29	0.28	0.28

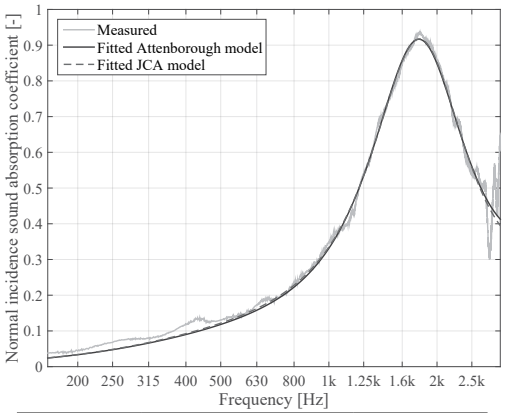

	Measured	JCA-model	Attenborough
SAA-value [-]	0.33	0.32	0.32

Figure G.9: Validation study of 25 mm thick WWCB 1.5 mm strand width (left) ρ=286.6 kg/m^3 and (right) ρ=327.2 kg/m^3

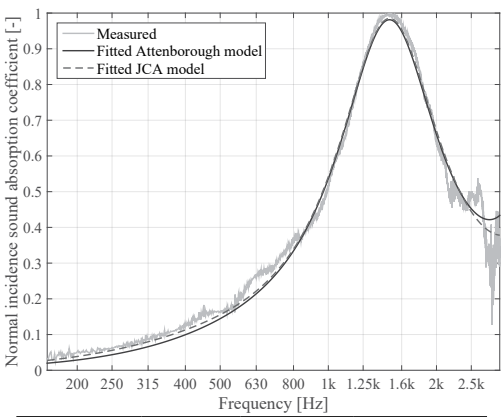

	Measured	JCA-model	Attenborough
SAA-value [-]	0.38	0.37	0.37

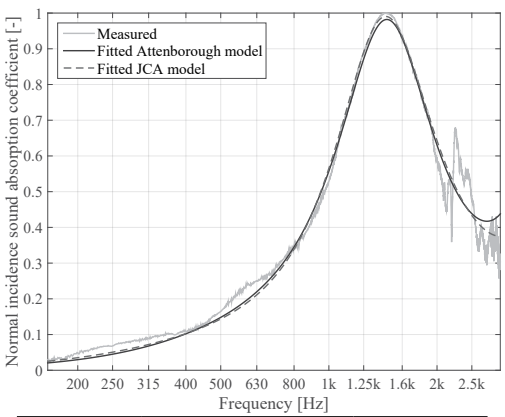

	Measured	JCA-model	Attenborough
SAA-value [-]	0.38	0.37	0.37

Figure G.10: Validation study of 25 mm thick WWCB 1.5 mm strand width (left) ρ=351.1 kg/m^3 and (right) ρ=464.8 kg/m^3

VALIDATION STUDY FOR THE ATTENBOROUGH AND JCA-MODEL
2.0 mm strand width (Belonging to Figure 4.10)

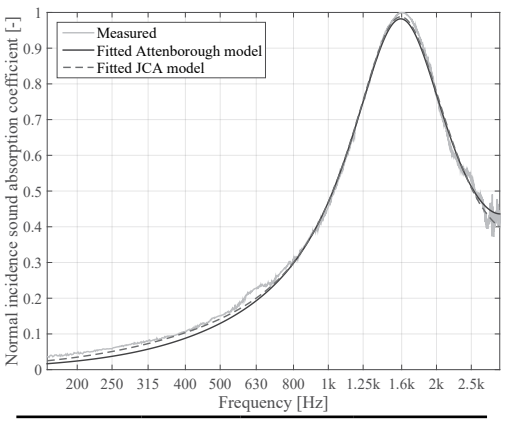

	Measured	JCA-model	Attenborough
SAA-value [-]	0.37	0.37	0.36

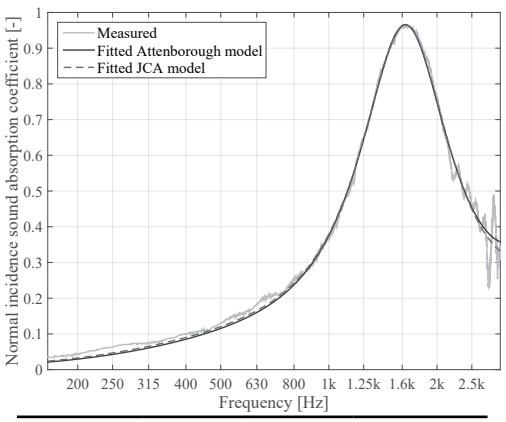

	Measured	JCA-model	Attenborough
SAA-value [-]	0.33	0.33	0.33

Figure G.11: Validation study of 25 mm thick WWCB 2.0 mm strand width (left) ρ=422.9 kg/m^3 and (right) ρ=395.7 kg/m^3

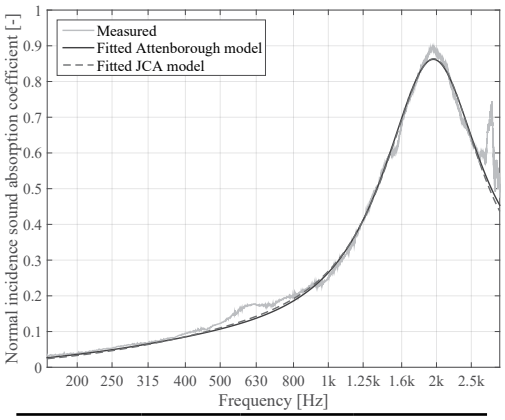

	Measured	JCA-model	Attenborough
SAA-value [-]	0.30	0.29	0.29

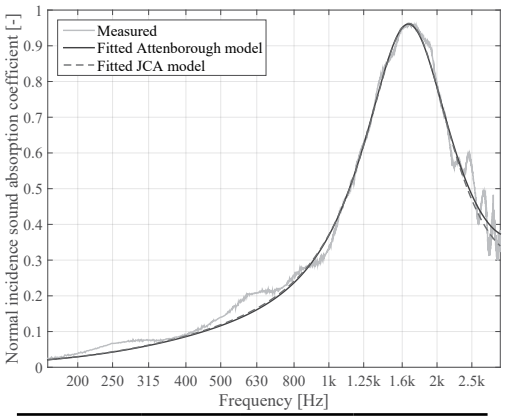

	Measured	JCA-model	Attenborough
SAA-value [-]	0.34	0.33	0.33

Figure G.12: Validation study of 25 mm thick WWCB 2.0 mm strand width (left) ρ=327.7 kg/m^3 and (right) ρ=390.9 kg/m^3

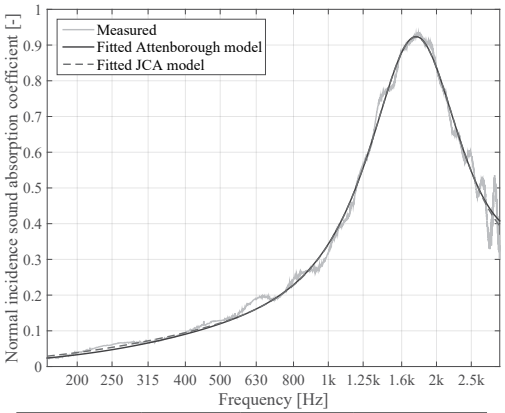

	Measured	JCA-model	Attenborough
SAA-value [-]	0.33	0.33	0.32

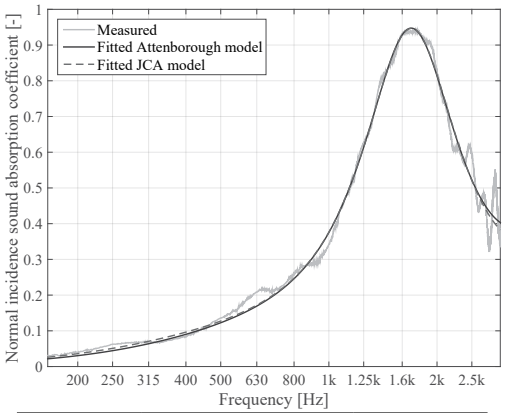

	Measured	JCA-model	Attenborough
SAA-value [-]	0.34	0.34	0.33

Figure G.13: Validation study of 25 mm thick WWCB 1.5 mm strand width (left) ρ=373.2 kg/m^3 and (right) ρ=367.1 kg/m^3

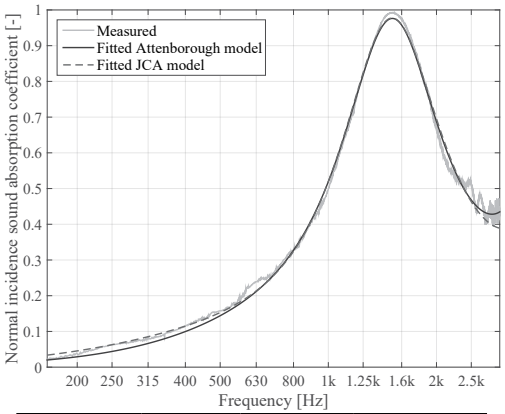

	Measured	JCA-model	Attenborough
SAA-value [-]	0.37	0.37	0.37

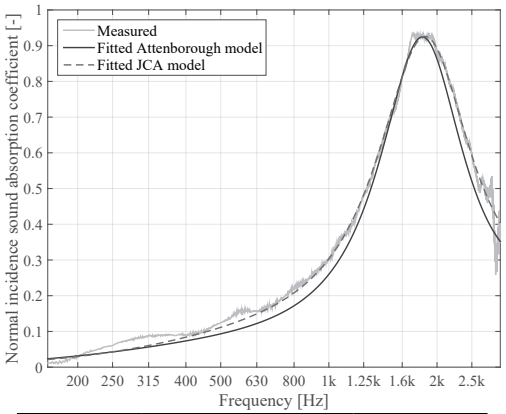

	Measured	JCA-model	Attenborough
SAA-value [-]	0.32	0.31	0.29

Figure G.14: Validation study of 25 mm thick WWCB 1.5 mm strand width (left) ρ=455.1 kg/m^3 and (right) ρ=328.1 kg/m^3

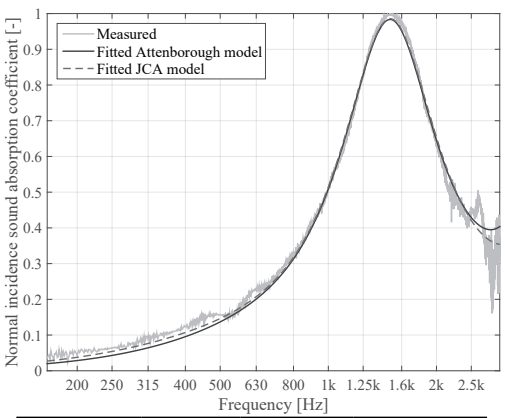

	Measured	JCA-model	Attenborough
SAA-value [-]	0.37	0.36	0.35

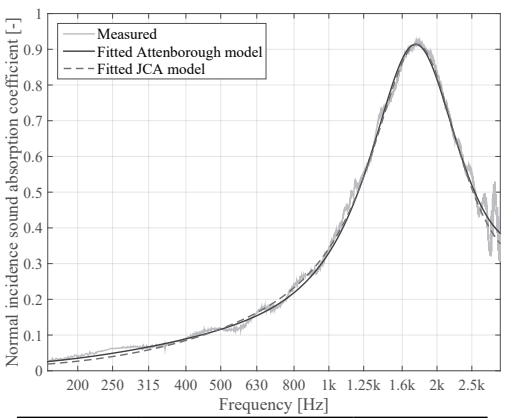

	Measured	JCA-model	Attenborough
SAA-value [-]	0.32	0.32	0.32

Figure G.15: Validation study of 25 mm thick WWCB 1.5 mm strand width (left) ρ=427.4 kg/m^3 and (right) ρ=341.5 kg/m^3

APPENDIX H

DEMONSTRATION OF THE JCA-MODEL FOR THE 'REGULAR' WWCB
25 mm thick WWCB
1.0 mm strand width

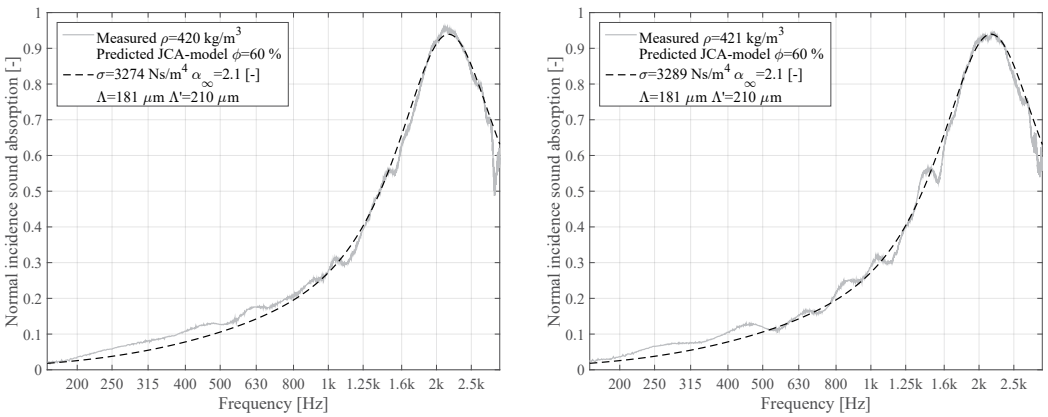

Figure H.1: 1.0 mm strand width (25 mm thick)

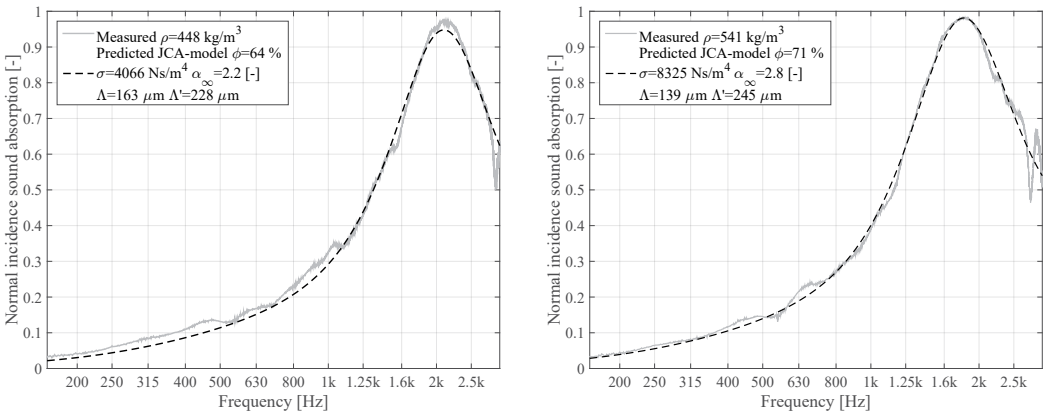

Figure H.2: 1.0 mm strand width (25 mm thick)

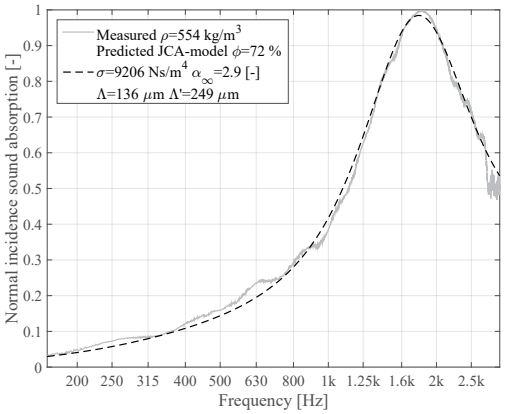

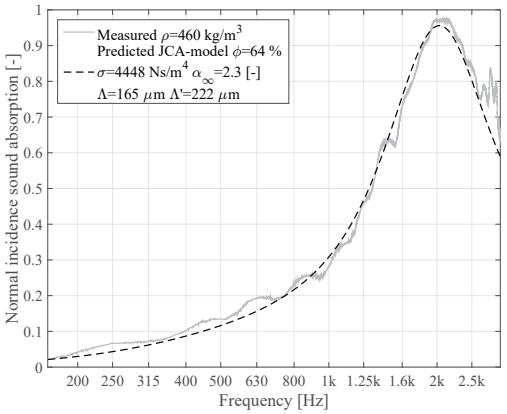

Figure H.3: 1.0 mm strand width (25 mm thick)

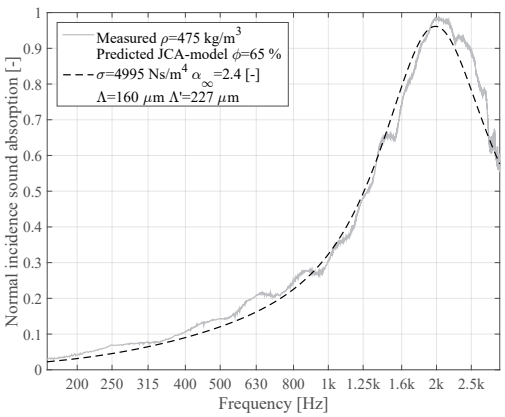

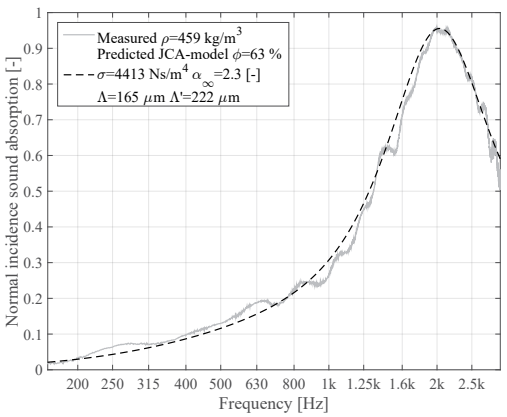

Figure H.4: 1.0 mm strand width (25 mm thick)

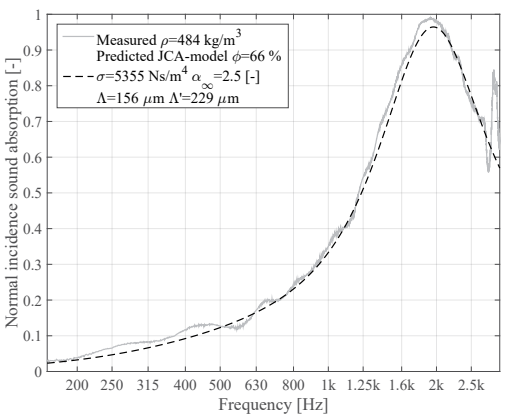

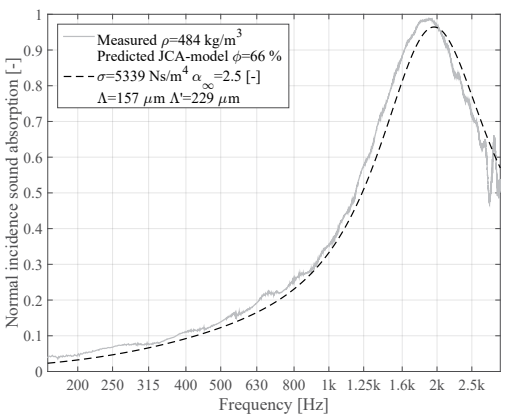

Figure H.5: 1.0 mm strand width (25 mm thick)

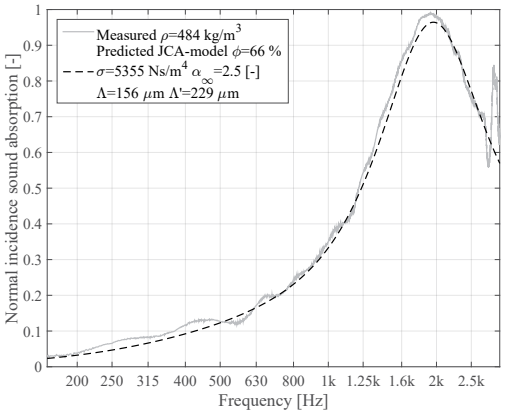

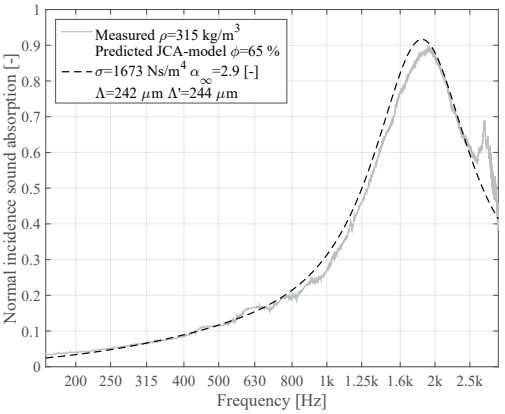

Figure H.6: 1.5 mm strand width (25 mm thick)

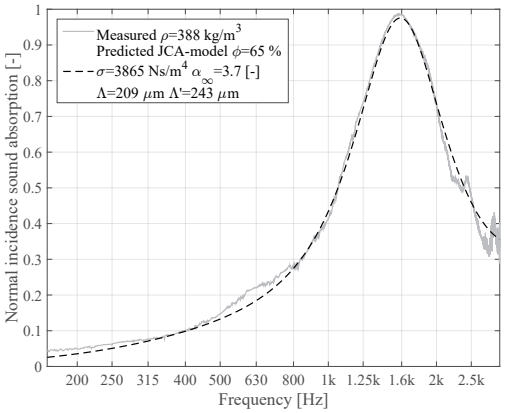

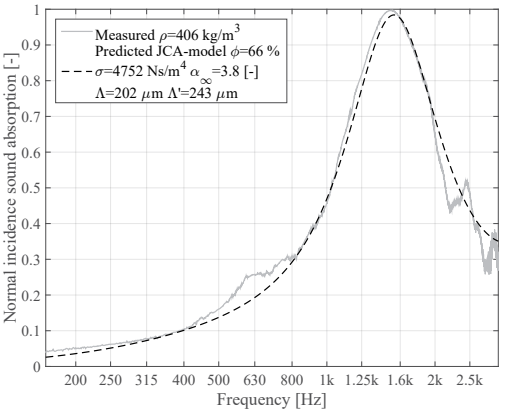

Figure H.7: 1.5 mm strand width (25 mm thick)

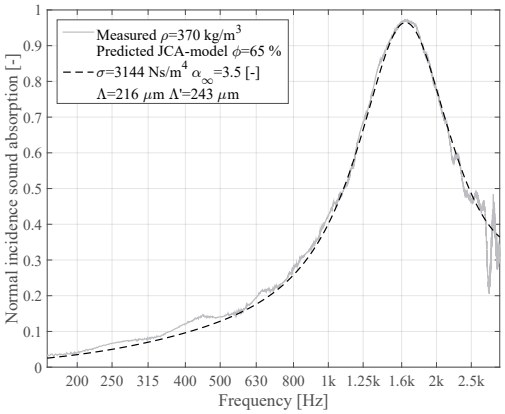

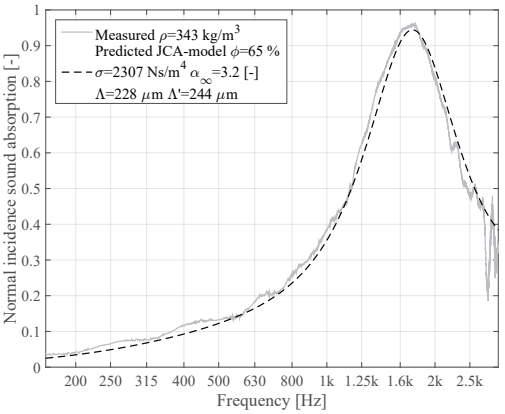

Figure H.8: 1.5 mm strand width (25 mm thick)

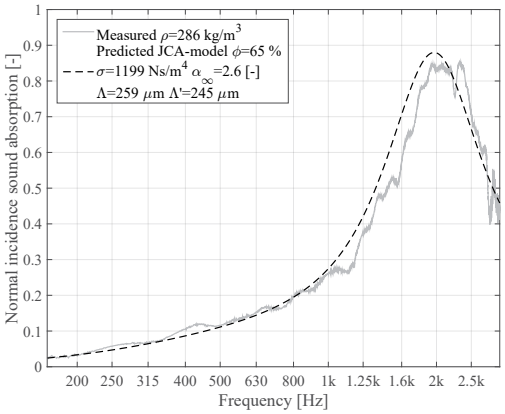

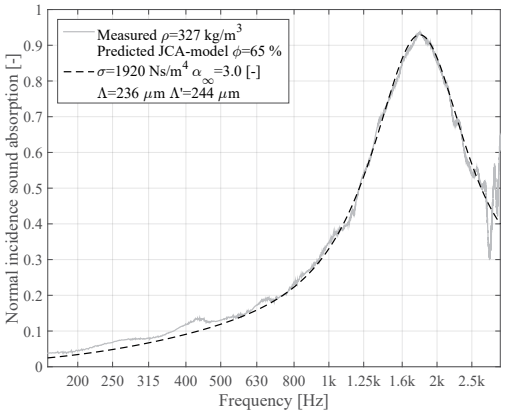

Figure H.9: 1.5 mm strand width (25 mm thick)

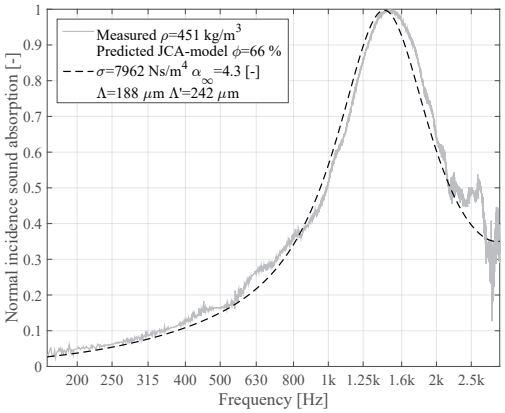

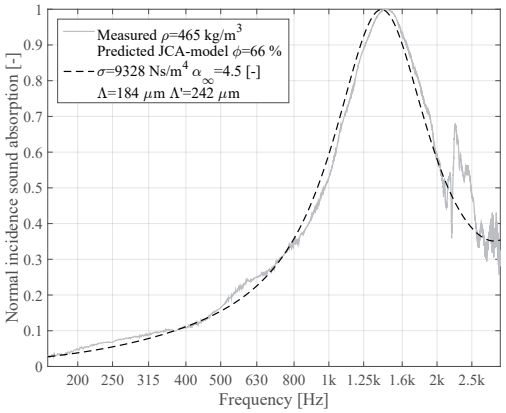

Figure H.10: 1.5 mm strand width (25 mm thick)

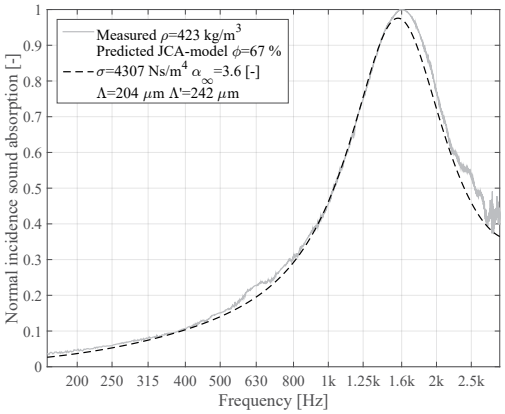

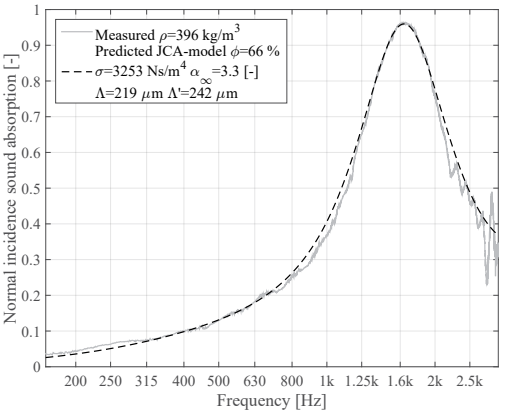

Figure H.11: 2.0 mm strand width (25 mm thick)

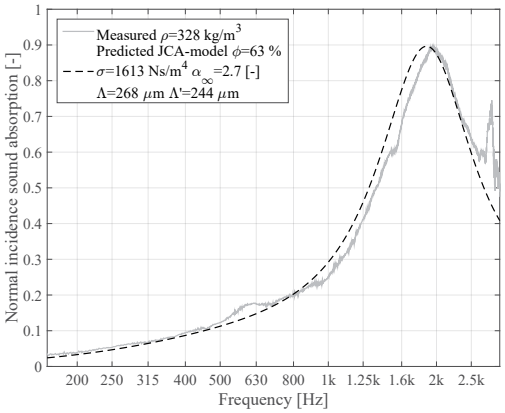

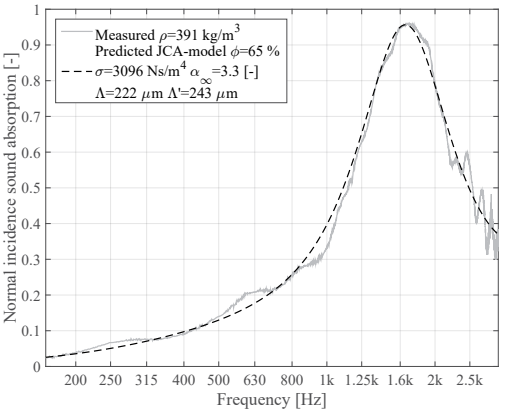

Figure H.12: 2.0 mm strand width (25 mm thick)

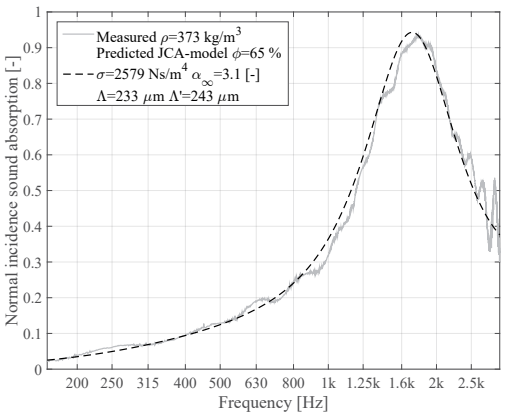

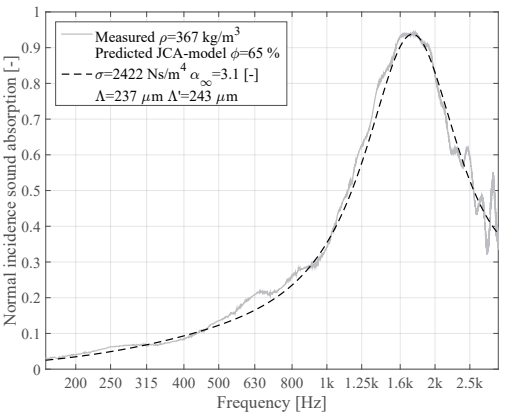

Figure H.13: 2.0 mm strand width (25 mm thick)

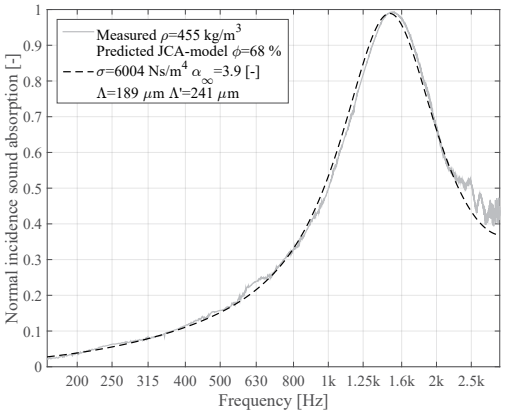

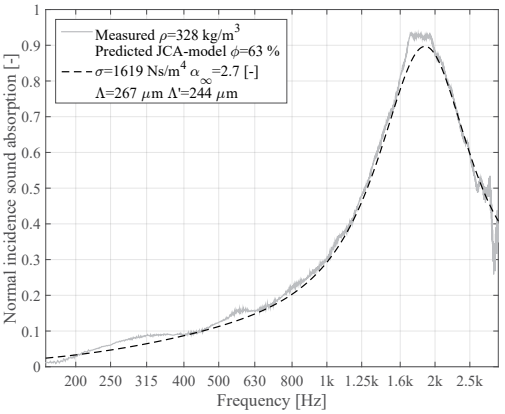

Figure H.14: 2.0 mm strand width (25 mm thick)

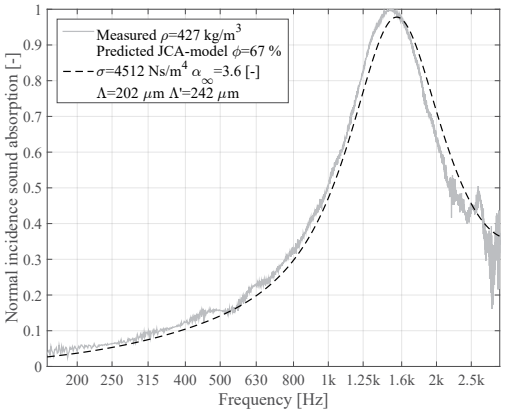

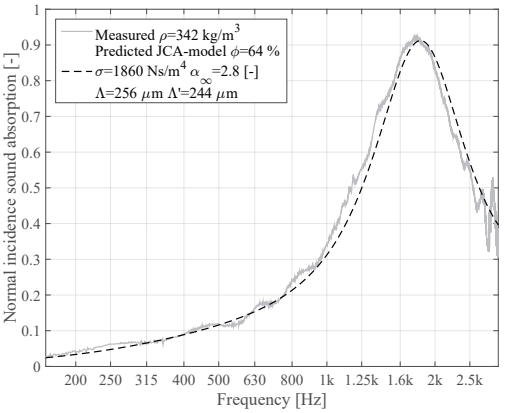

Figure H.15: 2.0 mm strand width (25 mm thick)

APPENDIX I

DEMONSTRATION OF THE JCA-MODEL FOR DIFFERENT THICKNESS'S

15, 35 and 50 mm thick WWCB

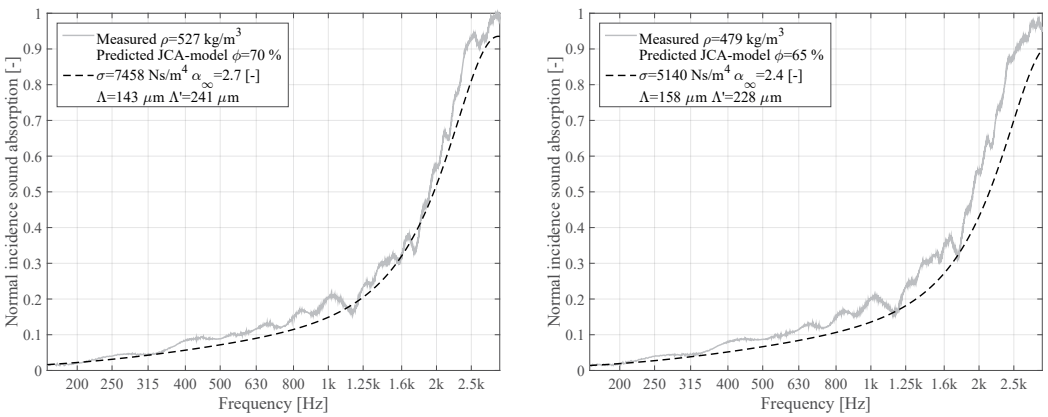

Figure I.1: 15 mm WWCB (1.0 mm strand width)

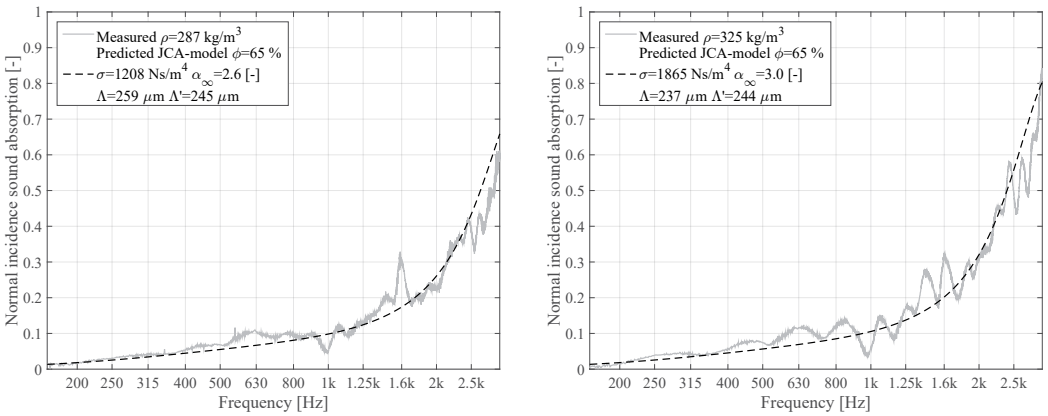

Figure I.2: 15 mm WWCB (1.5 mm strand width)

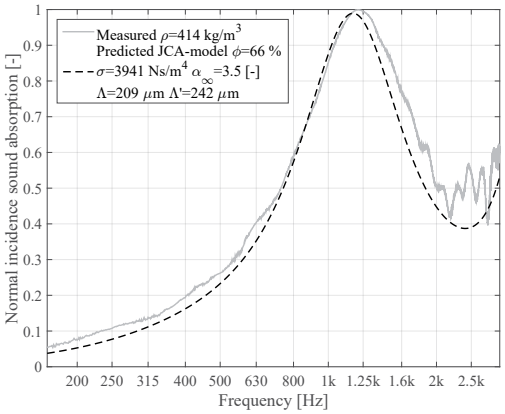

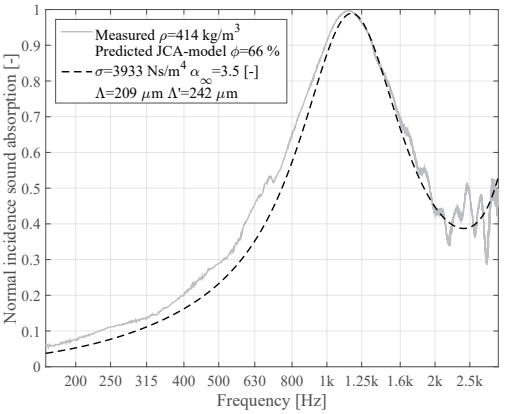

Figure I.3: 35 mm WWCB (2.0 mm strand width)

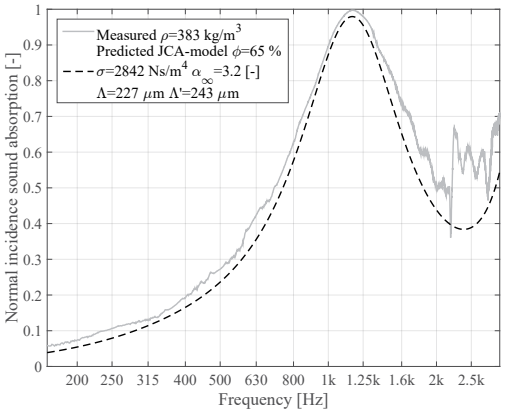

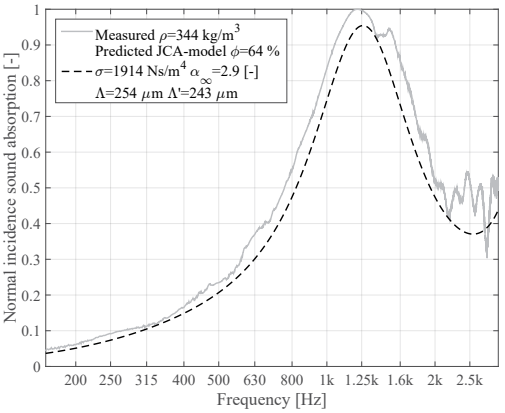

Figure I.4: 35 mm WWCB (2.0 mm strand width)

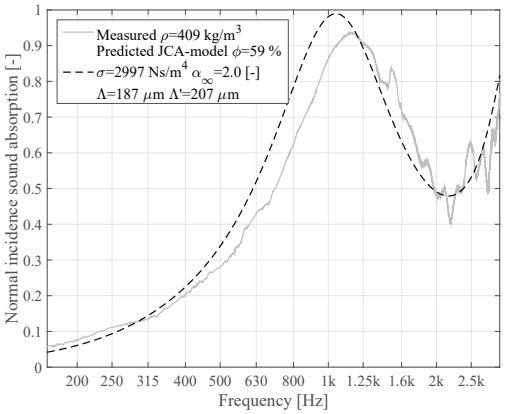

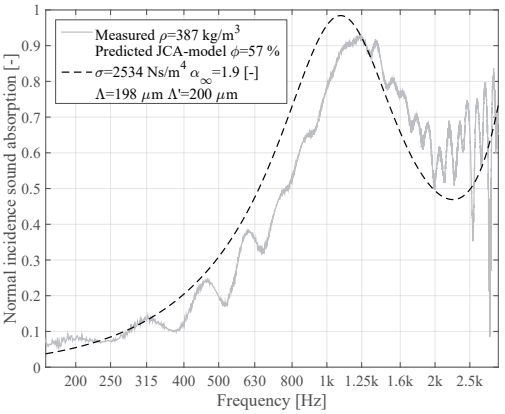

Figure I.5: 50 mm WWCB (1.0 mm strand width)

APPENDIX J

PAPER INTERNATIONAL CONGRESS ON SOUND AND VIBRATION
10-14 JULY 2016, ATHENS, GREECE

T08.SS01 Sound Absorption Materials

Sound absorbing materials have been widely used for the control of noise, the reduction of reverberant sound pressure levels and, consequently, the reduction of reverberation time in enclosures or rooms. This technical session will focus on topics related to sound absorbing materials. Papers related (but not limited) to advances, development, analysis and/or optimization of materials that have been produced for the specific purpose of providing high values of sound absorption are welcome. The papers can be related to fundamental research, and/or applications, related to design, modeling, testing, and/or manufacturing of sound absorbing materials. Due to the importance of the subject, this session will also welcome studies on environmentally friendly sound absorbing materials that are made of recycled products and/or through less contaminating processes.

23rd International Congress on Sound & Vibration
Athens, Greece 10-14 July 2016
ICSV23

CHARACTERIZING AND MODELLING THE SOUND ABSORPTION OF WOOD WOOL CEMENT BOARDS (WWCB)

Bram Botterman, Maarten Hornikx, Guillaume Doudart de la Grée, Qingliang Yu and Jos Brouwers

Eindhoven University of Technology, Department of the Built Environment, 7000 Eindhoven, The Netherlands
email: b.botterman@gmail.com

The present article aims to characterize and, by using impedance models, predict the sound absorption of wood wool cement boards (WWCB). The main challenge lies in the inhomogeneity of the WWCB; the samples taken from different commercial boards do not only greatly differ in density, but also in wood-to-binder ratio. Different models, able to predict the acoustic impedance of rigid-frame porous materials, have been analysed and their suitability for the WWCB has been evaluated. It is concluded that the Johnson-Champoux-Allard (JCA) model was found to be most appropriate to fit the normal incidence sound absorption values as measured in the impedance tube. From the five input parameters for this impedance model, the flow resistivity has been measured. The open porosity, tortuosity and viscous and thermal characteristic lengths, have been determined by making use of an inverse calculation method, a curve fitting approach, based on the measured acoustic absorption coefficients in the impedance tube. The tested WWCBs are made of three different strand widths (1.0, 1.5 and 2.0 mm) and of different thicknesses, densities and wood cement ratios. By making use of the found relations between the bulk density and the input parameters, it is concluded that it is possible to predict the normal incidence sound absorption of the WWCB by only making use of the bulk density and thickness as input parameters.

1. Introduction

A wood wool cement board (WWCB) is a building material produced since 1920, consisting of wood wool mineralized by Portland Cement (PC) [1]. The boards are mainly applied in parking lots and underneath balconies as in- and outdoor ceiling material and used as sound barriers. The boards possess a high fire resistance, are having a high durability and low maintenance, hence are still popular nowadays [2]. Due to the high open porosity (± 80%) and the internal pore structure, the boards can acoustically be considered as porous absorbers. Its sound absorption coefficient values have previously been measured [2]. However, no systematic study exists explaining the sound absorption behaviour of the WWCB, which would enable to increase and finally optimize its acoustical properties.

Furthermore, during this study, a wide range of densities was measured within the WWCBs, which makes them more difficult to characterize in comparison to homogeneous porous materials. To study the parameters influencing the acoustic impedance of the WWCB, impedance models are evaluated to predict its sound absorbing properties. Various studies have shown that impedance models are able to predict the acoustic impedance of rigid-frame porous materials by one to eight input parameters, depending on the internal pore structure. From Cox & Antonio [3] it is known the key parameters are the open porosity and the flow resistivity. Moreover, it is expected that for this material, having a complex internal pore structure, an impedance model taking into account this internal pore structure (i.e. by the pore shape factor or the viscous and thermal characteristic lengths), is required. Previous studies on other types of porous wood-based materials, found good agreements between theory and measurements by making use of the Attenborough model [4] or Johnson-Champoux-Allard model

[5-6] depending on the type of wood-based material [8-10]. In this study, WWCBs with three different strand widths (1.0, 1.5 and 2.0 mm) and different board thicknesses (15, 25 and 35 mm) are tested. Measurements of the density, wood-to-binder ratio, porosity, flow resistivity and surface impedance are performed. Due to the difficulty to measure them in practice, using the selected impedance model the remaining parameters are fitted to the normal incidence sound absorption values defined from measured impedance values in the impedance tube.

2. Material properties and modelling

2.1 Characterization of density, porosity, flow resistivity and surface impedance.

2.1.1 WWCB bulk properties

The bulk properties of the tested WWCB-samples, taken from a large number of samples per board, are presented in Table 1. The range in density per strand width and the difference in wood-to-binder ratio, which is a result of the production process and the used recipes, is showing the board's inhomogeneity.

Table 1: Properties of the tested WWCB.

Strand width (mm)	Density range (kg/m^3)	Thickness (mm)	Wood-to-binder ratio* (-)
1.0	365-544	15,25	0.43-0.50
1.5	300-400	15,25	0.53-0.55
2.0	310-486	25,35	0.54-0.57

*Indicative values defined by measuring the loss on ignition up to 750 ^{0}C.

2.1.2 Flow resistivity and open porosity

From a number of samples taken from different WWCBs, the flow resistivity (sample diameter 100 mm) was measured according to ISO 9053 with a flow resistivity meter and the open porosity (sample diameter 40 mm) with a helium pycnometer (Micromeritics AccuPyc II 1340). The results of the measurements including the regression lines and the belonging Root Mean Square Errors (RMSE), are shown in Figure 1a. The relations belonging to these regression lines will later on be used to create an impedance model for the WWCB, where for its practical use only the density and the thickness are input parameters.

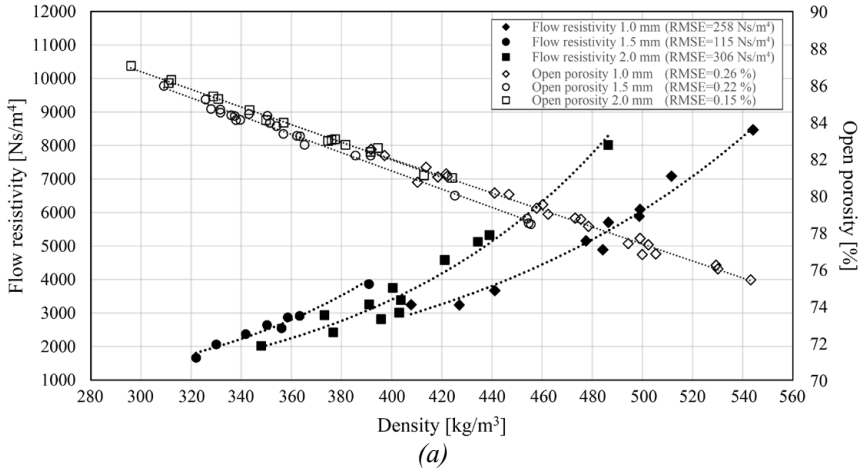

(a)

(b)

Figure 1: (a) Relations between the density and the porosity (linear) and flow resistivity (exponential) and (b) a picture of a WWCB-sample.

From Figure 1a, it can be concluded that the porosity values for boards having different strand widths are in the same order of magnitude. The observed difference in porosity-values, between the strand widths and for the same density, is attributed to the different wood-to-binder ratios but is not significant due to the small amount of solid volume present. The influence of the strand width and binder amount is greater for the flow resistivity values.

Regarding the binder amount, at the same porosity level, the flow resistivity is lower when having a higher binder amount. This indicates that the volume of wood fibres is a more influential with respect to the flow resistivity compared to the binder amount. In Table 1 it can be seen that the boards having a 1.0 mm strand width having a higher binder amount, which is a result of a different recipe. As a result, the flow resistivity is lower compared to the other strand widths having the same density. Comparing the same density for a 1.5 and 2.0 mm WWCB, meaning the same volume of wood fibres, the number of wood fibres inside the 1.5 mm board is higher due to the smaller strand width. This results in a board with smaller openings and a higher flow resistivity.

In Figure 3b, the wood-to-binder ratio for a 'standard' WWCB is compared to boards produced with other recipes, one with a low and one with a high binder amount having the same density. From this figure it can be seen that a lower wood-to-binder ratio, resulting in a lower porosity and a higher flow resistivity and the sound absorption will increase.

Based on a study by Wasselief [8] and after investigating the influence of the porosity on the sound absorption, it was concluded that not all the pores, measured by the helium pycnometer, take part in the acoustical process (some pores are too small). In Figure 3a this is confirmed by increasing the moisture content of different samples, which leads to a decrease of the micro-porosity (in the saturated variant it is assumed all the cell walls of the wood wool strands are filled with water). This figure indicates that closing the micro pores by moisture does not influence the sound absorption significantly. Hence, not all the micro pores take part in the acoustical process. Therefore, to compute the surface impedance from a prediction method, the open porosity measured with the helium pycnometer is not used but is instead determined by an inverse calculation method, see Section 3.1.

2.1.3 Impedance tube measurements

Surface impedance measurements were performed by making use of a six-microphone impedance tube. Out of the measured surface impedance, the normal incidence sound absorption of samples (diameter of 40 mm) are determined. Due to the reliability of the tube, the evaluated range in this study is from 200 to 2800 Hz. In Figure 2 the measured values are given for the three different strand widths.

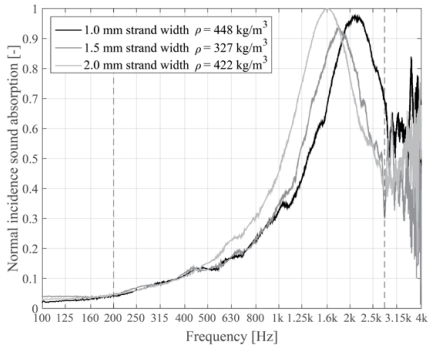

Figure 2: Typical measured normal incidence sound absorption curves for the three strand width samples.

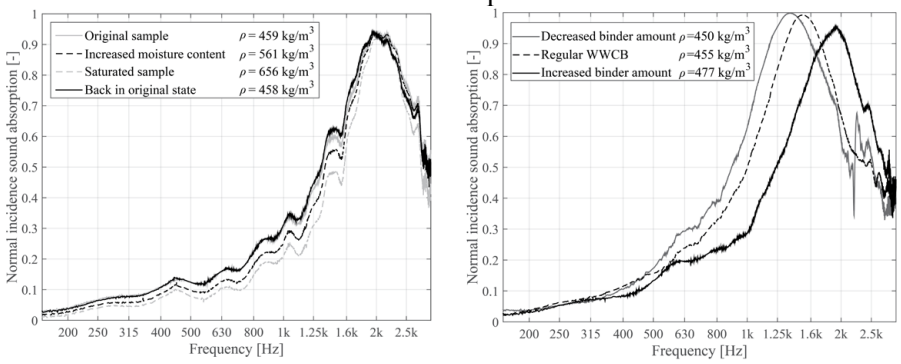

(a) *(b)*

Figure 3: Normal incidence sound absorption of WWCB samples for variation in (a) moisture content and (b) binder amount (d=25 mm).

2.2 Impedance models

Since the evaluated frequency range (200-2800 Hz) is much larger than the phase decoupling frequency (1-2 Hz) of the WWCB, the board is unable to support wave propagation and can be considered as a rigid frame for this range [11]. Therefore, to model the impedance and sound absorption of WWCB, different rigid-frame impedance models were evaluated. As the WWCB does not meet the requirements for the Miki [12] model, this model is considered being unable to predict the sound absorption. The Attenborough [4], Johnson-Champoux-Allard (JCA) [5-6] and Johnson-Champoux-Allard-Lafarge (JCAL) [5&7] models, ordered in the number of input parameters, have been implemented to fit the measured impedances and are all showing values close to the measured ones.

Due to the high number of fitting parameters for the JCAL model, no unique values for the input parameters were found making use of the inverse calculation method. For this reason only the Attenborough and JCA model are shown in this paper. Besides the open porosity, flow resistivity and tortuosity, the Attenborough model takes into account a pore shape factor and the JCA-model a viscous and thermal characteristic length. The calculated relative deviation (Eq. 1) from the measured normal incidence sound absorption per 1/3 octave band in the range from 200 to 2500 Hz for the best fit of the two models (for 30 samples in total) is presented in Figure 4.

$$\varepsilon_{1/3octaveband} = \frac{\alpha_{\text{model,1/3octaveband}} - \alpha_{\text{measured,1/3octaveband}}}{\alpha_{\text{measured,1/3octaveband}}}. \tag{1}$$

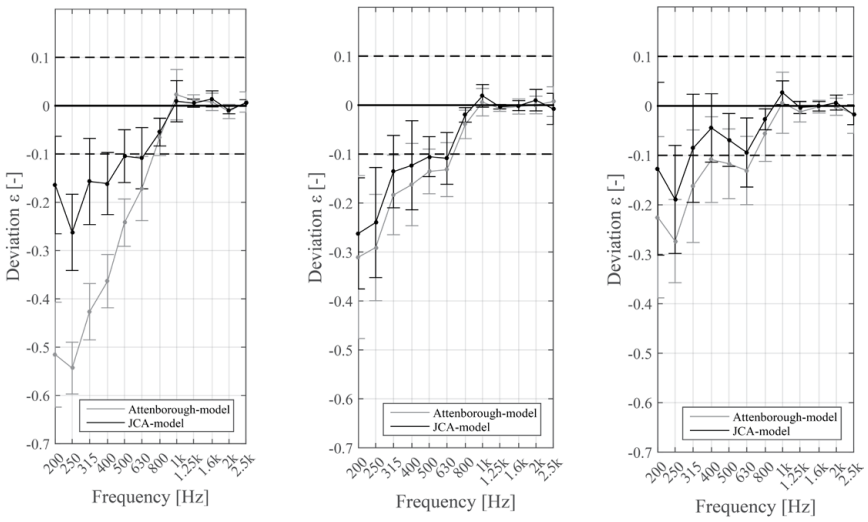

Figure 4: Relative deviation from the measured impedance tube values of the WWCB

From Figure 4 it can be seen that the absolute value of ε for both models is around the 0% above 1000 Hz, but increases below 500 Hz.

It can be concluded that the obtained deviation for the normal incidence sound absorption for the JCA model is lower, especially in the lower frequencies, in comparison to the Attenborough model and therefore better able to predict the sound absorption of the WWCB. Therefore, the JCA model will be used hereafter.

2.2.1 Johnson-Champoux-Allard (JCA) model

The JCA-model involves five physical parameters: the open porosity, flow resistivity, tortuosity and the viscous and thermal characteristic lengths. Based on these input parameters the effective density (Eq. 2), describing the viscous effects, and the effective bulk modulus (Eq. 3), describing the thermal effects, can be calculated.

$$\rho_e(\omega) = \frac{\alpha_\infty \rho_0}{\phi}\left(1 + \frac{\sigma\phi}{i\omega\rho_0\alpha_\infty}\sqrt{1 + \frac{4i\alpha_\infty^2\eta\rho_0\omega}{\sigma^2\Lambda^2\phi^2}}\right), \tag{2}$$

$$K_e(\omega) = \frac{\gamma P_0}{\phi}\left(\gamma - (\gamma-1)\left(1 + \frac{8\eta}{i\Lambda'^2 N_{pr}\omega\rho_0}\sqrt{1 + \frac{i\rho_0\omega N_{pr}\Lambda'^2}{16\eta}}\right)^{-1}\right)^{-1}, \tag{3}$$

with α_∞ is the tortuosity [-], ρ_0 the density of air [kg/m^3], ϕ the porosity [-], σ the flow resistivity [Ns/m^4], i the imaginary number [-], ω the angular frequency [1/s], η the viscosity of air (≈1.84 10^{-5}) [-], Λ the viscous characteristic length [μm], γ ratio of the specific heat capacity (≈ 1.4), P_0 the atmospheric pressure (≈101,320) [-], Λ' the thermal characteristic length [μm] and N_{pr} the Prandtl number (≈1.4) [-].

Based on these equations, the characteristic impedance Z_c $\left(Z_c = \sqrt{K_e(\omega)\cdot\rho_e(\omega)}\right)$ and the wave-number k $\left(k = \omega\sqrt{\rho_e/K_e}\right)$ can be determined. Out of these parameters the surface impedance Z_s $\left(Z_s = -jZ_c\cot(k_c d)\right)$ can be defined with d the board thickness and finally the normal incidence sound absorption can be calculated $\left(\alpha = 1 - \left|\left(Z_s - \rho_0 c\right)/\left(Z_s + \rho_0 c\right)\right|^2\right)$ with $\rho_0 c$ representing the impedance of air (Pa.s/m).

3. Results and characterization of the WWCB

3.1 Determining the input parameters

By making use of the measured normal incidence sound absorption in the impedance tube, an inverse calculation method was used to determine the tortuosity, open porosity and the viscous and thermal characteristic length. In Figure 5 an overview is given of the inverse calculation study for the JCA-model, where the open porosity, tortuosity and the characteristic lengths are fitted on the measured sound absorption curve. The values obtained from this fitting are visible in the legends of Figure 5 and this is done for thirty samples. The found values including the belonging regression lines are presented in Figure 6 and 7, where the grey areas correspond to the root mean square error ranges to the plotted regression lines. For the model's practical use, the input parameters for the impedance models are related to the WWCBs bulk density based on the equations belonging to these regression lines. This is done because the bulk density is easy to measure, where the input parameters are not.

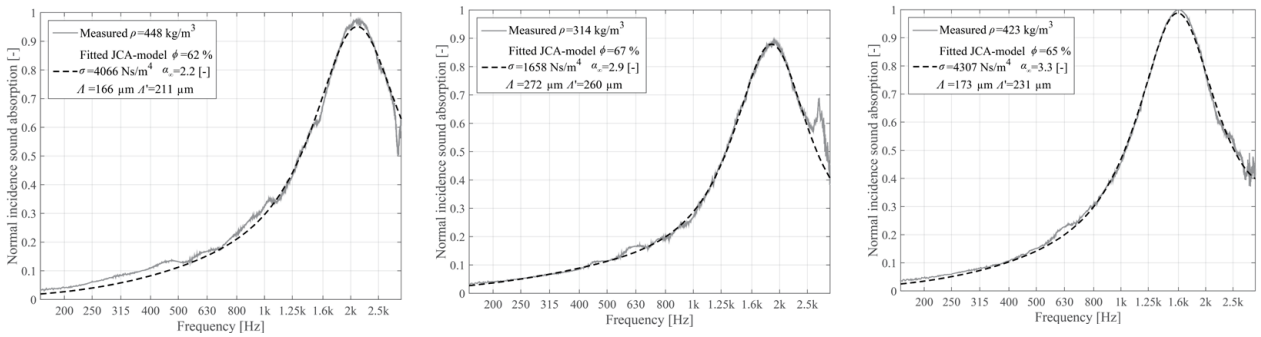

(a) 1.0 mm strand width *(b) 1.5 mm strand width* *(c) 2.0 mm strand width*

Figure 5: Curve fitting results of the JCA-model on measured values for one sample per board (d=25 mm).

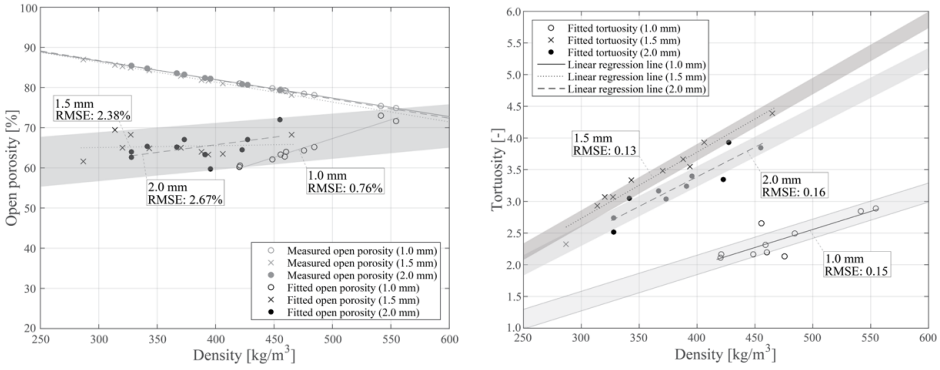

(a) *(b)*

Figure 6: Relations between the bulk density (kg/m^3) and (a) open 'acoustical' porosity (-) and (b) the tortuosity (-) from 30 samples.

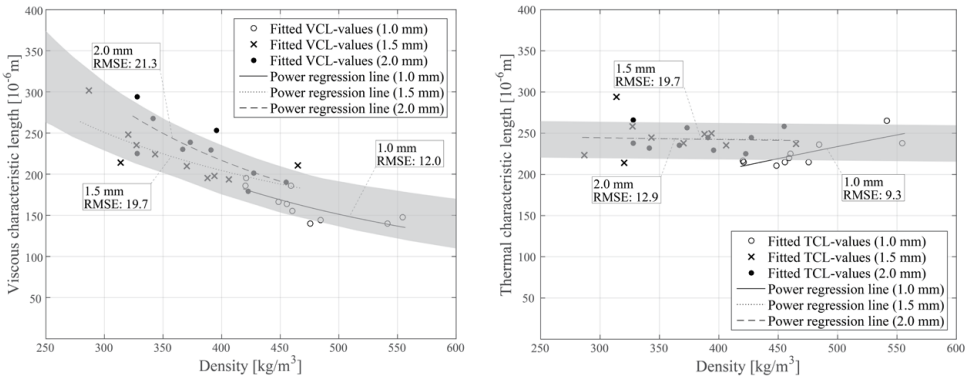

(a) *(b)*

Figure 7: Relations between the bulk density (kg/m^3) and (a) the viscous and (b) thermal characteristic lengths (µm) from 30 samples.

Increasing the bulk density leads to an increase of the acoustically effective open 'acoustical' porosity and the tortuosity and a decrease of the viscous and thermal characteristic length. The relations for the tortuosity, viscous and thermal characteristic lengths are in line with the expectations. While the measured porosity decreases when the density increases, the opposite appears when determining the 'acoustical' porosity. Besides the micro-porosity, the big pores in the lower densities are not efficiently taking part in the acoustical process. This can be explained by the same principle as perforated panel absorbers having bigger openings, where the wall friction is less efficient to damp the vibrations [13]. This finally results in an unexpected increased open porosity with increase of the density.

Table 2: WWCB parameters.

Strand width (mm)	Measured density range (kg/m^3)	Open porosity (%)	Flow resistivity (Ns/m^4)	Tortuosity (-)	Viscous characteristic length (µm)	Thermal characteristic length (µm)
1.0	400	58	2795	1.99	191	204
1.5	400	65	4436	3.78	204	242
2.0	400	65	3400	3.38	216	242

Now the impedance model is validated, the WWCB can be characterized. In Table 2 an overview is given of the WWCB input parameters for the model for the three strand widths with a density of 400 kg/m^3.

3.2 Demonstration of the model

To show the applicability of the model for other board thicknesses as well as boards on an air-cavity, the normal incidence sound absorption values for these WWCBs are predicted making use of the equations belonging to the regression lines from Figure 1, 6 and 7, and compared to the measured values. The results, presented in Figure 8 and 9, show that the created model is able to predict the measured sound absorption with a root mean square error of 0.02 for 1/3 octave bands in the range of 200 to 2500 Hz.

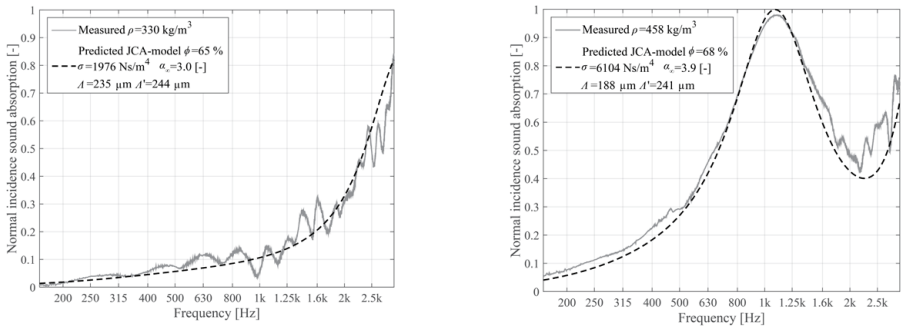

(a) d=15 mm (1.5 mm strand width) *(b) d=35 mm (2.0 mm strand width)*

Figure 8: Demonstration of the created JCA-model for WWCBs with different thicknesses.

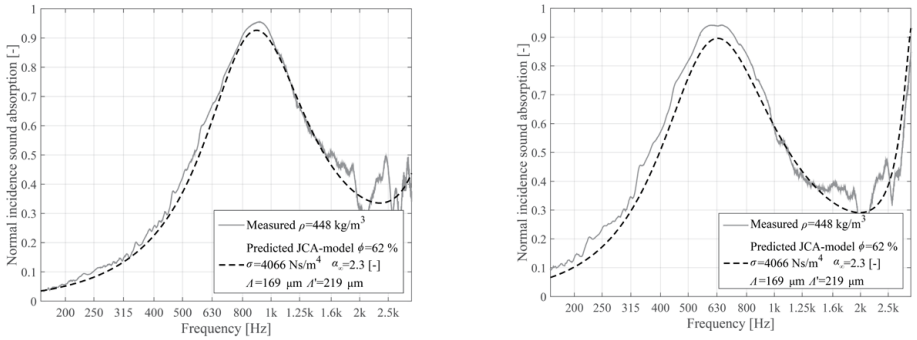

(a) 25 mm air-cavity (1.0 mm strand width) *(b) 50 mm air-cavity (1.0 mm strand width)*

Figure 9: Demonstration of the created JCA-model for WWCBs (d=25 mm.) on an air-cavity.

4. Conclusion

In this article, the sound absorption behaviour of WWCBs is studied. By making use of the Johnson-Champoux-Allard (JCA) model the sound absorption is characterized and predicted, allowing to evaluate properties like board thickness, density and strand width. The sound absorption was studied by using measured and predicted input parameters for the JCA-model. Moreover, the influence of the moisture content and wood-to-binder ratio was considered. Based on the obtained results the following conclusions can be drawn:

- The studied WWCB samples differ greatly in density and in wood-to-binder ratio.
- The five parameter JCA-model is able to predict the sound absorption of the inhomogeneous WWCB with a root mean square error between 0.01 and 0.03 for the 1/3 octave bands in the 200-2500 Hz frequency range in all the evaluated WWCBs.
- Not all the pores, measured by the helium pycnometer, take part in the acoustical process.
- For the evaluated WWCBs, the wood-to-binder ratio per strand width does not need to be treated separately; it is incorporated in the input parameters.
- In case the recipe is changed in comparison with the studied WWCBs by significantly in- or decreasing the wood-to-binder ratio, new relations between the bulk density and the input parameters need to be determined to be able to predict its sound absorption.

By making use of the model and the created relations, it is possible to increase and optimize the sound absorption, which is part of the future work of this study.

5. Acknowledgements

The authors would like to thank the STW-foundation, Knauf Insulation, Van Ganzewinkel Minerals, Eltomation, ENCI, and Wageningen UR for their provision of material, knowledge and financial support.

REFERENCES

1. Elten, G.J. van, Production of wood wool cement board and wood strand cement board (eltoboard) on one plant and applications of the products, *Proceedings of the 10th International Inorganic-Bonded Fiber Composites Conference*, Sao Paulo, Brazil, 15-18 November, (2006).

2. Doudart de la Grée, G.C.H., Yu, Q.L. & Brouwers, H.J.H. Wood-wool cement board: potential and challenges, *Proceedings of the International Inorganic-Bonded Fiber Composites Conference*, Da Nang, Vietnam, 15-19 September, (2014).

3. Cox, T.J. & D'Antonio, P. *Acoustic Absorbers and Diffusers: Theory, design and application*, Taylor & Francis, Abingdon, Oxon, (2009).

4. Attenborough, K. Acoustical characteristics of rigid fibrous absorbents and granular materials, *Journal of the Acoustical Society of America*, **73**, 785-799, (1983).

5. Johnson, D. L., Koplik, J. and Dashen, R. Theory of dynamic permeability and tortuosity in fluid-saturated porous media, *Journal Fluid Mechanics*, **176**, 379-402, (1987).

6. Champoux, Y. and Allard, J.F. Dynamic tortuosity and bulk modulus in air-saturated porous media, *Journal Applied Physics*, **70**, 1975-1979, (1991).

7. Lafarge, D., Lemarinier, P., Allard, J.F. & Tarnow, V. Dynamic compressibility of air in porous structures at audible frequencies, *Journal of the Acoustical Society of America*, **102**, 1997-2006, (1997).

8. Wassilieff, C., Sound absorption of wood-based materials, *Applied Acoustics*, **48**(4), 339–356, (1996).

9. Glé, P.,Gourdon, E. and Amaud, L. Modelling of the acoustical properties of hemp particles, *Construction and Building Materials*, **37**, 801-811, (2012).

10. Berardi, U. and Iannace, G. Acoustic characterization of natural fibers for sound absorption applications, *Building and Environment*, **94**(2), 840-852, (2013).

11. Zwikker, C. and Kosten, C.W. *Sound absorbing materials*, Elsevier, New York, (1949).

12. Miki, Y. Acoustical properties of porous materials - Modifications of Delany-Bazley models, *Journal of the Acoustical Society Japan (E)*, **11**(1), 19-24, (1990).

13. Fuchs, H.V. *Applied acoustics: Concepts, absorbers, and silencers for acoustical comfort and noise control: Alternative solutions – Innovative tools – Practical examples*, Springer, New York, (2013).

Wood Wool Cement Boards (WWCB)

Due to their good thermal insulating, fire resisting and sound absorbing properties, wood wool cement boards (WWCB) are widely applied, mostly as an in- and outdoor ceiling material and noise barriers. The sound absorbing performance of the WWCBs is, characterized, modelled and optimized in this study.

Different models, able to predict the acoustic impedance of rigid-frame porous materials, have been analyzed and their suitability for the WWCB has been evaluated. The Johnson-Champoux-Allard model, used to describe the effective density and dynamic bulk modulus, was found to be most appropriate.

The used WWCBs are made of different strand widths ,different thicknesses and different wood cement ratios. Using the JCA-model, the influence of the WWCB thickness, density, wood-cement ratio, strand diameters and air-cavity is evaluated and the results show that is it possible to improve and optimize the sound absorption of the inhomogeneous WWCB.

TU/e Technische Universiteit Eindhoven University of Technology